JNC TJ9400 99-004

鉛スペクトロメータを用いた
ネプツニウム-237の
中性子捕獲断面積測定

（核燃料サイクル開発機構　研究委託内容報告書）

１９９９年　３月

京都大学原子炉実験所

JNC TJ9400 99-004

鉛スペクトロメータを用いた
ネプツニウム-237の
中性子捕獲断面積測定

（核燃料サイクル開発機構　研究委託内容報告書）

１９９９年　３月

京都大学原子炉実験所

JNC TJ9400 99-004

１９９９年　３月

鉛スペクトロメータを用いたネプツニウム-237の中性子捕獲断面積測定

（核燃料サイクル開発機構　研究委託内容報告書）

小林捷平 ＊

要　旨

本研究の前半では、代表的なマイナーアクチニド(ＭＡ)核種であるNp-237について、まず、中性子核データの現状、評価済核データについて調査を行った。次に、京都大学原子炉実験所の電子線型加速器と組み合わせて付設されている京都大学鉛スペクトロメータ(KULS)を用いて、金及びNp-237の中性子捕獲断面積を熱中性子からkeV領域において測定した。中性子捕獲によって放出される即発ガンマ線は、アルゴンガス入り比例計数管を用いて測定した。入射中性子束／スペクトルの測定には、BF_3比例計数管を用い、捕獲断面積の絶対値は$^{10}B(n,\alpha)$反応による相対測定値を標準熱中性子断面積に規格化して求めた。金及びNp-237試料に対する共鳴領域の中性子自己遮蔽効果は、MCNPコードを用いた計算によって補正した。$^{197}Au(n,\gamma)^{198}Au$及び$^{237}Np(n,\gamma)^{238}Np$反応断面積の測定結果とENDF/B-VI、JENDL-3.2の評価済核データ値との間には全般的によい一致が見られたが、大きな共鳴ピーク領域では両反応とも評価済核データより低目の値を示した。

本研究の後半では、鉛スペクトロメータの原理とその構築、諸特性についてまとめた。中でも、KULSの特性として ①中性子減速時間ｔ(μs)とエネルギーE(keV)の関係（ビスマス孔:$E=190/t^2$、鉛孔:$E=156/t^2$）及び ②エネルギー分解能（ビスマス孔、鉛孔共に約40 %）に関しては共鳴フィルターを用いて実験的に求め、飛行時間分析法によって ③KULS 体系中の中性子スペクトルを測定した。一方、MCNPコードを用いてKULSの諸特性を計算した結果、実験値とは全体によい一致が得られた。

本報告書は、京都大学が核燃料サイクル開発機構の委託により実施した研究成果に関するものである。
契約番号： 100D0121
機構担当部課室：大洗工学センター　システム技術開発部　炉心技術開発グループ
＊　京都大学原子炉実験所

JNC TJ9400 99-004

March 1999

Neutron Capture Cross Section Measurement of Np-237 with Lead Slowing-down Spectrometer

Katsuhei Kobayashi *

Abstract

The present status of nuclear data for neptuniumu(Np)-237, which is a well-known minor actinide, has been reviewed and investigated. Making use of the Kyoto University Lead Slowing-down Spectrometer, the neutron capture cross sections of Au-197 and Np-237 have been measured in the energy range from thermal to keV energy neutrons with an Ar-gas proportinal counter. The neutron flux/spectrum has been monitored with a BF_3 proportional counter, and the relative measurement has been normalized to the well-known standard capture cross section value at 0.0253 eV. Self-shielding corrections, especially near the resonance peaks, were made by the calculations with the MCNP code. The evaluated cross sections for the $^{197}Au(n, \gamma)^{198}Au$ and $^{237}Np(n, \gamma)^{238}Np$ reactions in ENDF/B-VI and JENDL-3.2 are in general agreement with the measurements, although the experimental values are rather lower at the resonance peaks.

A lead slowing-down spectrometer was installed coupled to the 46 MeV electron linac at Research Reactor Institute, Kyoto University (KURRI). Characteristics of the Kyoto University Lead Slowing-down Spectrometer (KULS) were measured and ① the relation between neutron slowing-down time t(μs) and energy E (keV) ($E=190/t^2$ in Bi hole and $E=156/t^2$ in Pb hole) and ② energy resolution (~40 % in Bi and Pb holes) were experimentally investigated. ③ The neutron energy spectrum in the KULS was also measured by the neutron TOF method. The results obtained by the MCNP code were in general agreement with these experimental ones.

Work performed by Research Reactor Institute, Kyoto University under contract with Japan Nuclear Cycle Development Institute (JNC).

JNC Liaison: O-arai Engineering Center, System Engineering Technology Division Reactor Physics Research Group.

* Research Reactor Institute, Kyoto University

鉛スペクトロメータを用いたネプツニウム(Np)-237の中性子捕獲断面積測定

目　　次

第１章　ネプツニウム-237の中性子捕獲断面積測定

第２章　京都大学鉛スペクトロメータ

付　録

第１章　ネプツニウム-237の中性子捕獲断面積測定

図のリスト

第１章　ネプツニウム-237の中性子捕獲断面積測定

表のリスト

第２章　　鉛スペクトロメータ

図のリスト

第２章　　鉛スペクトロメータ

表のリスト

第１章　ネプツニウム-237の中性子捕獲断面積測定

１．序論

ネプツニウム(Np)、アメリシウム(Am)、キュリウム(Cm)などは、いわゆるマイナーアクチニド（ＭＡ）と称される代表的な核種であって、核燃料の燃焼と共に原子炉内で生成蓄積される。図１は、これらのＭＡ核種の生成と変換の過程を示している。100万 kWe級の軽水炉一基あたり、ＭＡは一年間に約２０数ｋｇ生成されると言われている（表１）/1,2/。ＭＡ核種の大部分は、超長半減期の高レベルアルファ放射性廃棄物(ＨＬＷ)であるため、燃料再処理時の取扱い、放射性廃棄物の保管・管理において問題となる。図２は、ＨＬＷの潜在的放射性毒性指数の経年変化を示している。ここで言う毒性指数はＨＬＷ及び核分裂生成物（ＦＰ）中のある核種の存在量(Bq単位)を経口年摂取限度(Bq単位)で割った値として定義している。この図を見ると、Tc-99やI-129などの長半減期ＦＰが存在するものの絶対量はＭＡに比べて遙かに少なく、ＦＰ全体では数百年経てば著しく減少することが分かる。しかし、ＭＡは長半減期の核種が多く、200年以上経つと毒性指数全体としてはＭＡが占めるようになる。こうしたＭＡやＦＰなどを負の遺産として、またそのリスクを次の世代に残さないためにも、これらの高レベル放射性廃棄物をどの様に処理処分するかが、今日の我々に課せられた大きな課題となっている/1,2/。

現在、放射性廃棄物の処理処分法の中で最も有力視されている方法に地層処分が挙げられる。核種の半減期が短く、人が直接管理できる低レベル放射性廃棄物の場合には、比較的浅い地層中で保管管理することも考えられるが、半減期の長いＦＰやＭＡ核種のように長半減期の高レベル放射性廃棄物の場合は、人が住む環境に影響を及ぼさない地下約1000ｍの岩盤中に隔離貯蔵する深地層処分の方法が検討されている。このような場合でも、廃棄物の量をできるだけ減量しておくことが望まれる。

ＭＡは単なる放射性廃棄物ではなく、中性子と反応させれば核分裂を起こしてエネルギー源にもなり、中性子を吸収させれば核変換する点が注目される。消滅処理とは、ＭＡやＦＰを原子炉や加速器で核分裂・消滅させたり、核変換によって半減期の短い核種や毒性の少ない核種に変換させることをいう。消滅処理が実用化できれば、放射性廃棄物の減量化と共に数100年以降の毒性も下がり、次世代の人々へのリスクを低減した地層処分ができるようになる。最近では、ＭＡの燃焼・消滅処理のみならず、核兵器解体から出てきた余剰Ｐｕの扱いについても世界的に強い関心事となっている。原子炉を用いた消滅処理法では、Ｐｕ、ＭＡの核的性質から高速炉による燃焼・消滅が有力視されている。しかし、高速炉の実用化には今少し時間を要することと、高速炉にこれらの核種を装荷した場合、ボイド係

数が正側に移行するなどの問題が存在すると言われている。最近では、Puの場合同様、MAを現有の軽水炉で燃焼させる考え(プルサーマル方式)が検討されている/3,4/。さらに、強力中性子源によるMAの燃焼特性を論じた研究も幾つか発表されている/3,4/。

MAに関連した核データは、原子炉の安全性・経済性評価のみならず、核燃料の燃焼特性や使用済燃料中に生成蓄積されるMA量の予測、MA消滅処理における有効性評価にとっても極めて重要な基礎データである。今日までに、MAに関する核データの実験研究は、主として1960年頃から1980年代中頃にかけてかなり行われてきたものの、測定値間の差異が著しく、評価済核データにおいてもまだ不十分である/5/。その主な理由として、MAは強いアルファ放射体で自発核分裂性核種も含んでおり、実験上その取扱いが難しくなること、バックグランドが高くなること、純度の高い試料が得にくいこと等が考えられる。Wagemans は、試料中の不純物が核データの測定値を大きく乱す（断面積を見かけ上大きくする）ことについて忠告している/6/。特に、MA核種は同位体元素も多く、不純物として混入し易いため、試料純度の問題は一層重要である。また、純度の高い試料であっても、試料自身の核変換/崩壊によって不純物となる核種が徐々に生成蓄積する場合もある/6,7/。一方、実験を行う中性子源の状況からは、熱中性子から高速中性子までの広いエネルギー領域をカバーできる一連の実験が実施できる強力中性子源は得難いため、多数の実験者による測定結果をつなぎ合わせて断面積評価が行われていることが評価済核データの結果に食い違いが生じている原因ともなっている。さらに、一般的には、エネルギー依存の中性子断面積の絶対値測定は必ずしも容易なことではないと言う問題もある。

表１　マイナーアクチニド（ＭＡ）の生成量

	3410MWt-PWR		2500MWt-FBR
冷却期間 / 核種	3年	10年	3年
^{237}Np	57.9%	41.3%	9.45%
^{241}Am	27.4	48.8	54.9
^{242m}Am	0.06	0.04	1.38
^{243}Am	11.9	8.33	25.4
^{243}Cm	0.03	0.02	0.29
^{244}Cm	2.67	1.44	7.73
^{245}Cm	0.15	0.10	0.89
全重量	23.8kg	33.9kg	24.0kg

計算　　：データ JENDL-2, 計算コード SRAC-FPGS
燃焼度　　：33GWd/MT(PWR) 150GWd/MT(FBR)
再処理から群分離までの冷却期間：5年
U,Puの回収率　：100％

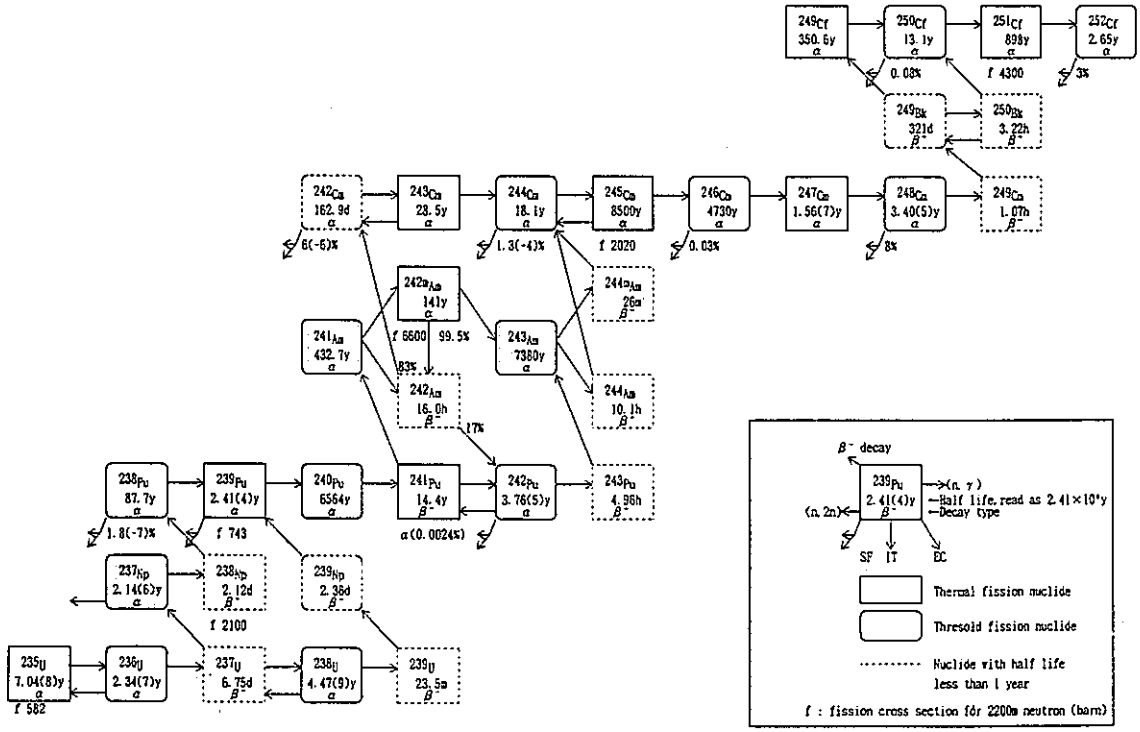

図１　アクチニド核種の生成と崩壊の図

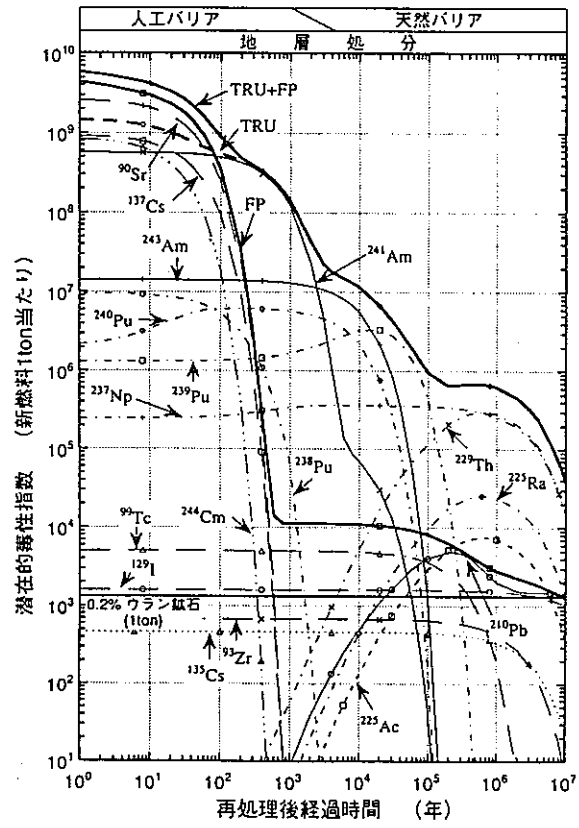

$$\text{潜在的毒性指数} = \frac{\text{HLW中の核種量 (Bq)}}{\text{核種の経口年摂取限度 (Bq)}}$$

使用済燃料：燃焼度33GWD/MT、3年冷却
再処理効率：99.5%U,Pu回収
TRU：全超ウラン元素、FP：全核分裂生成物

図２　ＨＬＷの潜在的毒性指数の経年変化

本研究の目的は、ＭＡ核種の中でも高燃焼燃料中に多量に生成蓄積すると言われる Np-237核種を取り上げ、その中性子捕獲断面積について評価値、実験値の現状を見た後、京都大学原子炉実験所の46MeV電子線型加速器と組み合わせて付設された鉛（減速）スペクトロメータ(KULS)/8/を用いて^{237}Np(n,γ)^{238}Np反応断面積を測定し、評価済核データファイルや既存実験データとの比較、及びこれらの核データ評価を行うことにある。

２．Np-237の中性子核データ

2.1　評価済核データファイル

核分裂で生まれた高速中性子は、核燃料及び原子炉構造材と相互作用を繰り返しながら、減速・拡散していく過程の中では、炉心や炉心周辺の物質／構造材による吸収、炉心からの漏洩など複雑な振る舞いをする。こうした中性子の挙動は、原子炉の核的特性として多群のエネルギー構造を持つ輸送計算/9/や連続エネルギー減速モンテカルロ計算/10/などによって求められる。これらの計算では、熱中性子から20MeV近辺までの中性子エネルギー領域における散乱、吸収／捕獲及び核分裂の断面積など、全てをカバーする一貫した核データが必要となる。ところが、個々の実験データはある特定のエネルギーや反応に限られたものであるため、これらをとりまとめて評価し、作成されたところの「評価済核データファイル」が必要となる。日本において作成された評価済核データファイルは、ＪＥＮＤＬ(Japanese Evaluated Nuclear Data Library：最新バージョンは JENDL-3.2) /11/と呼ばれ、水素からフェルミウムまでの殆んど全核種に対して中性子全断面積、中性子吸収／捕獲断面積、核分裂断面積、散乱断面積などが収納されている。同種の評価済核データファイルは、米国、ヨーロッパ、ロシア及び中国においても、それぞれ独自に ENDF/B-VI、JEF-2、BROND-2、CENDL-2 として作成されている。これらのファイルは熱中性子から20MeV領域の実験データをベースにして評価され、データの欠けている領域、反応については理論計算で補う形で作成される。しかし、実験データの不十分さ、評価法や計算上のモデルの違いなどによって評価済核データ間にも著しい差異が見受けられる場合がある。これらは、後の実験により検証、修正され、より信頼度の高い評価済核データファイルへとバージョンアップされて行くことになる。

最近では、研究の進展と共に核データに対する要請も具体的になり、上に挙げた一般的な評価済核データファイルの他に、ある特定の利用目的のためにDosimetry File、Fusion File, Actinide File (JENDLの場合、半減期が１日以上の核種で、Th(Z=90)からEs(Z=99)までの89核種）などが用意されている。

2.2 核データの現状

ＭＡ核種に関連した核データの実測値は、U-235、U-238、Pu-239 等のメジャーアクチニド核種の場合に比べて少なく、また、データ間の差異も依然大きいものがある/5,12/。今までに世界各国において測定された実験データは、殆んど全て NEA Data Bank に登録され、EXFORから作成されたNESTOR-2/13/を見ても、ＭＡの実験データ数は一般的に少ない。表２には、ＭＡに対する核分裂及び中性子捕獲反応断面積の現状がまとめられている。また、表３は、これらの核種、反応断面積に対し要求されている精度を示している/12/。これらを見ると、中性子捕獲断面積の実験データは、核分裂断面積に比べて質、量ともに乏しく、共鳴領域以上になるとさらにデータは不十分であることが分かる。本研究では、^{237}Np(n,γ)^{238}Np反応断面積の測定を取り上げることもあって、Np-237核種に対する主な中性子核反応の実験データと評価データの現状について調査した。その結果を図３～図１２にまとめる/12/。これらの図から分かることは、中性子捕獲断面積は一応測定データが存在するもののデータ数としては少ない、100keV以上の実験データ間に違いがある、共鳴領域から

表２　ＭＡ核種の核分裂及び中性子捕獲反応断面積に関する実験データの現状

	thermal～resonance			keV～MeV	
	fiss	capt	res	fiss	capt
			max. energy (eV)		
232U	○	○	200	○	×
234U	max	○	1500	○	×
236U	○	○	4000	○	○
237U	max	○	200	○	×
237Np	○	○	600	○	○
238Np	○	×	×	×	×
239Np	×	○	×	×	×
236Pu	○	×	×	○	×
238Pu	○	○	500	○	○
242Pu	max	○	3800	○	○
241Am	○	○	150	○	○
242Am	○	×	×	×	×
242mAm	○	○	20	○	×
243Am	○	○	250	○	○
242Cm	max	○	265	○	×
243Cm	○	○	66	○	×
244Cm	○	○	970	○	○
245Cm	○	○	60	○	×
246Cm	○	○	300	○	×

○:yes、×: no、max: maximum value only

表３　ＭＡ核種に対し、各反応断面積に要求される精度（%）

	σ_{fis}	σ_{cap}	σ_{inel}	σ_{2n}	ν
^{237}Np	5	5	10	20	5
^{238}Pu	5	5	20	20	5
^{242}Pu	10	10			20
^{241}Am	5	5	20	20	10
^{242}Am	20	20			30
^{242m}Am	10	10			15
^{243}Am	5	5	20	20	10
^{242}Cm	10	10			20
^{243}Cm	10	20			30
^{244}Cm	10	10			20
^{245}Cm	10	10			30
^{246}Cm	10	20			30

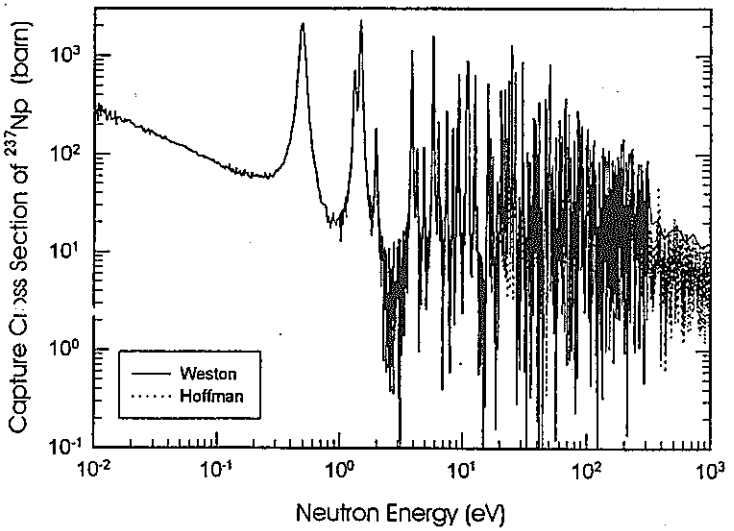

図３　^{237}Np(n, f)反応断面積の既存実験データ
（ 0.01 eV から 1000 eV 領域）

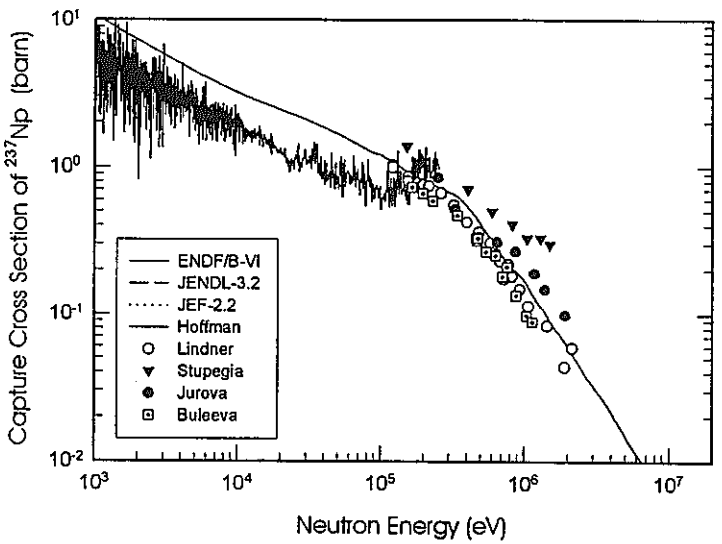

図４　^{237}Np(n, f)反応断面積の既存実験データ
（ 1000 eV から 20 MeV 領域）

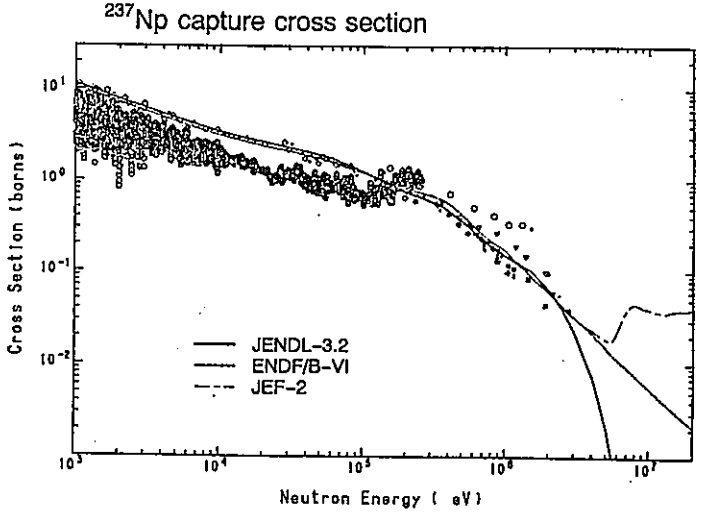

図５　^{237}Np(n, γ)反応断面積の既存実験データと
評価済核データの比較（１keV～20MeV領域）

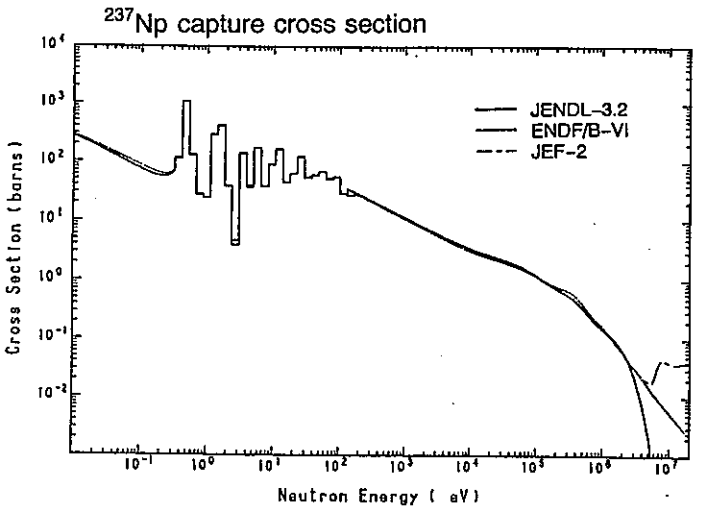

図６　^{237}Np(n, γ)反応断面積の評価済核データの比較

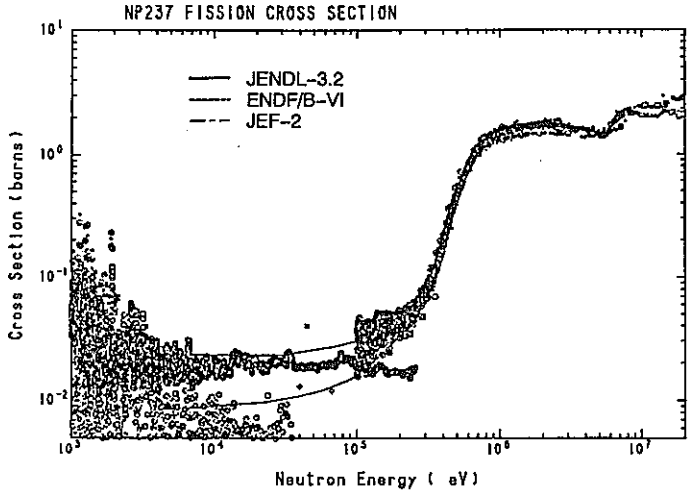

図７　^{237}Np(n, f)反応断面積の既存実験データと
評価済核データの比較（１keV～20MeV領域）

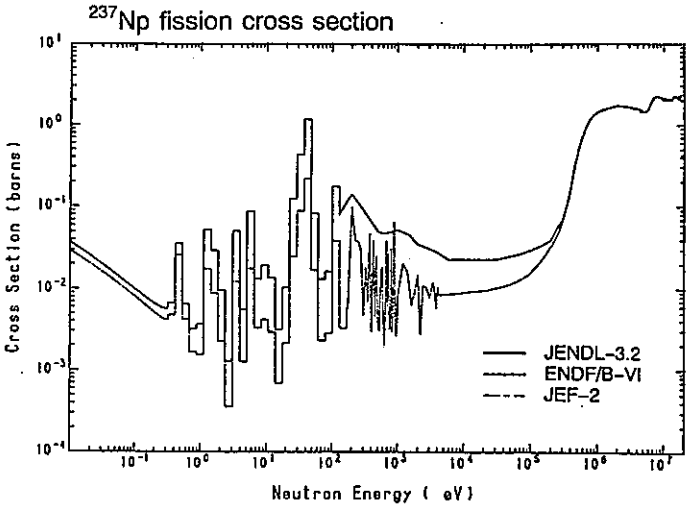

図９　^{237}Np(n, f)反応断面積の評価済核データの比較

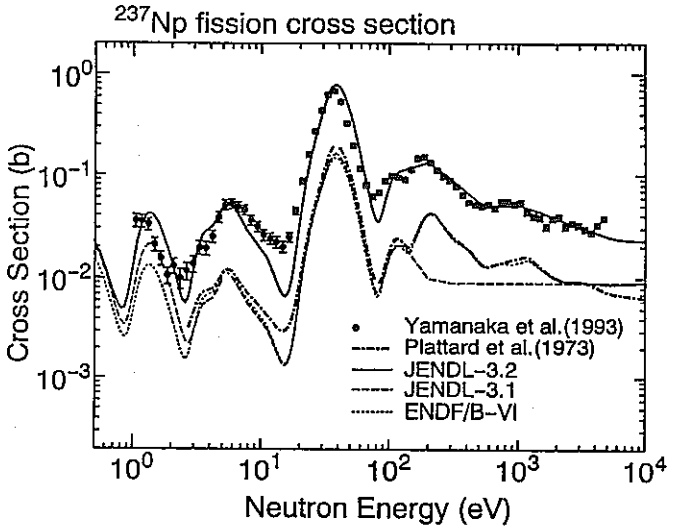

図８　^{237}Np(n, f)反応断面積のＫＵＬＳデータと
評価済核データの比較（１eV～５keV領域）

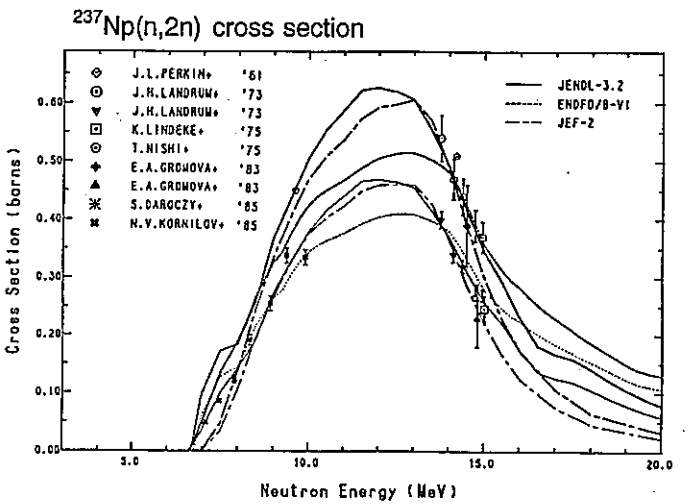

図１０　^{237}Np(n, 2n)反応断面積の既存実験データと
評価済核データの比較

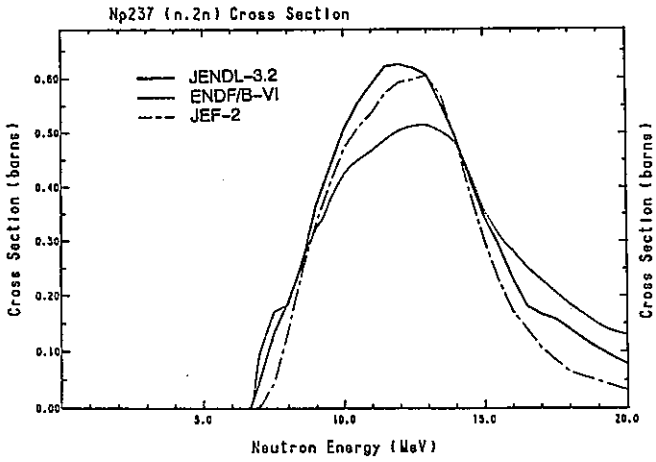

図１１ ^{237}Np(n,2n)反応断面積の評価済核データの比較

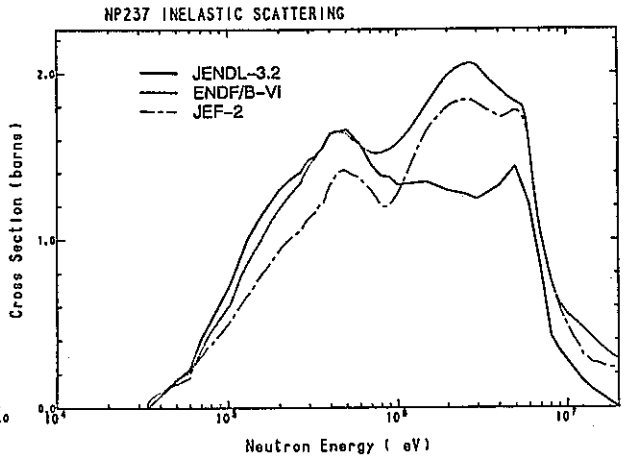

図１２ ^{237}Np の非弾性散乱断面積の評価済核データの比較

数100keV付近の評価値と測定値には差異が見られる、低エネルギー領域の核分裂断面積については、我々のグループによる測定結果/14/がJENDLの再評価に反映され修正が加えられた、(n,2n)反応や非弾性散乱断面積については実験データの不足もあって評価値間にも大きな差異が存在している、などを挙げることができよう。こうした核データの現状、表３の状況からみて、ＭＡ核種に対する核変換／消滅処理を検討評価する観点からも、新たな核データの測定が望まれるところである。

３．鉛スペクトロメータを用いた ^{237}Np(n,γ)^{238}Np反応断面積の測定

3.1 はじめに

ネプツニウム(Np)-237 は、高燃焼燃料中に生成蓄積される主たる超ウラン（ＴＲＵ）元素の１つであって、その半減期は214万年である。そこで、この超長半減期の高レベルアルファ放射性廃棄物（ＨＬＷ）の処理処分法の１つとして、核反応によってこのNp-237を減量・消滅させる方法が検討されている/1,2/。即ち、核分裂反応によってNp-237核そのものを破壊する方法と、中性子捕獲反応によって核変換させ、短半減期(2.12日)のPu-238、さらにPu-239として核分裂・消滅させることへの期待が持たれている。^{237}Np(n,f)反応断面積は、低エネルギー側において極めて小さくなっているのに対し、図７にも見られるように、数百keVから立ち上がる一種のしきい反応断面積のような形状を示し、１MeV付近では２ﾊﾞｰﾝ前後の断面積値に至る。一方、^{237}Np(n,γ)^{238}Np反応断面積は、図６に示されてい

るように、低エネルギー領域において大きな断面積（熱中性子断面積：約180ﾊﾞｰﾝ）を持っている。

Np-237の中性子捕獲反応断面積は、熱中性子領域からMeV領域にかけて一応実験データは存在するものの（図３、図４）その数は少なく、特に100keV以下の領域では Hoffman/15/、Weston/16/のデータが存在するのみである。既存の評価済核データ ENDF/B-VI,JENDL-3.2,JEF-2.2は、何れもほぼ同じデータを示しており、数10eVから100keV領域においてHoffmanのデータより高目になっている。

本研究では、京都大学原子炉実験所の46MeV電子線型加速器と組み合わせて設置された鉛スペクトロメータ(KULS)/8/を用いて、共鳴領域から熱中性子に至る領域の $^{237}Np(n,\gamma)^{238}Np$反応断面積を測定する。実験に使用するNp-237は、円盤形状をした密封線源であることと、実験では中性子捕獲に際して放出される即発ガンマ線を測定することから、検出器として円筒状のアルゴンガス入り比例計数管を使用する。Np-237試料をこの計数管のそばにセットし、一緒にして鉛スペクトロメータの実験孔に挿入して実験を行う。また、中性子束／スペクトル測定用には、マイクロBF_3比例計数管を使用し、得られたエネルギー依存断面積の相対測定値を、別途実測された熱中性子の標準断面積値に規格化することによって$^{237}Np(n,\gamma)^{238}Np$反応断面積を求める。

$^{237}Np(n,\gamma)^{238}Np$反応断面積の測定に先立ち、本実験では、まず、標準的な断面積としてよく知られ、データとしても信頼度の高い測定・評価結果が得られている$^{197}Au(n,\gamma)^{198}Au$反応断面積/17/を測定することとした。金に対する中性子捕獲断面積が従来の標準値をほぼ再現し、本実験手法が妥当であることを確認した上で、今回目的とする$^{237}Np(n,\gamma)^{238}Np$反応断面積の測定を行う。

3.2 Np-237 及び金の試料

Np-237試料は、Amersham社に依頼し、購入したもので、これに付された資料によると、酸化物とした後、670℃で約４時間焼結し、アルミニウム製の容器に封入したものである。作成時(1995年)のNp-237試料は、アルファ線測定によると Np-237：99.897%、Pu-238：＜0.103%であった。その後アルファ崩壊によってNp-237試料中には半減期27日のPa-233が生成蓄積されており、今日では放射平衡に達しているものと思われる。Np-237試料の分析データシートによると、重量純度は99.6wt%で、約４μgの不純物（主として Ga,K,P,Rb,S）が含まれている。

Np-237試料の放射能は、２６MBq（1997年12月10日）で、酸化物（NpO_2）として 1.1279±0.001 グラム封入されている。Np試料の封入容器は、円盤形状のアルミニウム製で、内径20mm(外径30mm)、内厚さ1.4mm(外厚さ2.2mm：円盤面のアルミニウム窓の厚さ0.4mm)の寸法をもつ密封放射線源である。当試料購入後、既に幾度かは中性子実験に使用しているが、図１３は、我々のもとでＧｅ検出器を用いて測定したNp-237試料のガンマ線スペクトルを

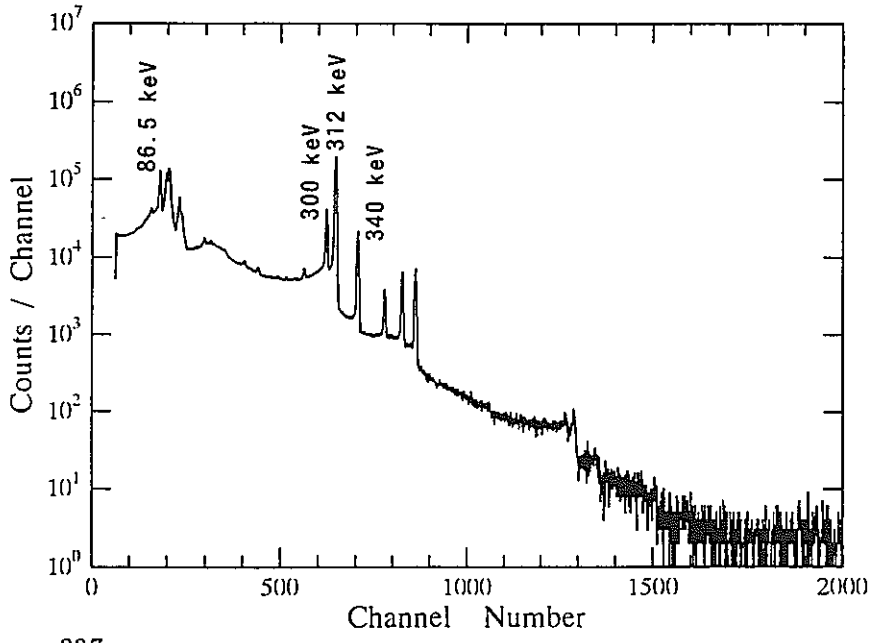

図１３ ^{237}Np のガンマ線パルス波高分布図（Ｇe検出器による測定）

示している。この図には、Np-237(86.5keV)及びPa-233(300,312,341keVほか３本)からのガンマ線ピークが観測されている。

金の試料は、市販されている金箔（厚さ50μm、５cm x 10cm）を丸めて円筒状にし、これにアルゴンガス比例計数管を挿入して実験に使用した。

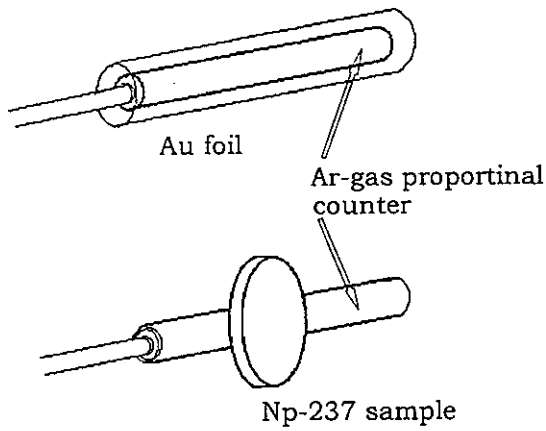

図１４　金箔及びNp-237試料とアルゴンガス比例計数管の実験配置図

3.3　アルゴンガス入り比例計数管

Np-237試料が中性子を捕獲すると、これから即発ガンマ線が放出される。我々は、このガンマ線測定に直径12.7mm、有効長約6.3cm、内圧１気圧（Ar:97%, CO_2:3%）のアルゴンガス入り比例計数管を用いた。使用した高電圧は1400ボルトである。この検出器によるガンマ線の測定効率は必ずしも高くないが、中性子に対しては殆んど感度を示さないことに大きな特徴がある。本実験のように、中性子場において即発ガンマ線を測定する場合には、中性子に感度を持たない測定器の使用が重要となる。^{197}Au(n,γ)^{198}Au反応断面積測定では、金箔の幅５cm側を丸めて長さ10cmの円筒形状にし、これをアルゴン比例計数管に巻き付けて実験を行った。図１４は、金箔、Np-237試料と比例計数管の実験配置を示しており、この状態で鉛スペクトロメータのビスマス実験孔に挿入した。

金箔やNp-237試料に対する中性子捕獲断面積は、BF_3比例計数管を用いて試料に入射する中性子束／スペクトルの測定を行い、$^{10}B(n,\alpha)$反応に対する$^{197}Au(n,\gamma)^{198}Au$、$^{237}Np(n,\gamma)^{238}Np$反応断面積の相対測定結果を別途求められているそれぞれの熱中性子断面積値に規格化する方法によって求めた。

3.4 中性子捕獲断面積の測定

鉛スペクトロメータ(KULS)を用いた$^{197}Au(n,\gamma)^{198}Au$および$^{237}Np(n,\gamma)^{238}Np$反応断面積測定の実験の手法は、先に我々が行ったNp-237、Am-241,242m,243 の核分裂断面積測定の場合と基本的には同じである/7,13,18/(付録Ａ，Ｂ，Ｃ）。これまでの核分裂断面積測定では、測定対象とする試料の電着膜とU-235の電着膜を背中合わせ（back-to-back 型）にセットして電離箱に封入し、実験に用いた。$^{235}U(n,f)$反応は、標準断面積値を与えるとして測定結果の規格化に使用された。しかし今回のKULSの実験では、図１４に示す実験配置において、アルゴンガス比例計数管による$^{197}Au(n,\gamma)^{198}Au$および$^{237}Np(n,\gamma)^{238}Np$反応断面積を測定した。マイクロ$BF_3$比例計数管は、$(n,\gamma)$反応のエネルギー依存断面積の相対測定を行うためのモニターとして使用されている。この場合もアルゴンガス比例計数管用、BF_3比例計数管用にそれぞれ一系統ずつ独立に実験回路系を用意した。各時間分析器のチャンネル幅は共に0.5μs、チャンネル数は8192である。図１５～図１８は、Au-197／アルゴン比例計数管、Np-237／アルゴン比例計数管、バックグランド(実験試料なし)／アルゴン比例計数管、マイクロBF_3比例計数管を用いた各測定に対する時間スペクトルの例を示す。図１５の200チャンネル付近には4.9eVの金の巨大共鳴ピークが観測される。図１６の数十チャンネル前後にNp-237の共鳴ピークが見られる。試料からのバックグランド放射線が高いため、全チャンネルにわたって計数値が高くなっている。図１７は、ビスマス実験孔のビスマス中に含まれる銀の不純物によるピーク(バックグランド)が測定されている。

本中性子捕獲断面積の測定は、アルゴンガス比例計数管を用いた即発ガンマ線測定法によって行ったが、この場合は先の核分裂電離箱の場合と異なり検出器周辺に存在するガンマ線に対しても感度が高く、これらのガンマ線がバックグランドの要因となる。また、比例計数管の特性として、パルス信号に対する時間応答がシンチレータなどより遅いことも実験上不利な条件である。今回の実験では、このような比例計数管を使用せざるを得なかったことがkeV以上のエネルギー領域における測定をより困難なものにしていると言える。鉛スペクトロメータの実験孔は周囲が鉛で覆われてはいるが、ガンマ線測定を行うという点で従来の核分裂実験に比べて、加速器から受けるγフラッシュは深刻な問題であった。そのためγフラッシュの影響をできるだけ少なくするために、加速器の運転条件を以下のような低出力状態に保って実験を行った：パルス幅：6.8 ns、パルスの繰り返し：200 Hz、ピーク電流：0.140 A、電子加速エネルギー：30 MeV。実験に要した時間は、合計してほぼ80時間余りであった。

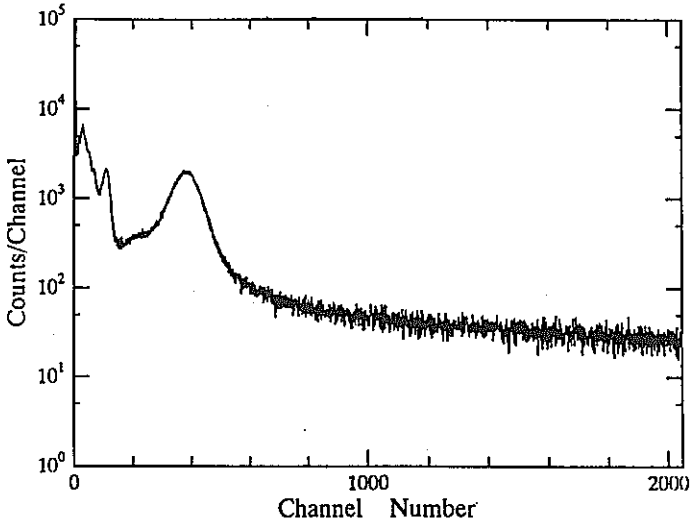

図１５　金箔による時間スペクトル測定の例

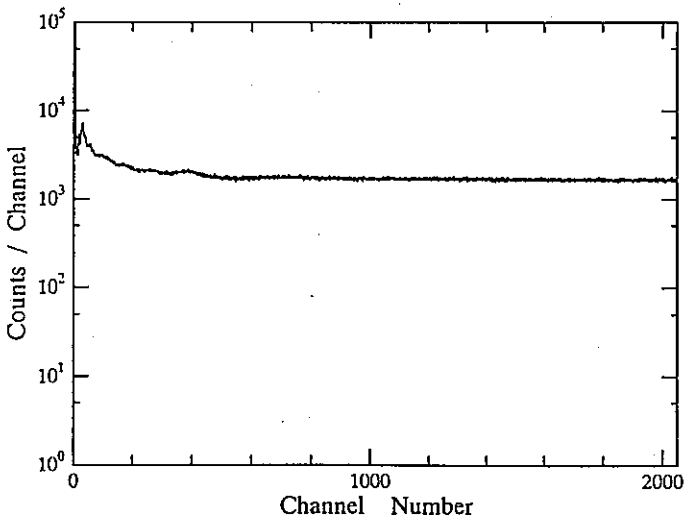

図１６　Np-237試料による時間スペクトル測定の例

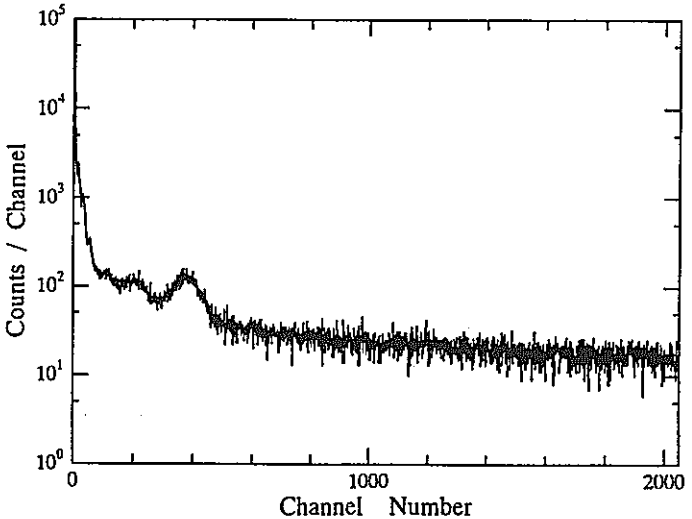

図１７　バックグランド（試料なし）測定の時間スペクトル測定の例

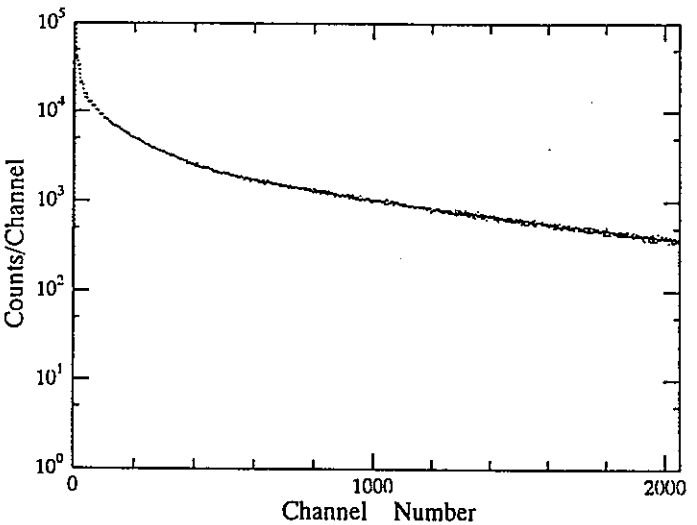

図１８　マイクロＢＦ$_3$比例計数管による時間スペクトル測定の例

中性子捕獲断面積σc(E)の相対測定は、次式によって行った：

$$\sigma_c(E) = \frac{\text{アルゴン比例計数管の計数率(捕獲事象測定－バックグラント')}}{\text{マイクロ}BF_3\text{比例計数管の計数率}} \times F(E) \times \sigma_B(E)$$

ここで、マイクロBF_3比例計数管は、入射中性子束／スペクトルのモニター-として使用している。$^{10}B(n,\alpha)$反応断面積$\sigma_B(E)$は、いわゆる1/v型の曲線を示し、標準断面積としてもよく知られている/19/。F(E)は、試料における実効的な中性子自己遮蔽に対する補正項（関数）で、次節で述べる計算によって求めた。また、アルゴンガス比例計数管の即発γ線測定に対する検出効率は、入射中性子のエネルギーに依存しないものと仮定した。

3.5 中性子自己遮蔽効果の補正

Np-237は 0.49, 1.49eVなどに、金は 4.9, 60eVなどに大きな共鳴ピークを持っている。そのため、本実験には比較的厚さが薄いNpO_2粉末(厚さ1.4mm、0.35ｸﾞﾗﾑ/cm^2)、金箔(厚さ50μm、0.095ｸﾞﾗﾑ/cm^2)を用いたとはいえ、これらの巨大共鳴付近では中性子の自己遮蔽効果について検討をしておく必要がある。本研究では、連続エネルギー減速モンテカルロコードMCNP/10/を用いて、それぞれの試料中における中性子の自己遮蔽効果について計算を試みた。KULS実験孔内では、中性子は試料の周囲から一様に入射するとして、iのエネルギーグループEi毎に次式に従い計算を行った。

$$\langle \sigma_c(Ei) \rangle = \frac{\int_r \int_{Ei} N \sigma_c(E) \ \phi(r,E) \ dr dE}{\int_r \int_{Ei} N \ \phi(r,E) \ dr dE}$$

N：試料の原子数密度、$\sigma_c(E)$：中性子捕獲断面積、$\phi(r,E)$：試料中の場所 r における中性子スペクトルを示す。各エネルギーグループには、ほぼ0.12レサジー幅を持たせている。さらに試料に関しては十分希釈した（密度を６桁落とした）状態の計算も行い、これら両者の比からエネルギーに依存した自己遮蔽の補正関数を算出した。これをKULSのエネルギー分解能関数でなまし、金、Np-237試料に対するそれぞれの(n,γ)反応断面積の測定値を補正した。図１９、図２０は、これらの補正関数を示している。これらの図に見られるように、本実験に使用した薄い試料の場合でも大きな共鳴エネルギー付近では中性子自己遮蔽に対する補正が必要となることが分かる。

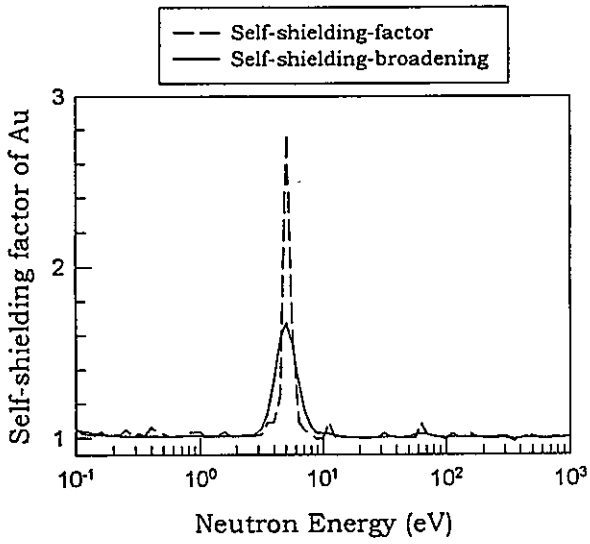

図１９　金箔に対する中性子自己遮蔽の補正関数

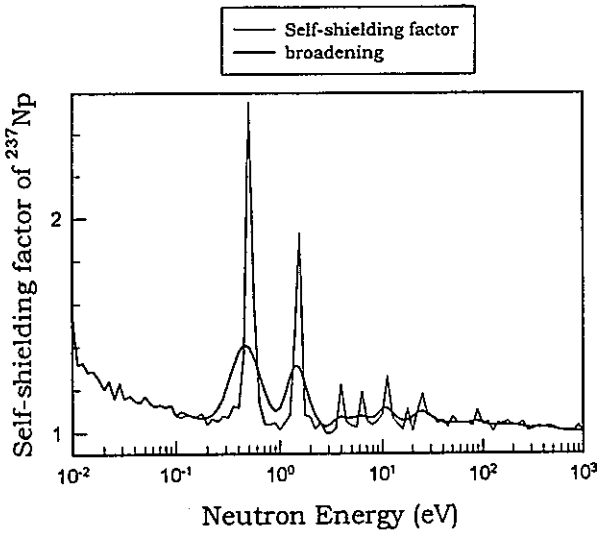

図２０　Np-237試料に対する中性子自己遮蔽の補正関数

3.6　測定結果

3.6.1　^{197}Au(n, γ)^{198}Au反応断面積

KULSを用いて測定した数keV以下の^{197}Au(n, γ)^{198}Au反応断面積の結果を図２１に示す。中性子共鳴領域／低エネルギーの領域では、実験に用いた鉛スペクトロメータのエネルギー分解能（半値幅）が、図２２に見られるように、～40%ないしそれ以上を示すため、図２１ではENDF/B-VIの評価済核データをKULSのエネルギー分解能（半値幅）関数を用いてなました(broadeningした)後、実験値との比較を行っている。また、本実験は相対測定であるため、0.0253eVにおける熱中性子断面積の標準値（98.65± 0.09ﾊﾞｰﾝ）に規格化している/20/。主たる誤差は、計数値に関わる統計誤差(0.63～6.9%)、^{10}B(n, α)反応におけるエネルギー依存性（1/v特性からのズレ：＜２%）、相対測定の規格化に伴う誤差(＜１%)、試料中での中性子自己遮蔽の補正に伴う誤差(ピーク近辺で＜16%)などが考えられ、全体で３～16%程度である。

図２１は、図１９に示した中性子自己遮蔽効果に対する補正を加えた結果である。本実験値は、4.9eVの主共鳴、60eVの共鳴ピークにおいて低目の値を示しているが、1/v領域を含め全体にENDF/B-VI評価値をよく再現していることが分かる。

3.6.2　^{237}Np(n, γ)^{238}Np反応断面積

^{237}Np(n, γ)^{238}Np反応断面積についても、KULSとBF_3比例計数管を用いて^{10}B(n, α)反応に対する相対測定を行い、熱中性子エネルギー0.0253eVにおける標準断面積値（付録Ｄ）に

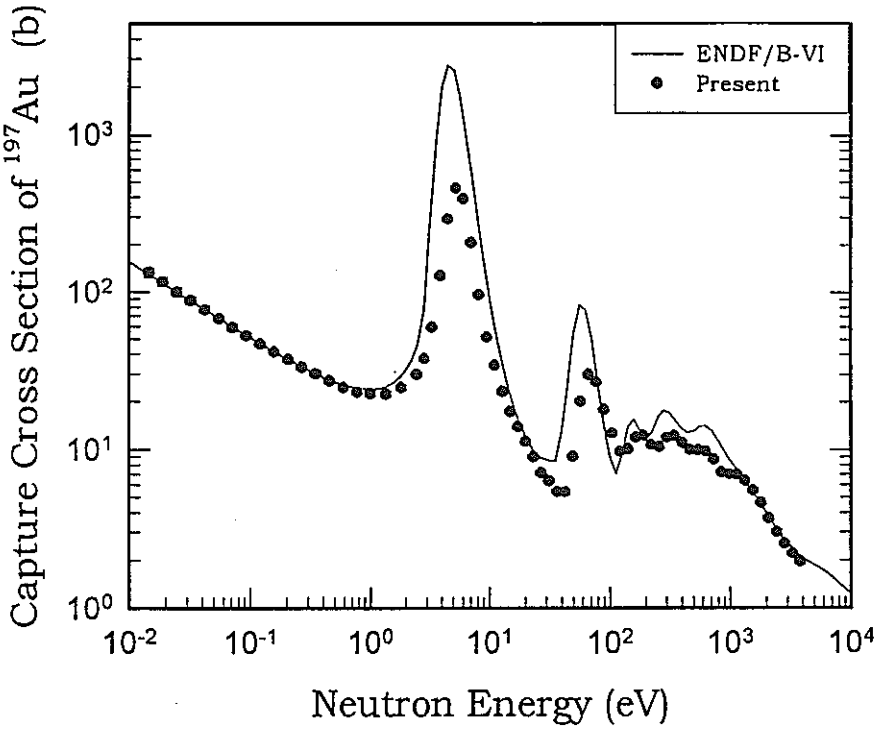

図２１ ^{197}Au(n, γ)^{198}Au 反応断面積の測定結果と評価値の比較
(KULSのエネルギー分解能でなましている)

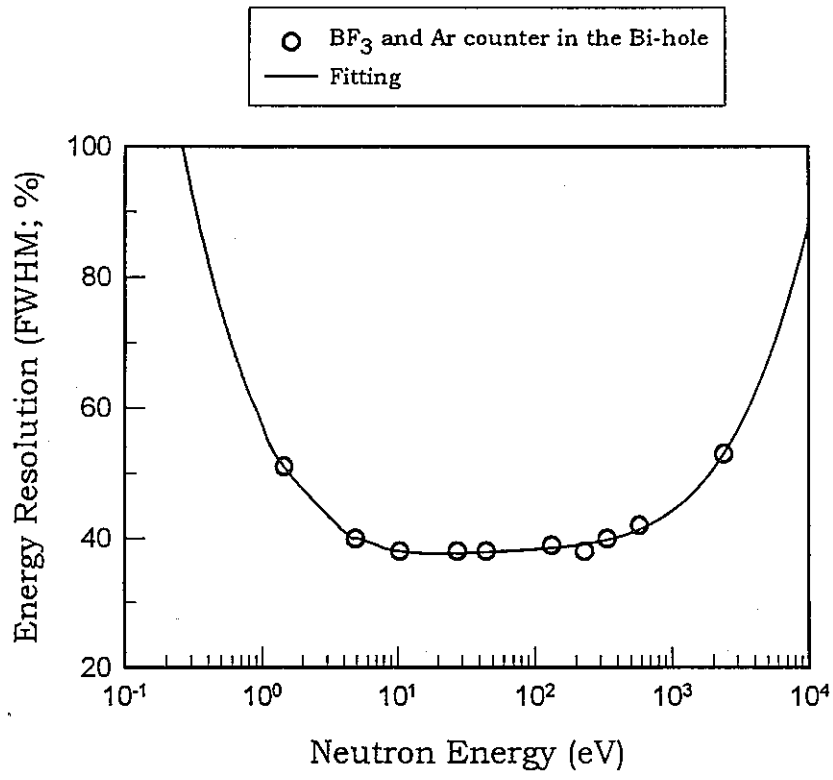

図２２　ＫＵＬＳのエネルギー分解能（半値幅）曲線

規格化した。本実験によって得られた熱中性子から数keV領域における測定結果を図２３に示す。ここでは、評価済核データ ENDF/B-VI、JENDL-3.2、JEF-2.2（３つの評価データ値は一致しており重なっている）のエネルギー依存性評価のためにも、0.0253eVにおけるENDF/B-VIの評価値（180ﾊﾞｰﾝ）に規格化している。また、図２３に描かれた評価済データは、鉛スペクトロメータのエネルギー分解能(半値幅)曲線を用いてなました(broadeningした)結果である。

本実験における主たる誤差は、計数値に関わる統計誤差(0.01～9.1%)、$^{10}B(n,\alpha)$反応におけるエネルギー依存性（1/v特性からのズレ：＜２%）、相対測定の規格化に伴う誤差（２%)、中性子自己遮蔽の補正に伴う誤差(ピーク近辺で＜14%)などが考えられ、全体で2.8～14%程度である。

図２３に示した$^{237}Np(n,\gamma)^{238}Np$反応断面積の評価値は、大きな共鳴ピークを除き、本測定結果と全体によい一致を示している。Np-237試料の場合も、大きな共鳴ピークにおいて実験値が評価値より低い値を示した。Np-237や金の共鳴ピークに見られるこのような差異については、今後の検討課題である。

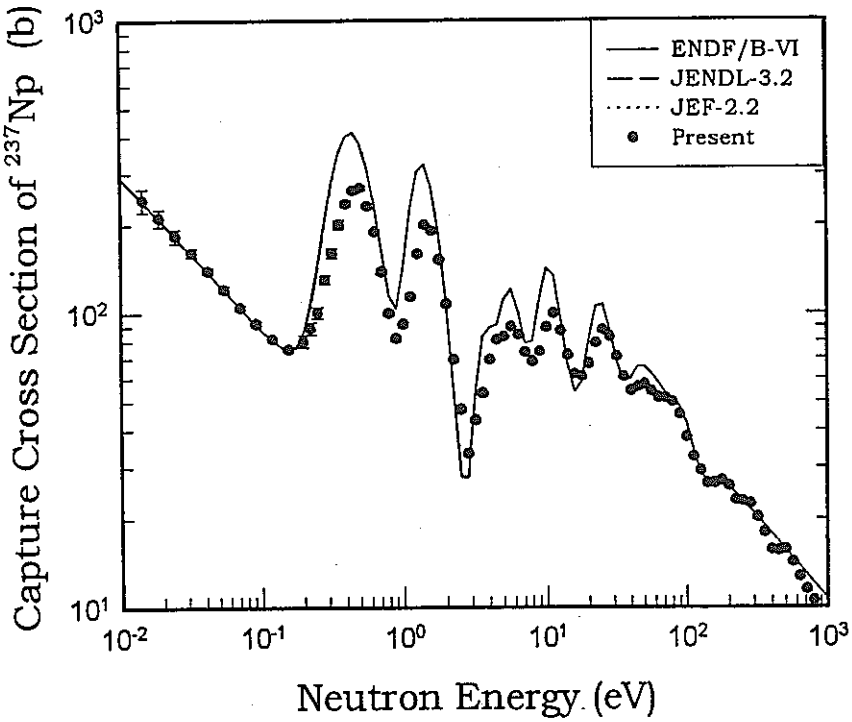

図２３ $^{237}Np(n,\gamma)^{238}Np$ 反応断面積の測定結果と評価値の比較
(KULSのエネルギー分解能でなましている)

４．まとめ

我々は、ここ数年来、アクチニド（ＭＡ）核種の消滅に関わる基礎的な核データとして、これらの中性子核反応断面積に関する実験的研究を進めてきた。こうした実験的研究の一環として、京都大学原子炉実験所の鉛スペクトロメータ(KULS)を用いて行ったNp-237、Am-241,242m,243に関する核分裂反応断面積の測定に続き、本研究ではNp-237の中性子捕獲反応断面積の測定を行った。本実験で得られた測定値を従来の実験データ及び評価済核データと比較、検討した。

本研究において得られた成果を以下にまとめる。

(1)Np-237に関する核データの現状を調査した結果、中性子捕獲断面積に関するデータ数は必ずしも豊富ではなく、共鳴領域から数100keV領域の評価値と実験値間にも差異が存在している。(n,2n)反応や非弾性散乱断面積に関する実験データが不足しており、評価値間にも大きな違いが見られる。

(2)本研究においては、京都大学原子炉実験所の46MeV電子線型加速器（ﾗｲﾅｯｸ）と組み合わせて設置されている鉛スペクトロメータ（エネルギー分解能は半値幅にして約40%）を用い、中性子捕獲反応断面積の測定ではアルゴンガス比例計数管（直径12.7mm、有効長約6.3cm、内圧１気圧）によって試料から放出される即発ガンマ線を測定する方法によった。この検出器の検出効率はシンチレータを使った検出器などに比べて低いが、実験場（鉛スペクトロメータの実験孔内）の中性子に対して殆んど感度を持たないことが特徴である。

(3)実験孔内の中性子束／スペクトルはBF_3比例計数管を用いて測定し、$^{10}B(n,\alpha)$反応断面積を利用して、Au-197及びNp-237の中性子捕獲断面積の相対値を求め、これを熱中性子(0.0253eV)の標準的な断面積値に規格化した。

(4)まず、標準的な中性子捕獲反応であって、実験／評価データ値も比較的よく知られている$^{197}Au(n,\gamma)^{198}Au$反応断面積を４keV以下のエネルギー領域において測定した。その結果、大きな共鳴ピーク領域を除き全体に従来値をよく再現するデータを得ることができた。

(5)同様に、$^{237}Np(n,\gamma)^{238}Np$反応断面積を熱中性子からkeV領域において測定し、ENDF/B-VIなどの評価済核データと比較した結果、全体に本測定データに近い結果を与えているが、大きな共鳴ピーク近辺では実験値が評価値を下回った。この傾向は金の場合にも見られる。

(6)金及びNp-237試料に対する中性子の自己遮蔽効果は、MCNPコードにより計算／補正を行っているが、大きな共鳴近辺に見られる実験値／計算値間の差異については、今後の検討課題である。

【参考文献】

/1/ 「消滅処理研究の現状」、日本原子力学会 消滅処理研究専門委員会 1994。

/2/ 「高レベル廃棄物の消滅処理研究開発」、日本原子力学会誌、Vol.37, No.3, p.159 (1995).

/3/ 例えば、向山武彦：私信 (1993)、1993 Future Nuclear System: Emerging Fuel Cycles and Waste Disposal Options を中心に。

/4/ 例えば、平川直弘：私信 (1996)、1995 Future Nuclear System: Emerging Fuel Cycles and Waste Disposal Options を中心に。

/5/ 菊池康之、中川庸雄、高野秀機、向山武彦、「アクチノイド核データの信頼性－微分データとその積分的検証」、日本原子力学会誌、Vol.36、No.３、211 (1994)。

/6/ C. Wagemans, Nucl. Instr. Methods in Phys. Res., A236, 429 (1985).

/7/ K. Kobayashi et al., J. Nucl. Sci. Technol., Vol.36, No.1, 20 (1999).

/8/ K. Kobayshi et al., Nucl. Instr. Methods in Nucl. Phys. Res. A, 385, 145-156 (1997).

/9/ 例えば、K. Tsuchihashi et al., "SRAC; JAERI Thermal Reactor Standard Code System for Reactor Design and Analysis", JAERI 1285 (1983), and "Revised SRAC Code System", JAERI 1302 (1986).

/10/ 例えば、"MCNP - A General Monte Carlo Code for Neutron and Photon Transport, Version 3A", LA-7396-M, Rev.2, Los Alamos National Laboratory (1986).

/11/ K. Shibata and T. Narita(Eds.) "Descriptive Data of JENDL-3.2", JAERI-Data/Code 98-006, Parts I & II, (1998).

/12/ 中川庸雄、日本原子力研究所 核データセンター発行「核データニュース」、No.50、p.13 (1995)、及び 中川庸雄氏私信(1995)。

/13/ T. Nakagawa, "Neutron Data Storage and Retrieval System", JAERI Nuclear Data Center (1995).

/14/ A. Yamanaka et al., J. Nucl. Sci. Technol., Vol.30, No.9, 863 (1993).

/15/ M. M. Hoffman et al., Bull. Am. Phys. Soc., 21, 655 (1976).

/16/ L. W. Weston & J. H. Todd, Nucl. Sci. Eng., 79, 184 (1981).

/17/ S. Yamamoto et al., J. Nucl. Sci. Technol., Vol.33, No.11, 815 (1996).

/18/ S. Yamamoto, et al., Nucl. Sci. Eng., 126, 201 (1997).

/19/ IAEA Technical Reports Series No.227, "Nuclear Data Standards for Nuclear Measurements", IAEA (1983).

/20/ S. F. Mughabghab, "Neutron Cross Sections", Vol.1,Neutron Resonance Parameters & Thermal Cross Sections, Part B, Academic Press, Inc., New York (1984).

第２章　　鉛スペクトロメータ

１．鉛スペクトロメータとその特徴

鉛のように重い物質であって、その中性子吸収断面積が小さい原子核できている大きな体系（一辺が 1.5～2m）にパルス状中性子を打ち込むと、中性子は体系から殆んど漏れ出ることなく、弾性散乱を繰り返しながら減速していく。この場合、散乱当たりに減速される割合が小さいため、多数回の散乱を繰り返す中で、比較的狭い velocity group に集まる傾向を示しながら、パルス打ち込み後の減速時間と共にgroup化した中性子の平均エネルギーが下がっていく。1950年頃、Lazarev & Feinberg は、こうした現象に着目し、これをスペクトロメータとして応用できないかと考えた/1/。Bergmanらは、1955年の第１回ジュネーブ原子力平和利用国際会議において、初めて鉛減速スペクトロメータ（または単に「鉛スペクトロメータ」とも言う）の原理と実験結果について報告している/1/。それ以後、世界各国で幾つかの鉛スペクトロメータが設置されたが、今日稼動状態にあるものは、米国のレンスラー工科大学(RPI)のRINS/2/、ロシアのクルチャトフ研究センターのスペクトロメータ/3/など数基程度かと思われる。

大きな鉛集合体のほぼ中央部にパルス状高速中性子が打ち込まれると、鉛は中性子吸収断面積が小さいため、中性子は弾性散乱（0.57 MeV以上では非弾性散乱も起こり得るが）を繰り返し減速して行く。高エネルギー側の中性子はそれだけ速くエネルギーを失うため、エネルギーの focus 現象が起こり、50～100keV 以下の中性子になると、減速時間に対応してほぼガウス分布に近いエネルギー分布を持つようになる。その平均中性子エネルギーは減速時間の自乗に反比例する関数として導かれる/1,4/。減速途中のvelocity group中性子が持つエネルギー分解能（半値幅）は、鉛スペクトロメータ固有の核的な特性により30～35%と広がっている/1,4/。この点が鉛スペクトロメータ最大の短所と言える。しかし、鉛スペクトロメータの最大の特徴は、中性子源より僅か数10cmの場所で実験が行えることもあって、強力な中性子束が得られることである。例えば、通常の飛行時間分析実験に比べ、中性子強度が数千倍から１万倍（飛行路が５ｍの場合）にもなると言われている/2/。この点に注目して、RPI では鉛スペクトロメータを用いて、keV 領域における U-238 の sub-threshold 核分裂断面積の測定/2/、100 keV以下でのトリウム、キュリウム、アインシュタニウム等に対する核分裂反応断面積の測定/5-8/が行われている。これらの実験においては、反応断面積が ﾏｲｸﾛﾊﾞｰﾝ(μｂ)オーダと小さい、または実験試料の入手量が極めて制限される等の実験上不利な条件下にあっても測定が可能であった。Block等は鉛スペクトロメータを用いて核分裂断面積を測定する場合、測定可能となる最低条件として「１μｇ

b」と言う表現を使っている/2/。即ち、1μg以上の試料があれば1bの核分裂断面積の測定が可能であり、1g以上の試料があれば1μbの核分裂断面積測定が可能となる一つの目安を示している。α崩壊、β崩壊を伴い、実験上のバックグランドが高くなるアクチナイド核種、試料量を十分入手できないFP核種、断面積の小さい核種等の核データ測定、物質のassay 等の基礎的な研究に対しても、鉛スペクトロメータは、その特徴を生かして活用されている/2,5-10/。

表1　中性子源としてのKULS、Linac、KURの比較

項　目	KULS	Linac	KUR
中性子発生の原理	Linacのパルス中性子源を使用	電子を加速し重金属を標的に照射光中性子を発生	ウランを核分裂させる
中性子発生の制御方法	Linacパワーを調整する	電子の加速状態を制御	制御棒で連鎖反応量を制御
中性子発生部位の体積	ｽﾍﾟｸﾄﾛﾒｰﾀ内全域(実験孔)	小さい：約10cmx10cmx10cm程度	容積は大きい約60cmx60cmx60cm程度
中性子発生の時間的様相	Linacパルスの発生に同じ	間欠的､ﾊﾟﾙｽ状毎秒数百回程度	連続的に発生定常中性子源
中性子エネルギースペクトル	0.1eV～100keV共鳴領域	熱中性子からMeV領域まで	熱中性子からMeV領域まで
中性子束強度	Linac条件と実験場による10^5～10^8n/cm^2/s	平均～10^{12}n/s ～10^{18}n/ﾊﾟﾙｽ	～10^{14}n/cm^2/s
利用できる放射線	共鳴中性子が主	中性子の他、電子、陽子、γ	中性子が支配的
中性子利用方法、形態	核データ、即発γ線分析assay	TOF実験、核データ、照射、放射光、物性･陽電子研究、RI製造	中性子を多量に、ビーム実験、照射、RI製造

中性子源としてみた場合、飛行時間分析実験に用いられる京都大学原子炉実験所の電子

線型加速器（Linac：最高電子エネルギー46MeV)/11,12/、原子炉中性子源としての５MWの京都大学研究用原子炉（ＫＵＲ)/13/、Linacと組み合わせて設置された京都大学鉛スペクトロメータ（ＫＵＬＳ)/14/について比較し、それらの特徴を表１にまとめた。ＫＵＬＳはエネルギー分解能の点でLinac飛行時間分析法に比べ遥かに及ばないが、実験場の中性子束は数千倍の強さがある。しかし、中性子束の高さから言うと、ＫＵＲはＫＵＬＳの場合より一段と高いが、定常中性子源であるため時間的にもエネルギー的にも得られる情報は積分量である。これらの中性子源には、それぞれ特徴があって、これらを生かした相補的使い方により一層充実した研究の遂行が期待できる。

２．鉛スペクトロメータの原理

鉛は、原子番号が 82、質量数が207.2と大きい物質であるため、中性子が鉛との衝突によって低エネルギーまで減速するためには（１衝突当たりのレサジーの平均増加量：$\xi = 0.0096$）、多数回の衝突を繰り返すことになる（例えば、１MeVの中性子が0.1eVになるまで：1680回）。また、鉛の中性子断面積は殆んどが散乱断面積（熱中性子で11.2ｂ）であり、中性子吸収断面積が小さいため（熱中性子で 0.17ｂ)、大きな鉛体系にパルス状の高速中性子が打ち込まれると、鉛によって中性子は殆んど吸収されることがなく、体系からの漏れも少ないため、中性子は体系内に長く留まって、その中性子束群は減速時間と１対１の対応関係を保ちながら、低エネルギーまで減速されていく。

鉛体系内に打ち込まれた高速中性子の時間的な振る舞いは、次のような時間依存減速方程式によって与えられる/4/：

$$\frac{dn(v,t)}{dt} = -v\Sigma_s n(v,t) + \frac{2v}{1-\alpha}\Sigma_s n(v',t)\frac{dv'}{v'} \qquad (1)$$

重核の均質媒質の内部では、弾性散乱によって減速して行く中性子の平均速さをｖとすると、中性子の減速時間ｔは、次のように導かれる/4/：

$$t = A\lambda \times \left(\frac{1}{v} - \frac{1}{v_0}\right) = \frac{A\lambda}{v} = \frac{A}{v\Sigma_s} \qquad (2)$$

ここで、v_0は中性子の初期速さ、Aは散乱媒質の質量数、λは散乱の平均自由行程、Σ_sは散乱断面積である。

$$E = \frac{1}{2}mv^2 = \frac{1}{2}m\left(\frac{A}{t\Sigma_s}\right)^2 = \frac{K}{t^2} \qquad (3)$$

となって、中性子の平均エネルギーE(keV)は、減速時間t(μs)の自乗に反比例することが分かる。Kは減速時間定数である。実際の測定においては、減速時間のゼロ時間補正項t_0が入るため、(3)式において一般的にはｔに代わって $t + t_0$が用いられる。エネルギー

分解能は中性子速度の広がり（分散）によって決まり、

$$\left(\frac{\triangle E}{E}\right)^2 = \frac{\langle E^2\rangle - \langle E\rangle^2}{\langle E^2\rangle} = \frac{8}{3A} \qquad (4)$$

で与えられる/4/。半値幅は標準偏差△E/Eの2.35倍であるから、鉛スペクトロメータにおける理想的な条件下でのエネルギー分解能（半値幅）は27%と導ける。

3．京都大学 鉛スペクトロメータ

3.1 京都大学鉛スペクトロメータ、ＫＵＬＳ

京都大学原子炉実験所に付設されている鉛スペクトロメータは、当初、東京大学工学部に設置され（昭和43年）、その後、同大学原子力総合研究センターに移管された「鉛減速時間スペクトロメータ(LESP)」/15/を、1991年（平成３年）になって京都大学原子炉実験所の方に譲り受けたもので、46MeV電子線型加速器(Linac)と組み合わせた京都大学鉛（減速）スペクトロメータ（ＫＵＬＳ）として実験に使用されることとなった/14/（**付録Ｅ**）。

本鉛スペクトロメータは、10x10x20 cm^3 の大きさを持つ高純度鉛(99.9%)ブロックを約1600個積み重ね、１辺が1.5mからなる立方体で総重量は約40トンである。図１に鉛スペクトロメータの断面図を示す。鉛ブロックを積み上げるとき、表面の酸化膜や油分、水分を除去するため、サンドペーパやワイヤブラシで１個ずつ丁寧に研磨し、エタノールで十分洗浄を行っている。

本鉛スペクトロメータKULSの設置に当たり、幾つかの工夫が加えられた/14/。

①京大原子炉実験所電子線型加速器(Linac)のターゲット室に鉛スペクトロメータを設置（図２）するとき、従来から進めてきた実験も支障なく行えるよう、ターゲット室の床面の補強工事を行い、鉛体系全体を頑丈な台車の上に乗せて移動できるようにした。

②LESPには、中心付近に貫通孔、その後方と上部にも実験孔があったが、図３に示すように、今回はさらに８ヶ所に角柱型（断面 10x10 cm^2）実験孔（奥行き50cm～60cm）を新設した。

③新設実験孔の内、１ヶ所はその周辺を厚さ10～15 cmのビスマス層で覆う構造とした。鉛からの中性子捕獲γ線は６～７MeVと高いのに比べ、ビスマスのそれは約４MeVと低い。核分裂率測定などの実験では、鉛から受ける中性子捕獲γ線により、実験試料に誘発核分裂（光核分裂）が起こることを避けるために低γ線量場としてビスマス実験孔を設けた。

④KULSのほぼ中央部に金属タンタルターゲットを置いて、パルス状高速中性子を発生させるが、Linacのドリフトチューブはスペクトロメータ入り口までとし、Linac側の真空系が実験系によって乱される恐れがないよう光中性子源用タンタルターゲットシステムから独

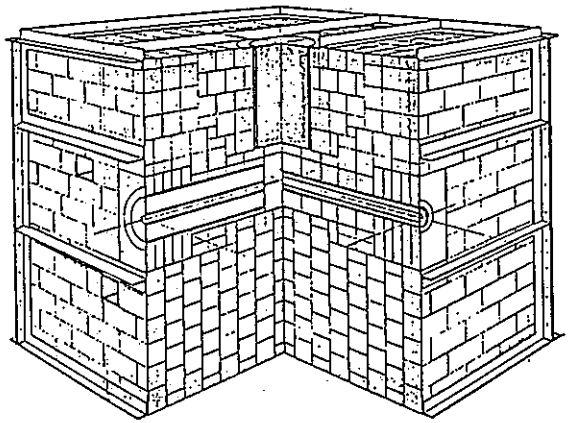

図１　鉛スペクトロメータKULSの断面図

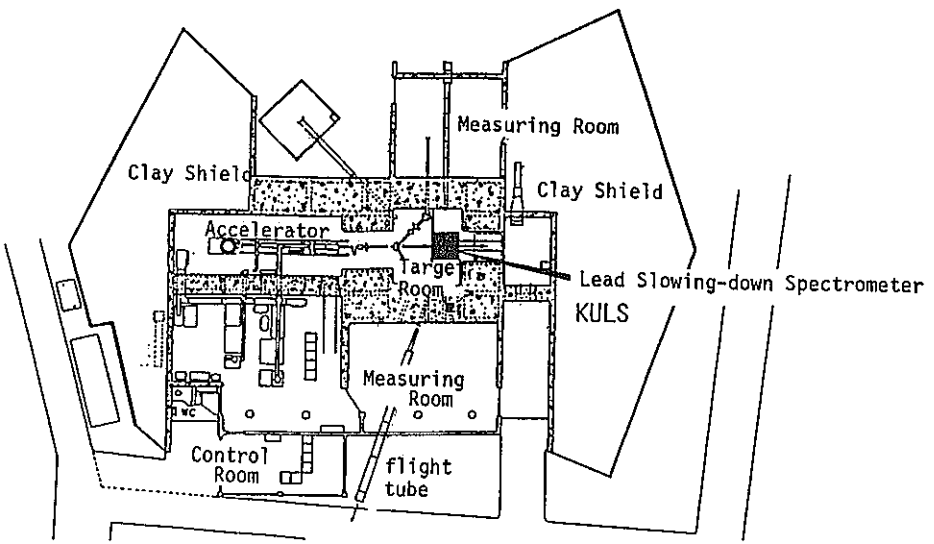

図２　電子線型加速器室と鉛スペクトロメータ
KULSの設置位置

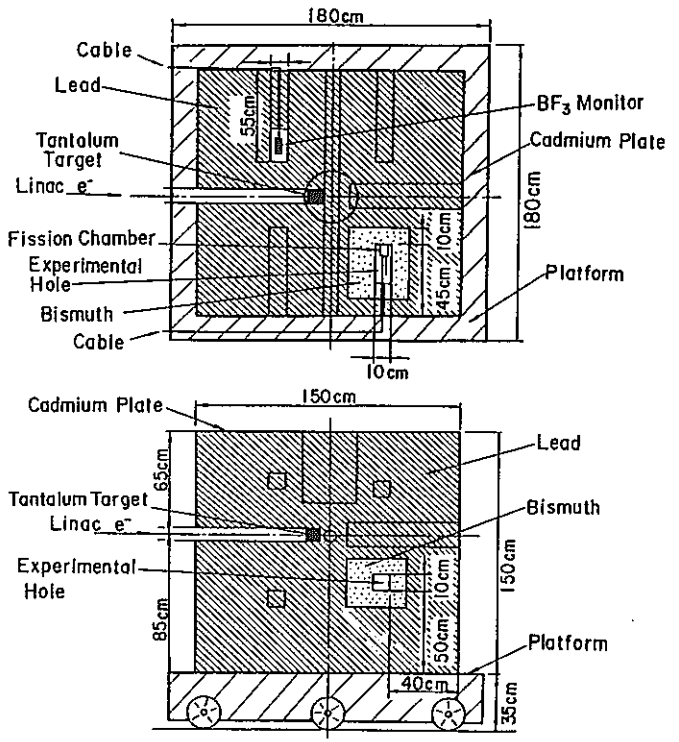

図３　鉛スペクトロメータKULSの
平面図（上）と垂直断面図（下）

立させている。

Linacの運転条件によっては、ターゲットに打ち込まれるパワーは500W前後にもなるが、圧縮空気を流す冷却方式によりターゲットケースの表面温度を200℃以下となるように抑えて実験を行うこととした。タンタルターゲットより得られる光中性子は、平均エネルギー約１MeV前後のものが多く、U-235の核分裂スペクトルを低エネルギー側に約１MeVシフトさせたような分布、広がりを持つスペクトル形状を示している/11,14/。

3.2　ＫＵＬＳ中の中性子輸送計算

京大原子炉実験所に付設された46MeV Linacからパルス状高速中性子が鉛スペクトロメータKULSに打ち込まれた後、鉛体系内で徐々に減速されていく中性子の時間的振舞いは、連続エネルギー減速モンテカルロコードMCNP/16/を用いた計算により求めた/14/。MCNPは中性子とγ線の輸送計算が行える計算コードとして知られているが、これに加えてパルス状中性子に対する固定中性子源問題では、中性子の時間的変化を10^{-8}秒間の間隔毎に追跡することが可能である。MCNPは鉛スペクトロメータ中での中性子の時間的な挙動を計算によって求めるコードとして適している。米国のRPIの研究グループにおいても、鉛スペクトロメータ中の中性子挙動（時間スペクトル、エネルギー分解能など）を求める計算に、本コードを使用している/17/。

本計算では、KULSを設置した台車を含めた３次元計算を行っている。さらに、KULS内部に設けたビスマス実験孔部についても考慮し、中性子源の位置、KULSを覆ったカドミウム板など、実際に即した計算配置を取っている。図４は、KULSのビスマス実験孔における時間依存スペクトルの計算結果で、Linacからパルス状中性子源打ち込み後、刻々と変化する減速時間に対応した時間スペクトルを示している。高速中性子のエネルギー領域では、入射中性子源スペクトルの広がりがそのまま広いエネルギー幅となっているが、やがてガウス分布に近い漸近形を保ちながら中性子が減速していく様子が分かる。本計算の結果、ビスマス実験孔における減速時間とエネルギーの関係（$E = K/t^2$）を示す定数Ｋとして、191 ± 3(keV･μs^2)が得られた。鉛の実験孔においても、ほぼ同様の時間依存スペクトルが観測され、Ｋとして 157 ± 4(keV･μs^2)が得られた。本MCNP計算による減速時間とエネルギーの関係をみると、ビスマス実験孔の方が鉛実験孔の場合に比べ中性子の減速が約18％程度遅いことが分かる。また、ガウス分布に近い漸近形を保つ中性子グループのエネルギースペクトル計算の結果から分解能（半値幅）を求めた。その結果、次節の表３にも見られるように、計算上にも些かばらつきが見られるものの、半値幅として30～40％前後の値を示した。

本KULSにおける中性子挙動・特性の１つとして、先にMCNPコードを用いて時間依存スペクトルを計算したが、これを時間積分すると定常中性子源としての中性子スペクトルが得られる。計算には、MCNPコード用にENDF/B-IVより作成された核データファイルを使用した

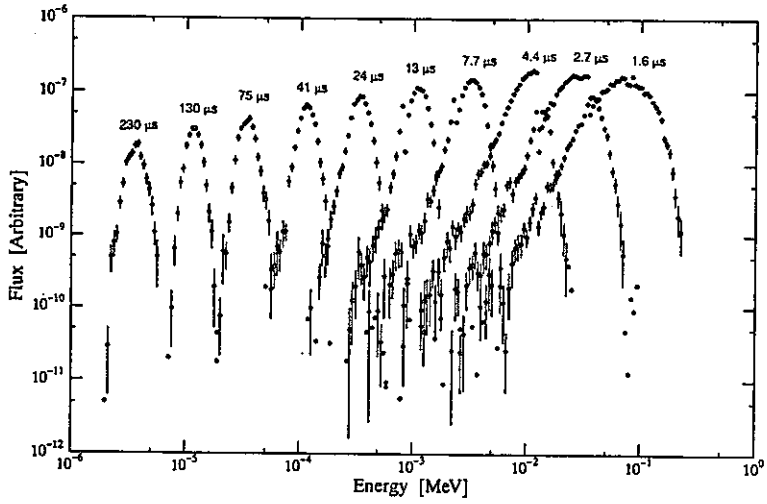

図４　KULSのビスマス実験孔における中性子の時間依存スペクトル

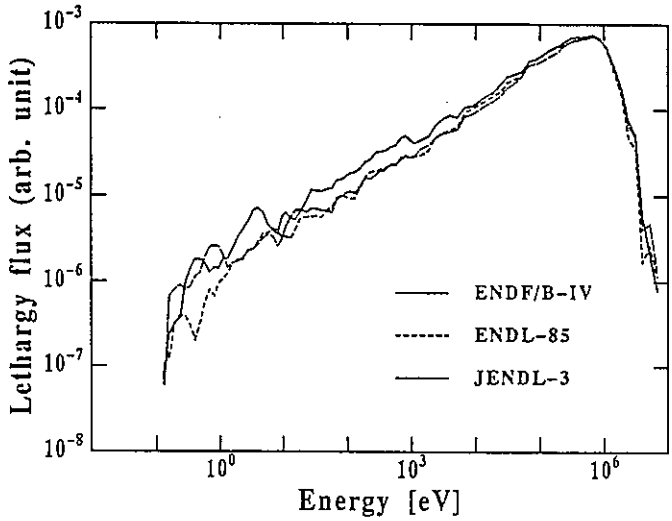

図５　KULS内の（定常）中性子スペクトルの計算結果

Material	Energy (eV)	Thickness (mm)	Form
In	1.46	0.2	foil
Te	2.33	7.0	powder
Ta	4.28	0.2	foil
Ta	10.4		
Au	4.91	0.05	cylinder
Ag	5.19	0.5	cylinder
Ag	16.3		
Cd	27.5	0.3	cylinder
Mo	44.9	7.0	powder
Co	132	0.3	cylinder
Cu	230	1.0	cylinder
Cu	579		
Mn	336	7.0	powder

表２　共鳴フィルターと共鳴エネルギー

が、他にJENDL-3、ENDL-85データファイルによる計算も比較のために実施した。これらの核データファイルによる計算結果を図５に示す。KULS内では、1/Eより硬い中性子スペクトルが得られ、熱中性子は少ないことが分かる。３つのデータファイルによる計算結果は全般的に一致しているが、10keV以下のエネルギー領域ではENDF/B-IVによる計算値が他のものより大き目となっている。

3.3 ＫＵＬＳの特性

3.3.1 中性子減速時間とエネルギーの関係

鉛スペクトロメータKULSのエネルギー較正は、表２に示した共鳴フィルターの透過中性子スペクトル測定及び共鳴中性子の捕獲γ線測定の方法によった/14/。まず、中性子透過率測定では、BF_3比例計数管（直径12mm、有効長50mm、内圧１気圧）を用意し、これを共鳴フィルターで巻き、減速時間の関数として中性子計数を行った。測定された時間スペクトルには、フィルターの共鳴エネルギーに対応した時間位置（即ちエネルギー点）に凹みが現れる。共鳴フィルターを交換して中性子の透過率測定を繰り返し、共鳴エネルギーと減速時間の関係を求めた。また、アルゴンガス比例計数管（直径0.5″、有効長2.5″、内圧１気圧：Ar:97%、CO_2:3%）を用いて共鳴フィルターから得られる中性子捕獲ガンマ線の測定を行ったが、その時間スペクトルには共鳴エネルギーに対応して凸みが現れる。これらの結果から共鳴エネルギーと減速時間の関係を求めた。図６は、BF_3比例計数管／アルゴンガス比例計数管と共鳴フィルターを用いて求めたビスマス及び鉛実験孔における中性子減速時間とエネルギーの関係の較正曲線を示す。これらの結果を最小自乗フィットすることにより減速時間定数Ｋを求めると、ビスマス及び鉛実験孔のそれぞれについて 190±2 および 156±2(k eV･μs^2)が得られ、BF_3比例計数管による測定結果 191±3(keV･μs^2)ともよい一致を示した。これらの測定値は、先のMCNPコードによる計算から求めた定数（191±3(keV･μs^2))ともよい一致を示している。また、鉛実験孔における定数は、以前に東京大学のLEPS時代に測定された値 155 (keV･μs^2)/15/ともよい一致を示した。

3.3.2 ＫＵＬＳのエネルギー分解能

鉛スペクトロメータKULSにとって、エネルギー分解能も重要な特性の１つである。エネルギー分解能の測定には、次の条件を備えた物質（フィルター）の使用が望まれる：①共鳴ピークが大きく、その幅が狭いこと、②共鳴エネルギーが既知で、隣の共鳴ピークから十分離れていること、③共鳴物質（フィルター）の厚さが薄いこと、などである。

本研究におけるエネルギー分解能測定も、先の表２に示したように、大きくて鋭いピークを持つ共鳴フィルターを使い、BF_3比例計数管を用いた中性子透過率測定法と、アルゴンガス比例計数管による共鳴捕獲γ線測定の方法によった/14/。まず、BF_3比例計数管では、中性子透過率測定において求めた時間スペクトルを凹型のガウス分布関数にフィット

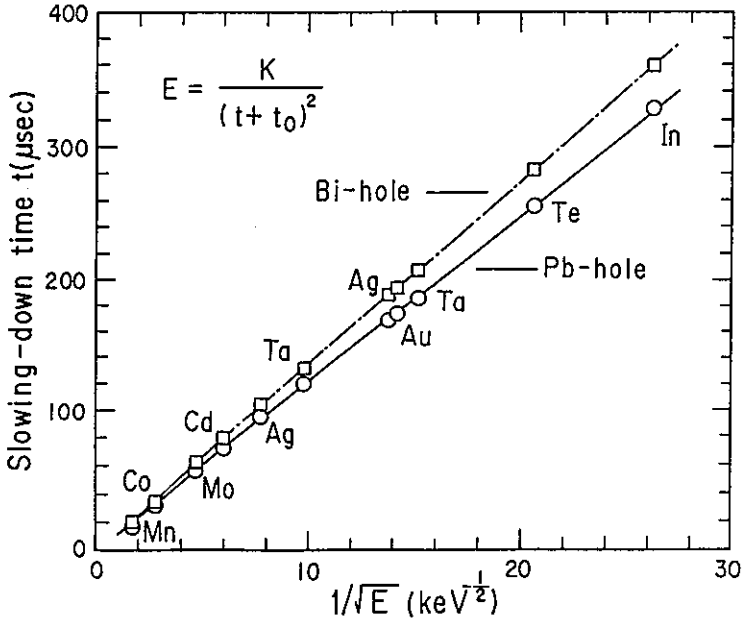

図６　KULSのビスマス実験孔と鉛実験孔における
中性子減速時間とエネルギーの関係

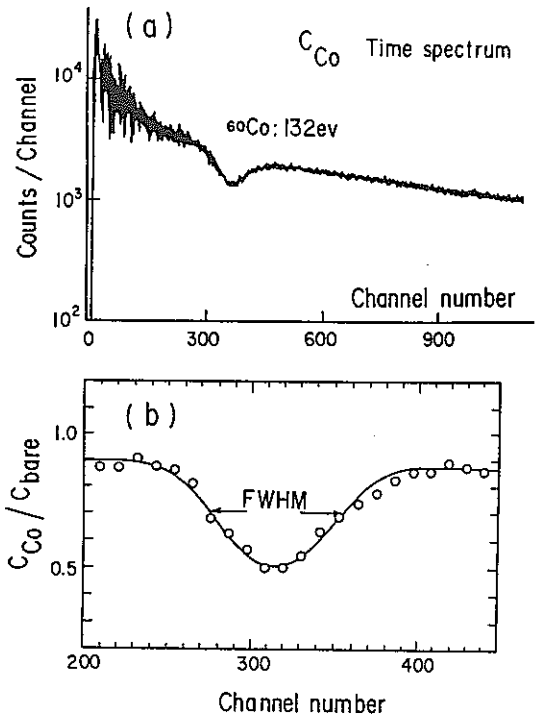

図７　中性子透過法によって測定された
時間スペクトルの例

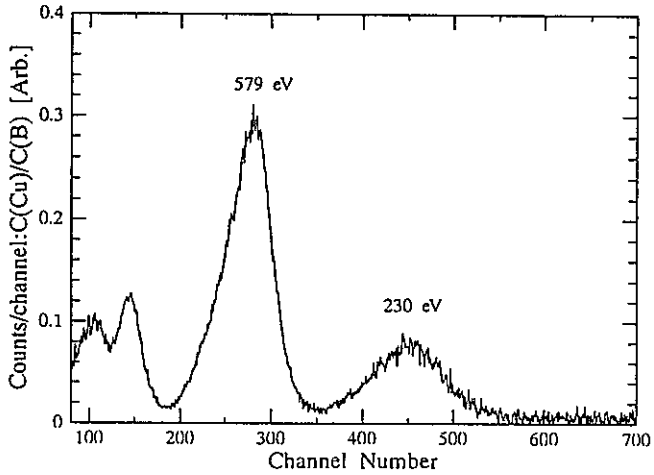

図８　共鳴捕獲γ線測定によるエネルギー
分解能測定の例

表３　ビスマス及び鉛実験孔におけるエネルギー分解能

Measurements				Calculations		
Energy	BF3 counter	Ar gas counter		Energy	MCNP code	
(eV)	Bi hole	Bi hole	Pb hole	(eV)	Bi hole	Pb hole
1.46	51±3			3.02		35.7
4.9	40±2			3.56	37.4	
10.4	38±1			10.0		28.5
27.5		38±2	37±2	11.6	31.6	
44.9	38±1			29.8		28.2
132	39±2			33.8	35.7	
230		38±3	40±3	99.1		29.8
336	40±3			113	34.5	
579		42±3	42±4	298		33.7
2370	53±3			339	38.3	
				990		38.1
				1091	43.2	
				2988		50.3
				3208	51.8	

して求め、その半値幅からKULSのエネルギー分解能を算出した。中性子透過率の時間スペクトル測定の例を図７に示す。アルゴンガス比例計数管を用いたエネルギー分解能測定では、BF_3比例計数管の測定に用いた大きな共鳴を持つフィルターより、むしろカドミウムや銅試料に見られるδ関数状の極めて狭く鋭い共鳴ピークに注目した。図８は、銅フィルターによる579eVと230eVの共鳴捕獲ピークについて測定した時間スペクトルの例である。KULSの持つエネルギー分解能の広がりを考えると、δ関数状の鋭い共鳴ピークを中性子透過率法によって測定することは困難である。また、透過率測定法では使用したフィルターの共鳴断面積にもある程度の幅があるため、これらに対する補正を必要とする場合がある。しかし、共鳴捕獲γ線測定法では鋭い共鳴ピークの場合でも測定が可能であり、むしろ共鳴ピーク幅を考慮せずに分解能測定が行える長所がある。KULSのビスマス及び鉛実験孔において、我々が求めたエネルギー分解能測定の結果を表３にまとめた。数eVから数keV付近までの実測値は約40%となり、これより高いエネルギー側、低いエネルギー側では、分解能が共に大きくなっている。表３には、MCNPコードによる計算結果も示されているが、実験誤差の範囲内とは言え、計算によるエネルギー分解能は実測値に比べ少し小さ目の値を示している。こうした要因及びKULSのエネルギー分解能が理論的な予測値（27%）よりかなり大きい値を示した点に関しては、(1)鉛スペクトロメータの寸法、(2)鉛ブロック中の不純物、(3)中性子源スペクトルの形状、鉛の非弾性散乱に関わる影響についてMCNPコードによる計算を行い、KULSの諸特性について検討を行った。その結果、KULSの分解能が理論値より大きくなった原因は、これらの要因が重なり合って生じたものと考えられる。この問題の詳細は、別報/14/（付録Ｅ）に譲る。

U-235やNp-237に関するENDF/B-VI、JENDL-3.2等の評価データによると、いわゆる共鳴領域（ eVオーダから200～300eV）においてはエネルギー幅が極めて狭く、鋭いピークを示す多数の共鳴が存在している。KULSによる実験では、第１章の図２２に見られるように、エネルギー分解能が～40%またはそれ以上にも及ぶため、後述の実験値と評価値の比較においては、ガウス分布型の分解能関数を使って評価データのなまし(broadening)を行っている。図９、図１０は、それぞれの評価データに対し、KULSの分解能でなます操作を行う前とその後のデータの例を示している。

3.3.3　ＫＵＬＳ内の中性子スペクトル

本研究では、KULSの特性実験の一環として、22m飛行路を用いた中性子飛行時間分析法により、鉛スペクトロメータ中の中性子スペクトルを測定した/14/。KULSのほぼ中央部にセットされたタンタルターゲット製の光中性子源の後方約15cmの位置に、直径８cmの貫通孔が設けられている（図３）。その中央部まで飛行路側の鉛プラグを抜き取り、設けられた実験孔（リエントラント ホール）の底部から、ターゲット位置に対し90度方向に取り出された中性子を測定した。本実験には、我々が従来より使用してきている^{6}Liガラスシンチレータ及び^{10}B-vaseline plug NaI(Tl)検出器/18/を用いた。図１１、図１２は、それぞ

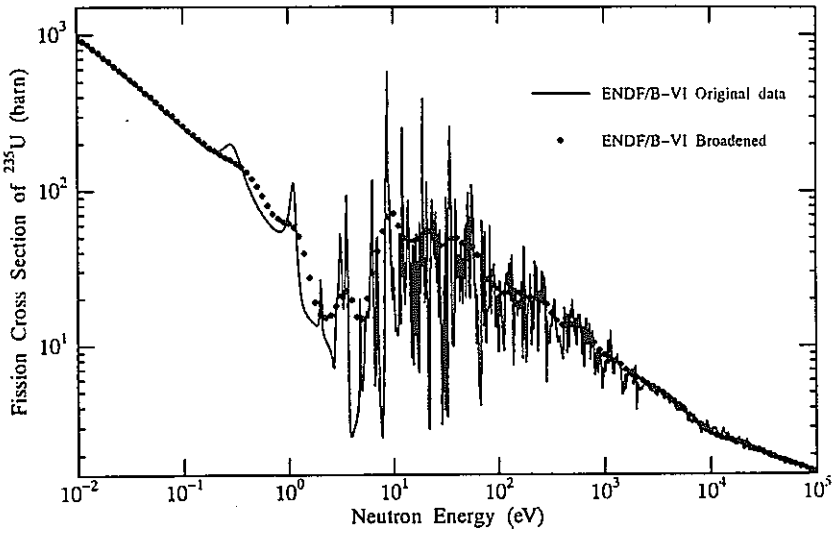

図９　^{235}U(n, f)反応のENDF/B-VI評価値と、
KULSの分解能関数でなました結果

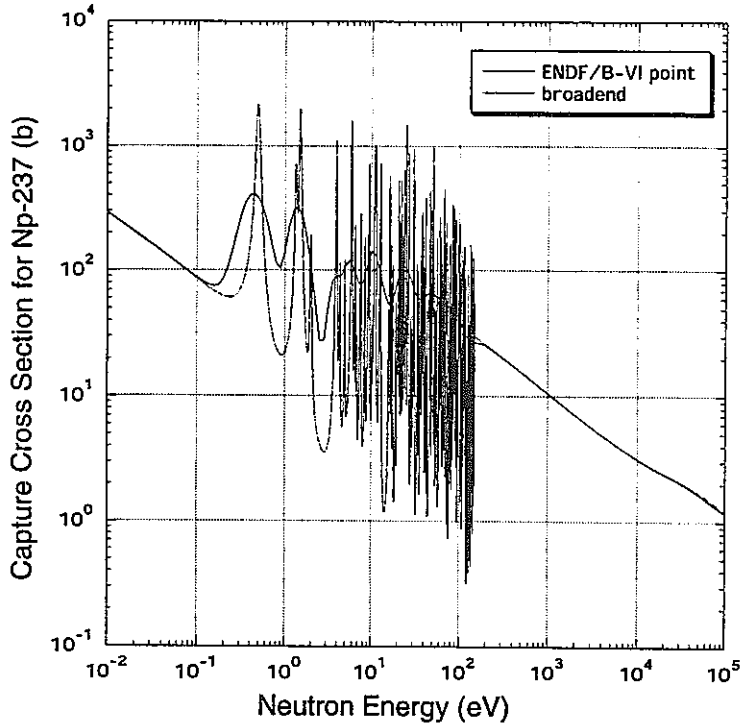

図１０　^{237}Np(n, γ)反応のENDF/B-VI評価値と、
KULSの分解能関数でなました結果

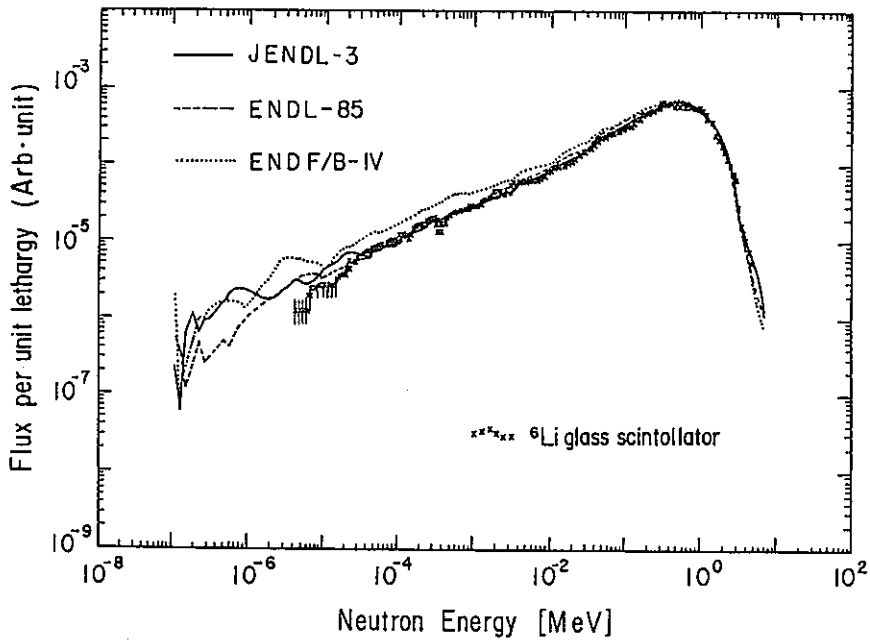

図１１　^{6}Liガラスシンチレータを用いて飛行時間分析法により測定した鉛スペクトロメータ内の中性子スペクトルとMCNPコードによる計算値の比較

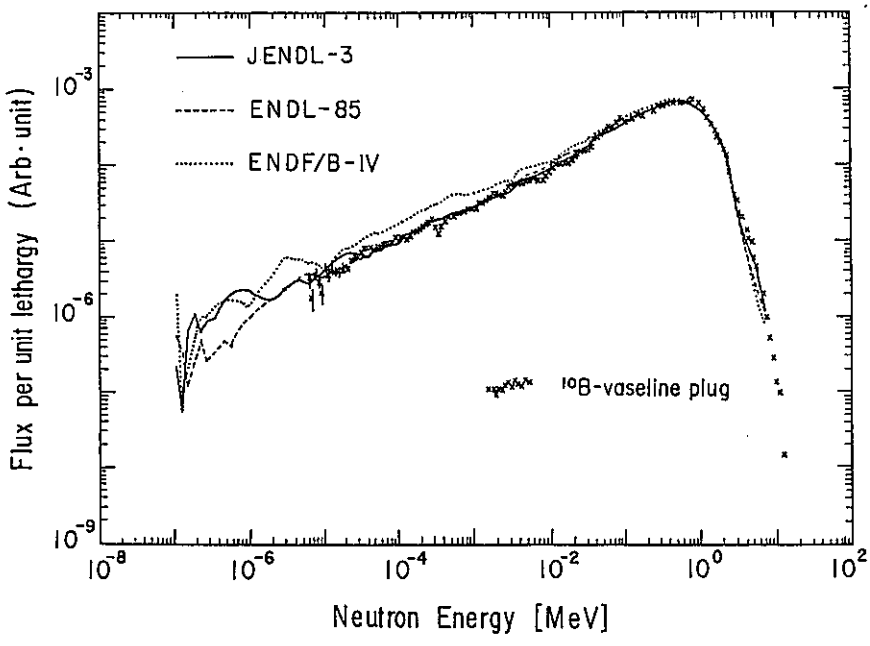

図１２　^{10}B-vaseline plug NaI(Tl)シンチレータを用いて飛行時間分析法により測定した鉛スペクトロメータ内の中性子スペクトルとMCNPコードによる計算値の比較

れの検出器を用いて測定したKULS中の中性子スペクトルを示す。また、これらの図では、ENDF/B-IV、JENDL-3、ENDL-85ファイルから作成された断面積セットを用いて計算した結果とそれぞれの実験値を比較している。計算値は実験値と全般的によい一致を示しているが、10keV近辺より下のエネルギー領域では、ENDF/B-IVによる計算値が他の定数による計算及び実験結果より高目になっていることが分かる。このことはENDF/B-IVの鉛の評価データについて再評価の必要性を示唆している。また、KULS内では低エネルギー、特に熱中性子は殆んど存在していないことが分かる。図１１、図１２を見ると、KULS内の中性子場は大型の高速炉における炉心スペクトルの形状に近くなっていることが分かる/19/。KULSでは、準標準的な中速中性子スペクトルの場が得られるとして、今後の利用が期待できよう。

3.4. まとめ

Linacをパルス状中性子源とした鉛スペクトロメータKULSについて、実験と計算によりその特性を明らかにした。本研究で得られた結果をまとめると、

(1)BF_3比例計数管による共鳴フィルターの中性子透過率測定とアルゴンガス比例計数管による共鳴フィルターの捕獲ガンマ線測定の結果から、中性子の減速時間とエネルギーの関係（$E = K / t^2$）を特徴づける減速定数Kを求めた。その結果、ビスマス実験孔で190±2(keV･μs^2)、鉛実験孔で156±2(keV･μs^2)を得た。

(2)同様の方法で、KULSのエネルギー分解能を実験的に求めた結果、数eVから数keVにおいて約40%（半値幅）、それ以上または以下ではこれを上回るU字型の分解能曲線を示した。

(3) MCNPコードを用いたモンテカルロ計算の結果、減速定数Kに関して実験値とよい一致を示したが、エネルギー分解能に関しては計算値が実験値より小さめ（30～40%）になった。その原因の１つは、鉛スペクトロメータ中の不純物の影響やKULSの持つ固有の特性（体系の大きさ、パルス中性子源のスペクトル、鉛の非弾性散乱）等が影響しているとも考えられる。

(4)KULS内の中性子スペクトルを計算により求めた結果と実験値を比較したところ、10keV以下でENDF/B-VIの評価済データによる結果は実験値より高目となったが、全般に計算／実験の両者はよい一致を示した。また、低エネルギー側の中 性子束は低く、高速炉・中速炉型のスペクトル形状を示すことが分かった。

(5)KULSを用いた実験として、既にNp-237、Am-241,242m,243の核分裂断面積が～0.1eVから10keV領域において測定されている。その結果を見ても、KULSはこうした核断面積測定を可能にする条件「１μｇｂ」を十分満たしていることが分かった。今後も強力中性子源としてのKULSの特徴を生かし、ＭＡ、ＦＰの核データ測定への応用が期待される。

【参考文献】

/1/ A. A. Bergman, et al.: Proc. 1st Int. Conf. on Peaceful Uses At. Energy, United Nations, 4, 135 (1955).

/2/ R. E. Slovacek, et al.: Nucl. Sci. Eng., 62, 455 (1977).

/3/ V. F. Gerasimov et al., Proc. of V-th Int'l Seminar on Interaction of Neutrons with Nuclei, NEUTRON SPECTROSCOPY, nUCLEAR STRUCTURE, RELATED TOPICS, ISINN-5, Dubna, p.348 and p.361 (1997).

/4/ K. H. Beckurts & K. Wirtz: "Neutron Physics", Springer-Verlag, New York, p. 167 (1964).

/5/ Y. Nakagome, et al.: Phys. Rev., C43, 1824 (1991).

/6/ H. T. Maguire,Jr. et al.: Nucl. Sci. Eng., 89, 293 (1985).

/7/ B. Alam, et al.: Nucl. Sci. Eng., 99, 267 (1988).

/8/ Y. Danon, et al., Nucl. Sci. Eng., 109, 341 (1991).

/9/ E. C. Vanterpool, et al.: Nucl. Sci. Eng., 110, 186 (1992).

/10/ N. M. Abdurrahman, et al.: Nucl. Sci. Eng., 115, 279 (1993).

/11/ K. Kobayashi, et al., Annu. Rep. Res. Reactor Inst. Kyoto Univ., Vol.22, p. 142 (1989).

/12/ K. Kobayashi and Y. Fujita, Annu. Rep. Res. Reactor Inst. Kyoto Univ., Vol. 26, p.92 (1993).

/13/ K. Kobayashi, et al., Annu. Rep. Res. Reactor Inst. Kyoto Univ., Vol.20, p. 1 (1987).

/14/ K. Kobayshi, et al., Nucl. Instr. Methods in Nucl. Phys. Res. A, 385, 145-156 (1997).

/15/ H. Wakabayashi, et al.: J. Nucl. Sci. Technol., 6, 487 (1970).

/16/ 例えば、"MCNP - A General Monte Carlo Code for Neutron and Photon Transport, Version 3A", LA-7396-M, Rev.2, Los Alamos National Laboratory (1986).

/17/ R. C. Little, et al.: Trans. Am. Nucl. Soc., 43, 119 (1982).

/18/ I. Kimura, et al., Nucl. Instr. Meth., 137, 85 (1976).

/19/ A. E. Walter and A. B. Reynolds, "Fast Breeder Reactors", p.710, Pergamon, New York (1981).

付　録

付録A

Journal of NUCLEAR SCIENCE and TECHNOLOGY, 30[9], pp. 863~869 (September 1993).

Measurement of Fission Cross Section of Neptunium-237 in Resonance Region with Electron Linac—Driven Lead Spectrometer

Akihiro YAMANAKA†, Itsuro KIMURA, Satoshi KANAZAWA,

*Department of Nuclear Engineering, Kyoto University**

Katsuhei KOBAYASHI, Shuji YAMAMOTO, Yoshihiro NAKAGOME, Yoshiaki FUJITA and Tadaharu TAMAI††

*Research Reactor Institute, Kyoto University***

Received December 14, 1992

Making use of a lead neutron slowing-down spectrometer combined with an electron linear accelerator and back-to-back type double fission chambers, we measured the fission cross section of ^{237}Np relative to that of ^{235}U from about 1 eV to about 5 keV with energy resolution ($\Delta E/E$) of about 40%. The experimentally obtained result has been compared with two newly evaluated data files, JENDL-3 and ENDF/B-VI, and with previously measured values by Plattard *et al.* and by Hoffman *et al.* Although the shape of the present energy dependent cross section agrees with that of ENDF/B-VI, that of JENDL-3 below 120 eV and that of Plattard *et al.*, the absolute values of above three are from 3 to 4 times smaller than those of the present data. However the Hoffman *et al.*'s data are rather closer to the present data.

KEYWORDS: ***fission cross sections, neptunium 237, subthreshold fission, fission ratio, uranium 235, lead slowing-down spectrometer, KULS, double fission chambers, transmutation, ENDF/B-VI, JENDL-3, energy resolution, energy dependence, comparative evaluations***

I. INTRODUCTION

Recently, several methods for the transmutation or the incineration of long-lived fission products and transuranium actinides have been proposed and studied. For the evaluation of the feasibility of those methods, basic data especially precise nuclear data are required.

Among several transuranium actinides produced by power reactors, neptunium-237 (^{237}Np) is thought to be one of the most burdensome ones, because of its large production rate in a reactor, very long half-life (2.14×10^6 yr) and α activities in its decay chain. In order to transmute ^{237}Np to nuclides with much shorter half-lives, it is proposed to use the ^{237}Np(n, f) and ^{237}Np$(n, \gamma)^{238}$Np reactions.

The cross section for the ^{237}Np(n, f) reaction increases above its threshold energy, and the precision of its cross section data in the MeV region is practically sufficient enough to evaluate the transmutation of ^{237}Np. Below the threshold energy of this reaction, Fubini *et al.*[1] found an intermediate structure from which the double humped barrier for the subthreshold fission of ^{237}Np was demonstrated. Several groups have measured this cross section below the threshold so far[2]~[6]. Jiacoletti

* *Yoshidahonmachi, Sakyo-ku, Kyoto 606-01.*

** *Kumatori-cho, Osaka-fu 590-04.*

† Present address: Nucl. Power Plant Eng. Dept., Hitachi Works, Hitachi Ltd., *Saiwai-cho, Hitachi-shi 317.*

†† Deceased in August, 1992.

et al. and Hoffman *et al.* measured it by the neutrons from the Physics 8[3][4] and Plattard *et al.* did with an electron linear accelerator[5]. However the absolute value of the data by the former two is about 3 times larger than that by the latter. In two newly evaluated data files, JENDL-3[7] and ENDF/B-VI[8], the data are close to those of Plattard *et al.* High resolution measurement of this cross section was carried out by Auchampaugh *et al.*[6], who mentioned that the experimental data of Plattard *et al.* were too low by a factor of 3. Therefore it has been strongly requested to check these data for the evaluation of the transmutation system by the ^{237}Np(n, f) reaction.

For the purpose of precise evaluation of nuclear data such as the fission cross section of ^{237}Np, required are ; (1) a neutron source with clearly known spectrum and with sufficient intensity, and (2) a detector with systematic errors as low as possible. In this work we utilized a lead neutron slowing-down spectrometer with an electron linear accelerator as an intense neutron source. The lead spectrometer affords more than 1,000 times higher neutron flux than an ordinary neutron time-of-flight system, although the energy resolution of the former is inferior to that of the latter. The lead spectrometer is not applicable to obtain individual resonance parameters but suitable to measure the absolute value of cross sections with very small amount sample mass. Before carrying out the fission cross section measurement, we obtained the neutron characteristics of the lead spectrometer very carefully. A special experimental hole covered by a bismuth layer was used to eliminate photofissions. For a detector with low systematic error, we adopted to use back-to-back type double fission chambers with a sample deposit of ^{237}Np and a reference one of ^{235}U and to measure the cross section for the ^{237}Np(n, f) reaction relative to that for the ^{235}U(n, f) reaction of which cross section can be thought to be quite precise.

II. Experimental Method

1. Lead Slowing-down Spectrometer

After pulsed fast neutrons are generated at the center in a sufficiently large lead pile, neutrons are initially slowed down by the $(n, 2n)$ reaction, inelastic scattering or elastic scattering. Below the threshold energies of the former two reactions, only the elastic scattering predominates the slowing-down process. Since the elastic scattering cross section for lead is nearly constant in the intermediate and epithermal regions, its absorption cross section is quite small and the mean logarithmic energy loss per an elastic scattering in lead is quite small as 0.0096, neutrons slow down continuously with asymptotically constant energy resolution $\Delta E/E$ and the slowing-down time t is simply related to energy E as below :

$$E=\frac{K}{(t+t_0)^2} .$$

Therefore we can use it as a neutron spectrometer[9]. Several groups have made lead spectrometers with a conventional pulsed neutron source[10]~[13] and have used them for capture cross section measurement and so forth. Slovacek *et al.* utilized an electron linear accelerator as a more intense pulsed neutron source for a lead neutron spectrometer[14], with which they succeeded in measuring very small cross sections such as the subthreshold fission of ^{238}U.

In this work, we took over a lead spectrometer of the University of Tokyo, named LESP[11], and reconstructed it beside an electron linear accelerator of Research Reactor Institute, Kyoto University (KURRI). This resuscitated lead spectrometer, abbreviated as KULS, was made by cleaning, polishing and reassembling lead blocks with the purity of 99.9%, covered by Cd sheet 0.5 mm thick and put on a movable steel table. The size and the weight of this lead spectrometer are 1.5 m cubic and about 38 t, respectively. An air cooled photoneutron source which consists of 12 Ta discs is placed at its center. We made 11 experimental holes, which were filled with lead blocks unless one was used for an experiment.

One of these holes was covered with a Bi layer about 10 to 15 cm thick to suppress high enegy γ-rays from the neutron capture of Pb[15]. The cross-sectional view of KULS is shown in **Fig. 1**.

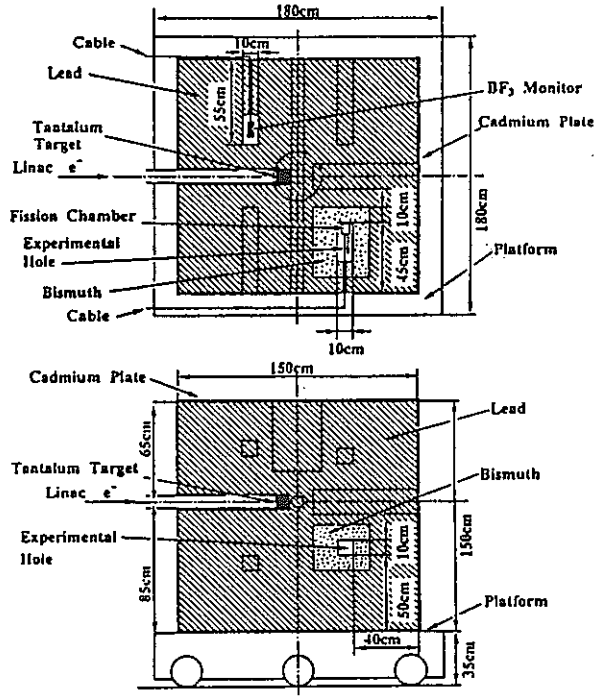

Fig. 1 Cross sectional view of Kyoto University Lead Spectrometer, KULS

The slowing-down characteristics of this lead spectrometer KULS were obtained with a BF_3 counter and an argon filled proportional counter with and without resonance filters (In, Ta, Au, Ag, Mo, Co or Mn). The measured slowing-down time behavior is depicted in **Fig. 2**. The energy resolution at 27.5 eV shows 39±1%. The details of the characterization of KULS were given elsewhere[16]. Since the size of KULS is smaller than most of other lead spectrometers, we could measure the fission cross section for the $^{237}Np(n, f)$ reaction about 1 eV. Upper limit of the neutron energy is thought to be about 5 keV.

2. Fission Chambers

The fission chambers employed in this work have two identical parallel plate type ionization chambers as shown in **Fig. 3**[17]. These chambers were originally designed for the incore fission ratio measurement in FCA of Japan Atomic Energy Research Institute. Since

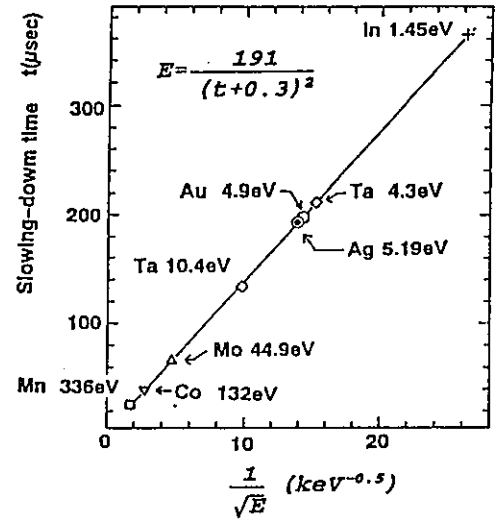

Solid line was obtained by the least square fitting (K=191 and t_0=0.3)

Fig. 2 Relation between slowing-down time and energy of neutrons in Bi covered hole of KULS

the back sides of a sample deposit on a stainless steel plate and a reference one are faced each other, it is called back-to-back type. The chambers were made of Al and filled with a mixed gas of 97%Ar and 3%N_2 at the pressure of 1 atm. The distance between the two electrodes was 8 mm. The operation voltage was 400 V.

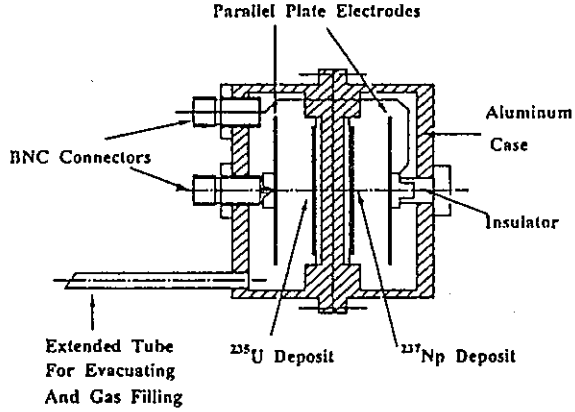

Fig. 3 Cross-sectional view of back-to-back type fission chambers

Neptunium oxide (NpO_2) of about 2 mg with high purity imported from Harwell Establishment of UKAEA was dissolved in hydrochloric acid of 0.2 N and 0.1 ml of this solution was mixed into 2-propanol of 5 ml. Therewith we electrodeposited NpO_2 on a stainless steel plate

28 mm in diameter and 0.2 mm thick. The applied voltage and the electric current were about 200 V and 2 mA, respectively. Electrodeposition was performed for 1 h. The diameter of the deposit was 2 cm. Highly enriched (99.91%) uranium oxide (UO_2) which we had purchased from Oak Ridge National Laboratory, USA was similarly electrodeposited on the stainless steel plate. After the electrodeposition, each plate was sintered with a gas burner, and the reference deposit became U_3O_8.

The number of atoms in the sample deposit and that in the reference one together with those of impurities were determined by the α-ray spectrometry with a Si surface barrier detector in vacuum. The numbers of ^{237}Np in the sample deposit and that of ^{235}U in the reference one are $(1.99\pm0.02)\times10^{17}$ and $(4.12\pm0.09)\times10^{17}$, respectively. In this determination, (1) statistical error, (2) uncertainties in the decay data, and (3) uncertainty introduced by background subtraction, 1% for ^{237}Np and 2% for ^{235}U, were taken into account. The thicknesses of the NpO_2 and U_3O_8 deposits are about 25 and 50 $\mu g/cm^2$, respectively.

In the sample deposit, we found small amounts of ^{238}Pu and ^{239}Pu, and their contents were 0.320 ± 0.003 and 1.10 ± 0.13 ppm, respectively. The α-rays from ^{234}U was counted for the reference deposit, and the content of ^{234}U became 464 ± 5 ppm.

3. Electronic Circuits

Two identical electronic circuits were prepared for both sample and reference chambers. As seen in **Fig. 4** the start signal for timing was taken from the electron linear accelerator. The channel number and time width of each time analyzer were 4,096 and 125 ns, respectively. Since we used quite thin sample and reference deposits, fission pulses were clearly discriminated from background pulses caused by α-rays.

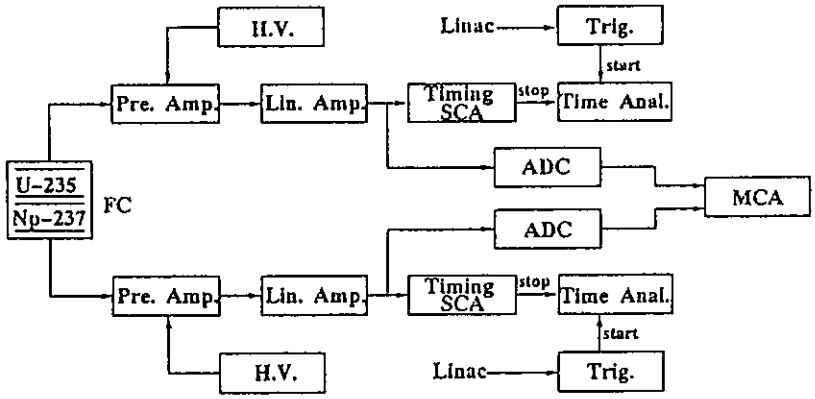

Fig. 4 Block diagram of electronic circuits to measure time dependent fission counts from double fission chambers

4. Fission Rate Measurement

Measurement of the fission ratio of ^{237}Np to ^{235}U was carried out in the Bi-covered experimental hole of KULS. The main reason to use this hole is to suppress the photofission of ^{237}Np and ^{235}U. The electron linear accelerator was operated by the following conditions: pulse repetition=180 pps, pulse width=33 ns, peak electron current=2A, accelerating energy =32 MeV, average neutron yield=10^{11} n/s and total operation time=50 h.

Background run was carried out by making use of the fission chambers without sample and reference deposits, and few background counts were observed.

III. Results and Discussion

From the fission counts of the sample and the reference, the cross section for the ^{237}Np (n, f) reaction is obtained by

$$\sigma_{Np}(E)=\frac{C_{Np}}{C_U}\cdot\frac{N_U}{N_{Np}}\sigma_U(E),$$

where C_{Np}: Fission counts of ^{237}Np
C_U: Fission counts of ^{235}U
N_U: Number of ^{235}U atoms in reference deposit

N_{Np}: Number of ^{237}Np atoms in sample deposit
$\sigma_U(E)$: Energy dependent fission cross section of ^{235}U.

We cited the numerical values of $\sigma_U(E)$ from ENDF/B-VI.

As it was described that the contents of ^{238}Pu and ^{239}Pu in the sample deposit were 0.32 and 1.10 ppm, respectively, the contribution of their fission counts to σ_{Np} was about 0.05%, and was neglected. The contribution of ^{234}U to σ_U is also estimated to be 0.01%.

Since we utilized the experimental hole covered by Bi, the highest energy of the capture γ-rays is about 4.6 MeV which is much smaller than that of Pb, 6.7 MeV. The photofission cross sections for ^{237}Np is in the order of 100 μb at 4.6 MeV and the shapes of both photofission cross sections for ^{237}Np and for ^{235}U are similar in their rise-up region. Therefore we can neglect the contribution of the photofission counts to σ_{Np}.

Grundl *et al.*[18] obtained the mean range of fission fragments in UO_2 to be 8.29 mg/cm^2. By using this value, Obu[17] showed the losses of fission fragments in the UO_2 layers 10, 20

Table 1 Obtained cross section data for $^{237}Np(n,f)$ reaction

Energy (eV)	Cross section (mb)	Error (mb)	Energy (eV)	Cross section (mb)	Error (mb)
1.05	35.6	5.3	73.7	61.9	3.9
1.17	35.0	5.1	82.7	68.1	4.2
1.32	32.6	4.4	92.7	88.3	5.1
1.48	21.0	3.1	104	98.7	5.6
1.66	15.5	2.4	117	95.6	5.4
1.86	10.6	1.9	131	91.3	5.2
2.08	13.1	2.2	147	114	6.2
2.34	10.0	2.2	165	148	7.7
2.62	11.7	2.3	185	152	7.9
2.94	13.7	2.5	207	134	7.1
3.30	19.6	3.0	233	112	6.0
3.70	19.3	2.9	261	97.9	5.3
4.16	25.0	3.3	293	88.7	4.9
4.66	38.2	4.7	329	77.4	3.9
5.23	50.7	5.7	369	64.0	3.3
5.87	51.8	5.7	413	54.5	2.9
6.58	48.4	5.5	464	51.4	2.9
7.39	45.3	5.0	520	49.9	2.9
8.29	36.0	4.1	584	51.8	3.1
9.30	31.2	3.5	655	48.1	3.0
10.4	25.8	3.1	735	55.3	3.5
11.7	24.0	2.9	824	55.9	3.6
13.1	22.2	2.8	925	52.5	3.6
14.7	20.0	2.4	1,040	53.7	3.8
16.5	24.7	2.6	1,160	44.0	3.1
18.5	44.5	3.8	1,310	39.8	2.8
20.8	87.0	5.9	1,470	38.4	2.6
23.3	159.4	9.1	1,640	31.4	2.1
26.2	270	14	1,840	37.6	2.5
29.4	432	21	2,070	39.2	2.6
32.9	618	30	2,320	31.4	2.1
37.0	680	33	2,600	34.0	2.2
41.5	530	26	2,920	32.4	2.1
46.5	326	17	3,280	29.7	1.9
52.2	196	11	3,680	27.7	1.7
58.5	116.7	6.7	4,120	32.6	2.0
65.7	80.0	4.9	4,630	37.9	2.3

and 50 $\mu g/cm^2$ thick. The loss of fission fragments in the both deposits was calculated by interpolating the above data, and was found to be negligible.

Angular distribution of fission fragments against the direction of an incident neutron beam shows an anisotropy for fast neutrons, but those for the neutrons in resonance region can be thought to be isotropic. Therefore we did not correct the data for the effect by the anisotropy of fission fragments. We compared the fission ratios of ^{237}Np and ^{235}U for two configurations; one case for which the sample deposit was placed at the inner position in the experimental hole and the other the oposite. The result shows little difference between them.

Loss of the fission counts for ^{237}Np and ^{235}U below the pulse height discrimination levels was determined by linearly extrapolating the fission count peaks.

After the above corrections, we obtained the result of the cross section for the ^{237}Np (n, f) reaction as **Table 1**, in which (1) the statistical error for the fission, (2) the error in the determination of the numbers of ^{237}Np and ^{235}U, (3) 2% as systematic error, and (4) the uncertainty in the fission cross sections for ^{235}U were taken into account.

In **Fig. 5**, the present result is compared with the evaluated values in JENDL-3 and in ENDF/B-VI. Since the energy resolution of the original data in both evaluated data files is much higher than that of the present experiment, we processed the evaluated data values by multiplying a resolution function of which energy resolution function is assumed to be a Gaussian with 40% of its full width at half maximum. In this figure, shown are the processed values of both files.

From this figure, it can be seen that (1) the evaluated values in both JENDL-3 and ENDF/B-VI are about 3 times smaller than the present result, (2) the gross shape of the present result is very similar to that of ENDF/B-VI in all range and to that of JENDL-3 below 120 eV, and (3) above 120 eV, the cross section in JENDL-3 is flat and differs from the present result.

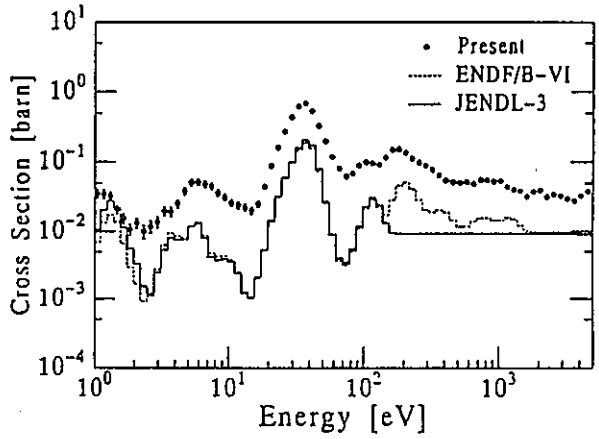

Fig. 5 Expermentally obtained cross section of $^{237}Np(n,f)$ reaction compared with those in evaluated data files

The present result is compared with earlier experimental data and is shown in **Fig. 6.** The original point wise data have been also processed as the same manner as the above. The data obtained by Hoffman *et al.*[4] are close to the present ones, but those measured Plattard *et al.*[6] are much smaller than the present ones. Too low normalization of Plattard *et al.*'s data was pointed out by Auchampaugh *et al.*, which is supported by the present result.

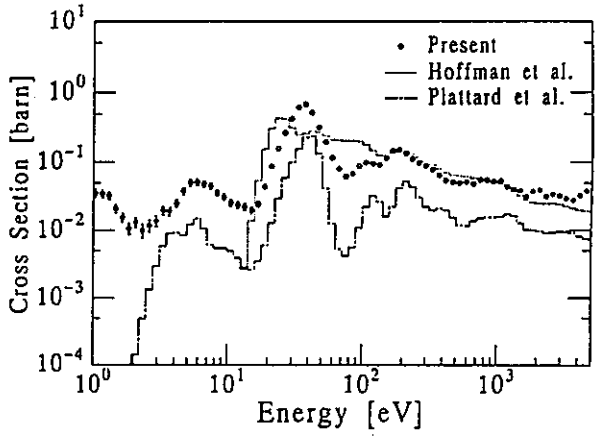

Fig. 6 Expermentally obtained cross section of $^{237}Np(n,f)$ reaction compared with two previously measured data

Reevaluation of the $^{237}Np(n, f)$ cross section in resonance and intermediate regions is recommended. If this cross section increases factor 3, the efficiency of the transmutation of ^{237}Np by the fission in resonance region would improve almost the same factor.

IV. CONCLUSION

We have measured the cross section for the $^{237}Np(n, f)$ reaction from about 1 eV to about 5 keV normalized to that for the $^{235}U(n, f)$ reaction with back-to-back type fission chambers by making use of a newly constructed lead neutron slowing-down spectrometer KULS. The absolute values of the data by Hoffman *et al.* are close to the present ones, but those by Plattard *et al.* are from 3 to 4 times less than the present ones. Gross shape of the present result is very similar to that of ENDF/B-VI in all range and that of JENDL-3 below 120 eV, however the absolute values in both files are also from 3 to 4 times smaller than those of the present data. Therefore we recommend to reevaluate the $^{237}Np(n, f)$ cross section in resonance and intermediate regions.

ACKNOWLEDGMENT

The authors would like to express hearty thanks to Prof. M. Nakazawa of University of Tokyo for the reconstruction of the lead slowing-down spectrometer and to Dr. M. Nakano of Japan Atomic Energy Research Institute (JAERI) for the supply of the fission chambers. They are also indebted to Mr. T. Nakagawa of the Nuclear Data Center of JAERI for supplying nuclear data. Technical assistance by Mr. K. Nishio of Kyoto University is appreciated.

This work was supported by the Grant-in-Aid of Scientific Research from the Ministry of Education, Science and Culture (No. 6346023 to Fujita and No. 03452302 to Tamai) and by the Cooperative Use Program of KURRI.

—REFERENCES—

(1) FUBINI, A., BLONS, J., MICHAUDON, A., PAYA, D: *Phys. Rev. Lett.*, 20, 1373 (1968).
(2) BROWN, W.K., DIXON, D.R., DRAKE, D.M.: *Nucl. Phys.*, A156, 609 (1970).
(3) JIACOLETTI, R.J., BROWN, W.K., OLSON, H.G.: *Nucl. Sci. Eng.*, 48, 412 (1972).
(4) SEMON, M.D., HOFFMAN, M., SANDERS, W.M.: *Bull. Am. Phys. Soc.*, 21, 655 (1976).
(5) PLATTARD, S., BLONS, J., PAYA, D.: *Nucl. Sci. Eng.*, 61, 477 (1976).
(6) AUCHAMPAUGH, G.F., *et al.*: *Phys. Rev.*, C29, 174 (1984).
(7) SHIBATA, K., *et al.*: *JAERI* 1319, (1990).
(8) ROSE, R.F. (ed.): *BNL-NCS*-17541 (4th ed.), (1991).
(9) BERGMAN, A.A., *et al.*: *1st Geneva. Conf.* Vol. 4, 135 (1955).
(10) MITZEL, F., PLENDL, H.S.: *Nukleonik*, 6, 371 (1964).
(11) WAKABAYASHI, H., SEKIGUCHI, A., NAKAZAWA, M. NISHINO, O.: *J. Nucl. Sci. Technol.*, 6, 487 (1970).
(12) CHOU, J.C., WERLE, H.: *J. Nucl. Energy*, 27, 811 (1973).
(13) SAWAN, M., CONN, R.W.: *Nucl. Sci. Eng.*, 54 127 (1974).
(14) SLOVACEK, R.E., *et al.*: *ibid.*, 62, 455 (1977).
(15) NAKAGOME, Y., BLOCK, R.C., SLOVACEK, R.E., EDGAR, B.B.: *Phys. Rev.*, C43, 1824 (1991).
(16) YAMANAKA, A., *et al.*: *JAERI-M* 92-027, p. 375 (1992).
(17) OBU, M.: *JAERI-M* 9757, (1981).
(18) GRUNDL, J.A., GILLIAM, D.M., DUDEY, N.D., POPEK, R.J.: *Nucl. Technol.*, 25, 237 (1975).

付録 B

NUCLEAR SCIENCE AND ENGINEERING: 126, 201-212 (1997)

Fission Cross-Section Measurements of ^{241}Am Between 0.1 eV and 10 keV with Lead Slowing-Down Spectrometer and at Thermal Neutron Energy

Shuji Yamamoto and Katsuhei Kobayashi

Research Reactor Institute, Kyoto University
Kumatori-cho, Sennan-gun, Osaka 590-04, Japan

Mitsuharu Miyoshi,* Itsuro Kimura, and Ikuo Kanno

Kyoto University, Department of Nuclear Engineering
Yoshida-honmachi, Sakyo-ku, Kyoto 606-01, Japan

Nobuo Shinohara

Japan Atomic Energy Research Institute, Department of Radioisotopes
Tokai-mura, Naka-gun, Ibaraki 319-11, Japan

and

Yoshiaki Fujita

Research Reactor Institute, Kyoto University
Kumatori-cho, Sennan-gun, Osaka 590-04, Japan

Received April 16, 1996
Accepted December 6, 1996

Abstract—*Making use of back-to-back type double fission chambers and a lead slowing-down spectrometer coupled to an electron linear accelerator, the cross section for the ^{241}Am(n,f) reaction has been measured relative to that for the ^{235}U(n,f) reaction in the energy range from 0.1 eV to 10 keV. To avoid the interference between the ^{241}Am and the ^{235}U resonances, the fission cross section below 1 keV was measured relative to the ^{10}B(n,α) reaction with a BF_3 counter, and the result obtained was normalized to the absolute value by the ^{235}U reference data between 200 eV and 1 keV. The measured result has been compared with (a) the evaluated nuclear data contained in the ENDF/B-VI and JENDL-3.2 libraries and (b) the existing experimental data, with the evaluated and measured data being broadened using the energy resolution function of the spectrometer.*

There is general agreement between the evaluated data and this measurement, although some discrepancies are found in the energy region where the cross-section shapes show a pronounced structure. The JENDL-3.2 data are underestimated by a factor in the range 1.2 to 2.3 between 22 and 140 eV, while the more recently measured data by Dabbs, Johnson, and Bemis and the evaluated data in ENDF/B-VI are in good agreement with the measurement within the uncertainties. In the energy range from 1 to 10 keV, the current result is 15 to 18% higher than the evaluations and the data of Dabbs, Johnson, and Bemis. Some of the earlier experimental data that were measured over part of the relevant energy region are not always in agreement with the current measurement.

The fission cross section for thermal neutrons was also measured in a pure Maxwellian neutron spectrum field with double fission chambers. The derived result at 0.0253 eV is 3.15 ± 0.097 b, which is obtained relative to the reference value of 586.2 b for the ^{235}U(n,f) reaction. The ENDF/B-VI data are in good agreement with the current measurement, while the JENDL-3.2 value is lower by 4.2%. The ratios of the earlier experimental data to the current value are distributed between 0.89 and 1.02.

*Current address: GE and Yokogawa Medical System, Inc., 4-chome, Asahigaoka, Hino-shi, Tokyo 191, Japan.

I. INTRODUCTION

Americium-241 is one of the burdensome minor actinides that are abundantly produced in power reactors. The nuclear data for ^{241}Am are of great importance for the design of reactors with mixed oxide or plutonium fuels and for the design of systems for spent-fuel reprocessing. In addition, the fission cross section of ^{241}Am is also of interest for its transmutation from the standpoint of the disposal of radioactive waste.[1-5]

Although the fission cross section of ^{241}Am rises ~500 keV up to ~2 b like a threshold reaction function, fission occurs to a certain extent in the thermal, intermediate, and resonance energy regions. This component of the fission should be taken into account in thermal reactor studies. Up to now, although numerous measurements of the cross section for the ^{241}Am(n,f) reaction have been made, there still exist marked discrepancies among the measured data <300 keV (Refs. 6 through 12). Dabbs, Johnson, and Bemis[6] measured the fission cross section in the wide energy range from 0.02 eV to 20 MeV using the neutron time-of-flight (TOF) method. Before this measurement, several experimental groups had measured the cross section in less broad energy ranges. Two recently evaluated data files appearing in ENDF/B-VI (Ref. 13) and JENDL-3.2 (Ref. 14) are close to the data obtained by Dabbs, Johnson, and Bemis.[6] However, other experimental data measured by Leonard et al.,[7] Bowman et al.,[8] Gerasimov,[9] Seeger et al.,[10] Derrien et al.,[11] and Gayther and Thomas[12] are not always in agreement with these evaluated data. Concerning the thermal neutron fission cross section of ^{241}Am, the evaluated values are in general agreement with each other.[13-16] Most of the experimental data were obtained from the 1950s to the 1970s, and they range between 2.8 and 3.2 b (Refs. 17 through 22).

A difficulty in the measurement of the fission cross section of ^{241}Am has often been caused by strong alpha-particle activity or pileup pulses because of its alpha decay with a short half-life of 432 yr. In addition, the fission cross section in the energy region from 1 to 300 keV is <0.1 b. Therefore, an intense neutron source is required for the cross-section measurement, especially in the intermediate or resonance energy region, to have enough signal-to-background ratio. A lead slowing-down spectrometer is a powerful tool and is often used for this kind of fission cross-section measurements because the neutron flux is ~10^4 greater than that of a conventional TOF experiment at a 5-m flight path, although the energy resolution of the spectrometer is ~35% full width at half maximum.[23]

Another problem for fission cross-section measurements of transuranium nuclides is often due to the lack of isotopically pure samples, though the utilization of high-purity samples is one of the most important requirements for nuclear data measurement. Wagemans suggests the usefulness of thermal neutron experiments to check the sample quality.[24] In an earlier measurement, we had the experience of obtaining a much larger fission cross section for ^{241}Am, the measurement being made with a sample on the market.[25] Through the careful and systematic investigation of the ^{241}Am sample by alpha-ray spectrometry, we found that the problem was mainly caused by plutonium impurities (~0.3%) in the sample.[26]

In the current measurement, we have prepared a pure ^{241}Am sample by means of the anion-exchange method to remove impurities of transuranium nuclides. The chemical solution of the sample was electrolyzed, and the ^{241}Am layer was deposited on a stainless steel disk, which was put into back-to-back (BTB) type fission chambers[27] together with the disk with the layer of ^{235}U. The fission cross section for the ^{241}Am(n,f) reaction was measured at energies between 0.1 eV and 10 keV relative to that for the ^{235}U(n,f) reaction by making use of the double fission chambers and the lead slowing-down spectrometer coupled to the 46-MeV electron linear accelerator (linac) of the Research Reactor Institute, Kyoto University (KURRI) (Ref. 28). To avoid the interference between the ^{241}Am and ^{235}U resonances, the ^{241}Am fission cross section was measured relative to the ^{10}B(n,α) reaction using a BF_3 counter below 1 keV, and the result was normalized to that measured with the BTB chambers at energies between 200 eV and 1 keV. The experimental technique is almost the same as that of the previous measurement of the fission cross section for ^{237}Np (Ref. 29). The current measurement is compared with the evaluated data in ENDF/B-VI and JENDL-3.2 and with the existing experimental data.

The thermal neutron cross section for the ^{241}Am(n,f) reaction was also measured with the aforementioned fission chambers in a standard neutron spectrum field having a pure Maxwellian distribution in the Kyoto University Reactor (KUR) at KURRI (Ref. 30). The result is compared with the evaluated and the previous experimental data.

II. EXPERIMENTAL METHOD

II.A. Lead Slowing-Down Spectrometer

The lead slowing-down spectrometer is installed at the 46-MeV electron linac at KURRI. This Kyoto University lead slowing-down spectrometer (KULS) is composed of 1600 lead blocks (each is 10 × 10 × 20 cm^3, and purity is 99.9%), and these are piled up to make a cube of 1.5 × 1.5 × 1.5 m^3 (~40 t) without any structural materials.[28] The KULS is covered with 0.5-mm-thick cadmium sheets. At the center of the KULS, we have placed an air-cooled photoneutron target of tantalum to produce pulsed fast neutrons. Four sets of thermocouples were attached to the surface of the photoneutron target case to monitor the temperature.

The linac was operated in such a way as to keep the temperature <300°C. The KULS has eight experimental/irradiation holes (10 × 10 cm^2, 55 or 45 cm in depth), and one of the holes is covered by bismuth layers of 10 to 15 cm in thickness to shield high-energy gamma rays (6 to 7 MeV) produced by the Pb(n,γ) reaction in the spectrometer.[28] The cross-sectional view of the KULS is shown in Fig. 1.

Characteristics of the behavior of neutrons in the KULS have been studied by calculations with the continuous energy Monte Carlo code MCNP (Ref. 31) and by experiments using the resonance filter method.[28] The energy E, in kilo-electron-volts, is related to the neutron slowing-down time t, in microseconds, by the relation $E = K/t^2$, where K is the slowing-down constant.[32,33] The neutron slowing-down time and the energy resolution of the KULS were measured with a BF_3 counter (12 mm in diameter, 50 mm in length, and 1 atm) and an argon gas counter (12.7 mm in diameter, 63.5 mm in length, and 1 atm). Measurements were made both with and without resonance filters of indium, tellurium, tantalum, gold, cadmium, molybdenum, and manganese. To measure the slowing-down constant K, the BF_3 counter was used to make neutron transmission measurements with the filters in place, and the argon gas counter was applied to the capture gamma-ray measurement with the filters. The dips or the bumps that were observed in the slowing-down time spectrum corresponded to the resonance energies of the filter material. The slowing-down constant K was determined to be 190 ± 2 and 156 ± 2 (keV·μs^2) for the bismuth and the lead experimental holes, respectively.[28] The energy resolution was ~40% for both experimental holes at energies from a few electron volts to ~500 eV and was larger in the lower and the higher energy regions.[28] The relation between neutron slowing-down time and energy and the energy resolution was also obtained by the MCNP calculations, and the results were in good agreement with those measured by the BF_3 and the argon gas counters. More detailed characteristics of the KULS are given in other references.[28,29]

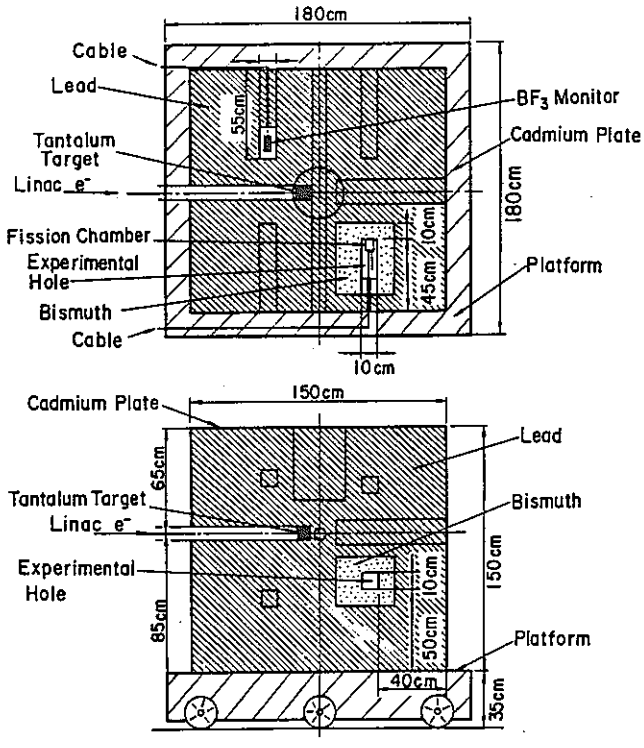

Fig. 1. Cross-section view of the KULS.

II.B. The ^{241}Am and ^{235}U Samples

The americium solution obtained from the International Atomic Energy Agency was purified at the Isotope Products Laboratory of the Japan Atomic Energy Research Institute (JAERI) by the anion-exchange method using nitric acid-methyl alcohol mixed media[34] to remove uranium, neptunium, plutonium, and curium from the americium sample. The purified americium solution and isopropyl alcohol were mixed thoroughly and electrolyzed on a stainless steel disk (28 mm in diameter and 0.2 mm in thickness) to produce an americium deposit (radioactive area of 20 mm in diameter).[35] After electrodeposition, the sample was sintered with a gas burner to fix the americium layer on the disk by making americium oxide.

The alpha rays from the deposit were measured with a silicon surface barrier detector. No traces of ^{237}Np, ^{238}Pu, ^{239}Pu, ^{240}Pu, ^{243}Am, or ^{242}Cm impurities in the americium deposit were observed in the measured alpha-ray spectrum. Therefore, the isotopic composition of ^{241}Am in the deposit was estimated to be >99.9%. The number of ^{241}Am atoms was determined by analyzing the alpha rays having energies in the range 5.322 to 5.544 MeV. The 59.5-keV gamma ray from ^{241}Am was also measured with a high-purity germanium detector. The number of ^{241}Am atoms was determined by both detectors, and the result was (1.734 ± 0.020) × 10^{16}, as given in Table I, where the errors were estimated by taking account of (a) statistics of the activity measurements, (b) geometrical detection efficiencies, and (c) uncertainties in the decay data used.

The deposit of highly enriched uranium oxide (99.91% of ^{235}U) purchased from Oak Ridge National Laboratory was prepared using almost the same technique as for the americium sample and was electrodeposited on a stainless steel disk at KURRI. This ^{235}U sample was used to monitor the neutron flux in this study by means of the well-known reference cross section of the ^{235}U(n,f) reaction. Alpha-ray and gamma-ray spectrometry measurements were carried out to determine the number of uranium atoms as was done for the americium sample. By the analyses of the alpha rays with energies in the range of 4.152 to 4.597 MeV and the 185.7-keV gamma ray from ^{235}U, the number

TABLE I

Determination of the Number of Atoms for the ^{241}Am and ^{235}U Oxide Deposits

Method	^{241}Am Deposit	^{235}U Deposit
Alpha spectroscopy	$(1.722 \pm 0.022) \times 10^{16}$	$(3.289 \pm 0.039) \times 10^{17}$
Gamma spectroscopy	$(1.796 \pm 0.053) \times 10^{16}$	$(3.253 \pm 0.094) \times 10^{17}$
Weighted mean value	$(1.734 \pm 0.020) \times 10^{16}$	$(3.283 \pm 0.036) \times 10^{17}$

of ^{235}U atoms was determined to be $(3.283 \pm 0.036) \times 10^{17}$, as shown in Table I.

Uniformity of the electrodeposited layer was investigated by using a solid-state track detector of CR-39 (Ref. 36). The exposure times for measuring the tracks from ^{241}Am and ^{235}U were a few seconds and 2 h, respectively, under the condition that the distance between the layer and the track detector was 0.5 mm. After etching the exposed plastics with KOH solution, the detector surface was examined with a microscope, and the number of the etched pits was counted in every area of 3×3 mm^2. The number of pits per unit area was between ~25 and 40 for ^{241}Am and between ~60 and 75 for ^{235}U except at the edge of the radioactive region of the deposit. Considering that the layer thickness is 2.2 μg/cm^2 for the ^{241}Am deposit and 41 μg/cm^2 for the ^{235}U deposit, most of the fission fragments can easily pass through the layers so that the nonuniformity in the current deposits could not perturb the fission cross-section measurement.

II.C. Fission Chambers

The fission chambers that are employed in the current experiment are composed of two identical parallel plate-type ionization chambers, as shown in Fig. 2. These chambers were originally designed for in-core fission ratio measurements.[27] Because it is the back sides of the stainless steel plates having the americium deposit and the reference uranium deposit that face each other,

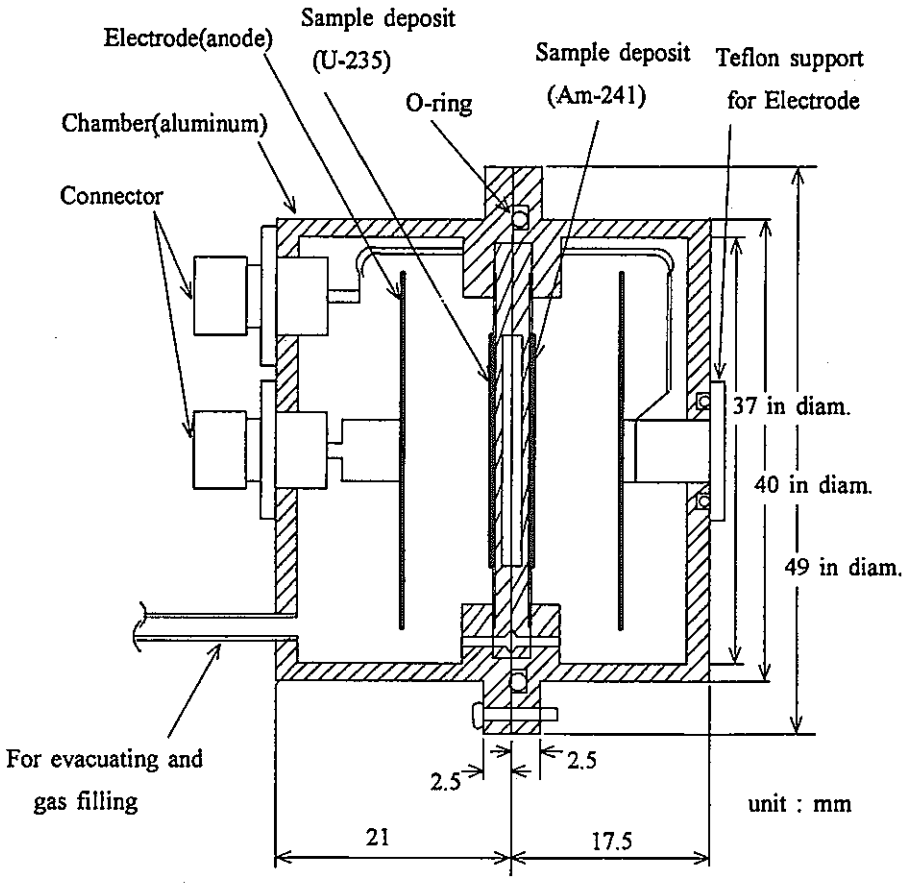

Fig. 2. Cross-section view of the BTB chambers.

it is called the back-to-back type. The double fission chambers are made of aluminum and filled with a mixed gas of 97% argon and 3% N_2 at a pressure of 1 atm. In this gas pressure, the mean range of alpha particles reaches 36 mm, while that of fission fragments is ~20 mm. Therefore, the fission chambers are designed so as to collect most of the energy of the fission fragments, although the chambers are designed not to collect most of the alpha particles, in order to get a good discrimination between the alpha and the fission fragment pulses. The distance between the electrode and the deposit layer is designed to be 8 mm. The operation voltage is 400 V. Figure 3 shows a typical pulse height distribution of fission fragments for 4 h of measurement for the americium layer. Because we used thin ^{241}Am and thin ^{235}U deposits, fission pulses were clearly discriminated from background pulses caused by the alpha rays.

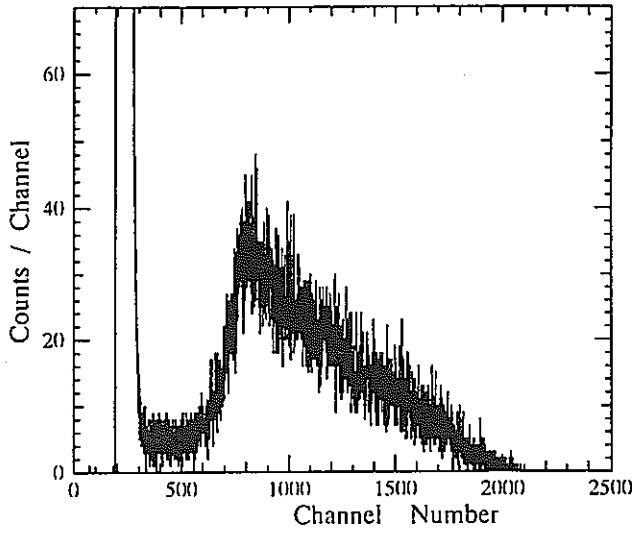

Fig. 3. Pulse height distribution of fission fragments for ^{241}Am with the BTB chambers.

II.D. The BF_3 Counter

The $^{10}B(n,\alpha)$ reaction is well known to be one of the standard cross sections and is often applied to cross-section measurements as a reference. The BF_3 counter[a] was used for the fission cross section measurement of ^{241}Am in the resonance interference energy region of ^{241}Am and ^{235}U fission cross sections. The counter was of a cylindrical type, 50 mm in effective length, 12 mm in diameter, and 1 atm, and its high-voltage bias was 1100 V. Instead of the ^{235}U fission chamber in the BTB chambers, the BF_3 counter was employed to measure the energy dependence of the neutron flux spectrum.

II.E. Fission Ratio Measurement

The fission cross section of ^{241}Am has been measured relative to that of ^{235}U by making use of the BTB chambers in the bismuth hole. As both ^{241}Am and ^{235}U nuclei have neutron resonances in the relevant energy region, the fission ratio data may be difficult to interpret. For this reason, we have employed not only the BTB chambers but also a BF_3 counter that is well known as a good $1/v$ detector in the energy range of the current measurement. The relative fission cross section of ^{241}Am was measured below 1 keV with the BF_3 counter, and the result was normalized to the fission cross section between 200 eV and 1 keV measured relative to the $^{235}U(n,f)$ reaction using the BTB chambers.

The lead slowing-down spectrometer KULS was driven by the 46-MeV electron linac at KURRI, and the typical operating conditions during the experiments were as follows: pulse repetition rate of 150 Hz, pulse width of 22 ns, electron peak current of ~0.8 A, and the energy of ~31 MeV. After the linac had operated for more than 120 h, the deposited plates of ^{241}Am and ^{235}U in the BTB chambers were interchanged, and another measurement was made for ~130 h in the bismuth hole. After the chambers were inserted into the bismuth hole, the hole space was filled with bismuth bricks so as not to let neutrons leak.

II.F. Electronics and Data Taking

Two identical electronic circuits were employed for both fission chambers, as shown in Fig. 4. Through the amplifiers and the discriminators, signals from the fission chambers were fed into a time digitizer, which was

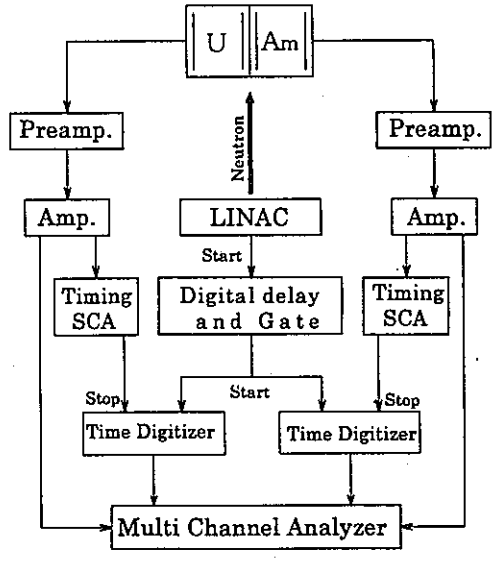

Fig. 4. Block diagram of electronic circuits to measure time-dependent fission counts with the BTB chambers.

[a]Purchased from Mitsubishi Electric Company.

initiated by the linac electron burst, and the slowing-down time data of neutrons were stored for each measurement of 4 to 5 h duration in a data acquisition system.[b] Two sets of 4096 channels were allotted to the slowing-down time measurements for the BTB chambers, and the channel width was 62.5 ns to 0.5 μs. Pulse height distributions of fission events from the ^{241}Am and the ^{235}U deposits were also measured with each 4096 channel analyzer in parallel with the slowing-down time measurements.

For the measurement of the relative fission cross section of ^{241}Am, output signals from the BF_3 counter were also led to the time digitizer through the amplifiers and the discriminators. The data of the slowing-down time of neutrons were stored in the same way as for the BTB chambers.

III. FISSION CROSS-SECTION MEASUREMENT

III.A. Fission Cross Section

The fission counts at the slowing-down time t (in microseconds) can be converted to those at energy E (in kilo-electron-volts) by using the relation of $E = K/(t + t_0)^2$, where t_0 is the zero time correction.[28] From the fission counts of the ^{241}Am and the ^{235}U deposits, the energy-dependent cross section for the ^{241}Am(n,f) reaction is given by

$$\sigma_{Am}(E) = \frac{C_{Am}(E)}{C_U(E)} \frac{N_U}{N_{Am}} \sigma_U(E) ,$$

where

$C_{Am}(E)$ = fission counts of ^{241}Am at energy E

$C_U(E)$ = fission counts of ^{235}U at energy E

N_U = number of ^{235}U atoms in the ^{235}U deposit

N_{Am} = number of ^{241}Am atoms in the ^{241}Am deposit

$\sigma_U(E)$ = energy-dependent fission cross section of ^{235}U.

We used the values of $\sigma_U(E)$ from ENDF/B-VI (Ref. 13), the accuracy of the fission cross section having been estimated as shown in Table II. The reference data were broadened using the energy resolution function that was fitted to the previous measurements in the relevant energy region,[28] the unbroadened fission cross section in ENDF/B-VI having sharp resonances in the energy range of the measurements. Below 200 eV, since strong neutron resonances occur in the fission cross sections of the ^{241}Am and ^{235}U, we have employed the ^{10}B(n,α) reaction that shows a smooth and good $1/v$ energy dependence in the relevant energy region, instead of the ^{235}U(n,f) reaction. In the relative cross-section measurement with the BF_3 counter, $C_U(E)$ and $\sigma_U(E)$ in the aforementioned relation can be interpreted to be the counts and the cross section for the ^{10}B(n,α) reaction. The ratio of N_U/N_{Am} can be considered as a field constant in this case. For the data processing, we have written Fortran programs for the personal computer.

TABLE II

Experimental Uncertainties for the Current Measurement

Causes of Uncertainties	Error (%)
Statistical error for ^{241}Am	0.08 to 6.2
Statistical error for ^{235}U	0.06 to 1.1
Assignment of fission counts for ^{241}Am	<1.9
Assignment of fission counts for ^{235}U	<0.65
Number of atoms of ^{241}Am	1.3
Number of atoms of ^{235}U	1.2
Reference cross section for the ^{235}U(n,f) reaction	2 to 4
Reference cross section for the ^{10}B(n,α) reaction	2
Correction for the setting position of the ^{241}Am and ^{235}U deposits in the BTB chambers	<0.3
Correction for scattering of inscattered neutrons by the chambers	<0.2
Correction to background subtraction	<0.2 to 0.4

	Energy Range (eV)	Error (%)
Total uncertainties	0.1 to 0.89	4.1
	0.89 to 3.55	4.6
	3.55 to 20.0	4.2
	20.0 to 200	4.4
	200 to 1000	5.7
	1000 to 10 000	8.6

The systematic difference between the ^{241}Am and the ^{235}U deposit positions in the BTB chambers was experimentally investigated by interchanging the plates. Before and after the deposits were exchanged, the measured ratio for $C_{Am}(E)/C_U(E)$ was charged by $\sim 1.06 \pm 0.05$, which was almost independent of neutron energy. For the derivation of the fission cross section, we took the average value for the $C_{Am}(E)/C_U(E)$ ratios obtained by exchanging the positions for the ^{241}Am and the ^{235}U deposits.

III.B. Background Correction

As the pulse height of fission events is bigger, it is easy to distinguish fission pulses from noise pulses or

[b]Canberra's Series-88 MPA analyzer.

alpha pulses from the sample deposit. Because the radioactivity of the ^{241}Am deposit was $\sim 8.8 \times 10^5$ Bq, the pileup problem due to the alpha pulses is negligible. Background counts that are due to the overlap of neutrons from the previous pulses of the linac are also negligible because of the low pulse repetition rate of 150 Hz and of the low thermal neutron flux in the KULS. Delayed neutrons could be neglected considering the emission rate $[\nu_d/(\nu_p + \nu_d) = 0.0016]$ to the fission neutrons. The background due to the photo-fission events has to be taken into account in the data analysis. Because the BTB chambers were put into the bismuth hole, background counts due to the photofission of ^{235}U and ^{241}Am by the Pb(n,γ) reaction in the KULS could be reduced.

A background run was carried out using the BTB chambers without sample deposits. A very limited number of counts in total were observed in the slowing-down time spectrum for a run of more than 30 h. It was found that the background counts for the ^{241}Am chamber might affect the minimum cross-section region for the ^{241}Am(n,f) reaction by 0.2 to 0.4% on average, at most, whereas the background counts for the ^{235}U chamber could be neglected completely.

Neutrons may be scattered by the structural materials of the BTB chambers before arriving at the deposit layers. The inscattered neutrons, which are not directly observable, may be another source of background for the current measurement. To investigate the inscattered background, we have made calculations using a continuous energy Monte Carlo code, MCNP (Ref. 31). The BTB chambers are made of aluminum and the size is 40 mm in diameter, 39 mm in length, and ~2 mm in thickness, as shown in Fig. 2. The electrodes, deposit layers, backing plates, and their supports by which neutrons may also be scattered are represented in the calculations. It was assumed that the neutrons entered the chambers almost isotropically from the surrounding region. The energy-dependent reaction ratio data for ^{241}Am to ^{235}U were calculated with 5 000 000 random histories to see how the measured cross section was affected by the inscattered neutrons. The current calculations have shown that a very small correction may be required, making the ^{241}Am(n,f) cross section lower by 2 to 6% at most in the energy region from 1 to 10 eV and larger by ~7% at most at energies between 0.3 and 0.8 eV, even taking account of the calculation uncertainties. Other small corrections were also made around 100 eV.

IV. MEASUREMENT OF THE THERMAL NEUTRON CROSS SECTION

IV.A. Thermal Neutron Spectrum Field

The KUR at KURRI has a thermal neutron facility that consists of a 1.4-m-long heavy water tank.[30,37] The irradiation room is $\sim 2.4 \times 2.4 \times 2.4$ m^3 and is surrounded by 90-cm-thick heavy concrete shields. The leakage neutrons from the heavy water tank can be used as a thermal neutron source of a plane-type in a large space.

Kanda et al. measured the neutron spectrum from the heavy water tank by the TOF technique using a fast chopper.[37] The measured spectrum showed good agreement with a Maxwellian distribution having a neutron temperature of 60°C. The cadmium ratio measured by gold foils with and without a cadmium cover of 0.7 mm in thickness was more than 5000, and so the contribution of epithermal neutrons can be neglected.[37]

IV.B. Experimental Methods

The heavy water thermal neutron facility has been employed for the measurement of the thermal neutron cross section for the ^{241}Am(n,f) reaction, making use of the BTB-type double fission chambers. The chambers were set in the irradiation room and exposed to thermal neutrons for ~10 h during the nominal power operation of 5 MW of the KUR. The irradiation was repeated by exchanging the ^{241}Am and the ^{235}U sample positions. Fission pulses from the samples were led to their 2048 channel pulse height analyzers through the amplifiers and the discriminators. Each of the fission counts was obtained by integrating the pulse height distribution above the discrimination level.

IV.C. Measurement of the Cross Section

The thermal neutron cross section σ_{th} averaged over the Maxwellian distribution spectrum is defined as

$$\sigma_{th} = \frac{\sigma_{th}(v_0)}{1.128}\, g(T_n) \left(\frac{T_0}{T_n}\right)^{1/2} ,$$

where

$v_0 = 2200$ m/s

$T_0 = 293.6$ K

T_n = neutron temperature

$g(T_n)$ = g factor.

The thermal neutron cross section σ_{Am} for the ^{241}Am(n,f) reaction at a neutron energy of 0.0253 eV (corresponding to a velocity of 2200 m/s) is obtained in almost the same way as in the case of the KULS measurement, by rewriting the relations as follows:

$$\sigma_{\mathrm{Am}} = \frac{C_{\mathrm{Am}}}{C_{\mathrm{U}}} \frac{N_{\mathrm{U}}}{N_{\mathrm{Am}}} \frac{g_{\mathrm{U}}(T_n)}{g_{\mathrm{Am}}(T_n)}\, \sigma_{\mathrm{U}} ,$$

where

C_{Am} = fission counts of ^{241}Am

C_{U} = fission counts of ^{235}U

$g_{\mathrm{U}}(T_n)$ = g factor of ^{235}U

$g_{Am}(T_n)$ = g factor of ^{241}Am

σ_U = fission cross section at 0.0253 eV of ^{235}U.

The reference fission cross section was taken from the evaluated data file of ENDF/B-VI, and the g factors for ^{241}Am(0.996) and ^{235}U(0.9761 ± 0.0012) were obtained from the Mughabghab compilation,[16] although Gryntakis et al.[38] gave values of 1.0220 and 0.9665, respectively. The ratio of C_{Am}/C_U data obtained by exchanging the deposit positions of ^{241}Am and ^{235}U in the BTB chambers was 1.04 ± 0.03. We took an average of the values before and after the deposits were exchanged to derive the fission cross section.

V. RESULTS AND DISCUSSION

Making use of the BTB chambers and the KULS, the cross section for the $^{241}Am(n,f)$ reaction was measured relative to that for the $^{235}U(n,f)$ reaction at energies from 0.1 eV to 10 keV. In the resonance energy region for ^{241}Am and ^{235}U below 1 keV, the fission cross section of ^{241}Am was measured relative to the $^{10}B(n,\alpha)$ reaction and was normalized to the absolute value between 200 eV and 1 keV obtained in the measurement relative to the $^{235}U(n,f)$ reaction, to avoid the resonance interference between ^{241}Am and ^{235}U. The current result from 0.1 eV to 10 keV is shown in Fig. 5 and is compared with the ENDF/B-VI and the JENDL-3.2 data, which have been broadened by the energy resolution function of the KULS.

The dead time correction for the ^{235}U fission chamber was <0.03%, and that for the ^{241}Am was negligibly small. Concerning the effects of (a) loss of the fission fragments in the ^{241}Am and the ^{235}U deposits, (b) anisotropic angular distribution of the fission fragments, and (c) photofission in the deposits on the resultant fission cross section of ^{241}Am, we have assumed that they are negligible as described in an earlier paper.[29] Because the pure ^{241}Am sample was carefully prepared and no impurity could be observed, no correction was made for an impurity effect.

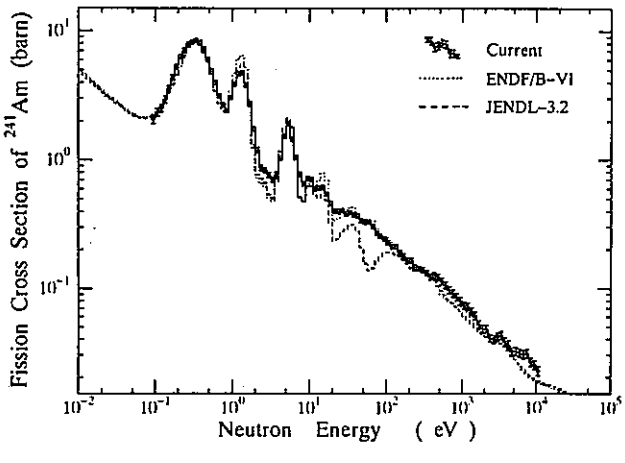

Fig. 5. Comparison of the evaluated fission cross section of ^{241}Am with the current measurement. The evaluated data are broadened by the energy resolution of the KULS.

The cross-section data were obtained by summing up the slowing-down time data in intervals of ~0.115 lethargy width. The experimental uncertainties for the current measurement are summarized in Table II. The discrimination level was set in the minimum count region between the fission and the noise counts in the pulse height distribution. The uncertainty in the determination of the fission counts was estimated to be 1.9% for ^{241}Am and 0.65% for ^{235}U, respectively. Considering the gain shift in the detection system, the discrimination level was checked and determined every 10 to 20 h during the experiment. The numbers of atoms in the ^{241}Am and the ^{235}U deposits were derived from the mean average by the alpha- and gamma-ray measurements. The gamma-ray measurement supported the result by the alpha-ray measurement within the experimental uncertainty, as seen in Table I. Uncertainties for the reference cross sections of the $^{235}U(n,f)$ and the $^{10}B(n,\alpha)$ reactions[13,39] were estimated to be 2 to 4% and 2% in the relevant energy region, respectively. [It is only the uncertainty in the $1/v$ form of the $^{10}B(n,\alpha)$ reaction that affects the measurement.] The uncertainty in the measured value of the ^{241}Am fission cross section is estimated to be 4.1 to 8.6% in the relevant energy range.

In Fig. 5, good agreement can be seen in the general shape and absolute values between the current measurement and the evaluated data in ENDF/B-VI and JENDL-3.2, and both of the evaluated data show good agreement with each other, except at energies from ~22 to 140 eV. Some discrepancies can be seen between the evaluated data and the measurement in the dip and the bump cross-section region. Both sets of evaluated data in the energy range of the dip from 2 to 4 eV are lower by ~30%, but the average value over a wider energy range agrees to within ~10%. The difference could be due to the resolution broadening function being broader than that assumed. The same problem of the resolution broadening is seen at the sharp dip near 8 eV. Comparing the evaluated values with the current measurement, we find the JENDL-3.2 data between 22 and 140 eV are underestimated by a factor ranging from 1.2 to 2.3, while the ENDF/B-VI data are in good agreement with the measurement.

The existing experimental data have also been broadened by the energy resolution function of the KULS and are compared with the current data in Fig. 6. The data measured by Dabbs, Johnson, and Bemis, which is the primary source used for the fission cross section in the evaluation for the ENDF/B-VI file, are in general agreement with the current values. The fission cross sections obtained by Gayther and Thomas[12]

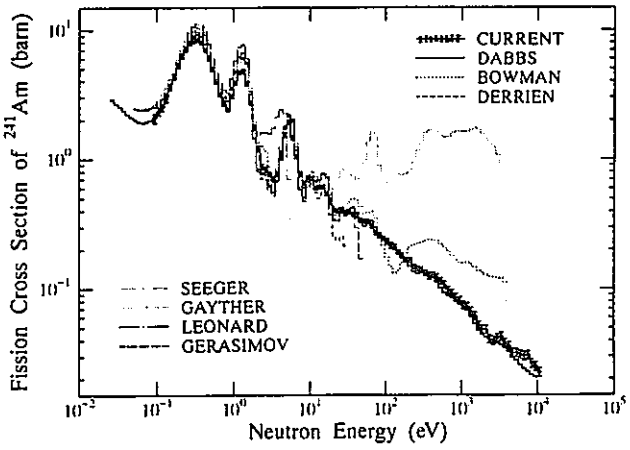

Fig. 6. Comparison of the existing experimental data with the current measurement. The experimental data are broadened by the energy resolution of the KULS.

are higher above 55 eV by 50 to 100% than the current measurement. The data by Bowman et al.,[8] Gerasimov,[9] and Derrien et al.[11] are close to the current cross section below several tens of electron volts, although Bowman et al. gave two times higher data above 200 eV. Leonard et al.[7] gave higher values between 2 and 5 eV. Seeger et al.[10] measured the cross section with a nuclear explosion technique and obtained much higher values than the current data above 20 eV.

In Table III, comparisons are made between the mean values of the ^{241}Am fission cross section from the current work and the results from ENDF/B-VI, JENDL-3.2, and the data by Dabbs, Johnson, and Bemis.[6] As seen in the table, the ENDF/B-VI data are within the uncertainties of the current measurements in the energy ranges 0.1 to 0.89 eV and 20 to 200 eV, but they are higher by 4.5 to 7% between 0.89 and 20 eV and lower by 12 to 15% between 200 eV and 10 keV. The JENDL-3.2 data show lower values by 7 to 25% in the energy range 0.89 eV to 10 keV, although good agreement is seen between 0.1 and 0.89 eV. The data by Dabbs, Johnson, and Bemis are in general agreement with the current measurements considering that the uncertainties of their measurements[6] are more than 6% in the relevant energy region, except for the energy range 0.89 to 3.55 eV, where their measured value is 14% higher than the current average cross section. The current result above 1 keV is higher by 16.5 ± 1.5% than the evaluations and the data of Dabbs, Johnson, and Bemis.

The cross section of the ^{241}Am(n,f) reaction for 2200 m/s neutrons was obtained relative to the reference value of 586.2 b for ^{235}U(n,f) given in ENDF/B-VI. The current result at 0.0253 eV is 3.15 ± 0.097 b, which is close to the extrapolated value of the KULS data as seen in Fig. 5. Fission counts were determined by linearly extrapolating the pulse height distribution curve near the discrimination level. The main sources of uncertainties in the current measurement are due to the statistical error (0.04 to 0.4%), assignment of C_{Am} and C_U by integrating the pulse height spectrum above the discrimination level (estimated to be ~1.5% for C_{Am} and 1.1% for C_U, respectively), the g-factors for ^{241}Am and ^{235}U, the reference cross section for the ^{235}U(n,f) reaction (estimated to be <1%) (Refs. 13 and 16), the number of atoms in the deposit samples as seen in Table I, and the correction assigned for the setting position of ^{241}Am and ^{235}U deposits in the BTB chambers (0.25%). We have estimated that the uncertainty of the g-factor for ^{241}Am is ±1.3%, because we could see such a difference between the g-factors given by Mughabghab[16] and Gryntakis et al.,[38] while the g-factor for ^{235}U is well determined.[16] Other uncertainties and corrections are considered to be small and may be neglected as in the aforementioned KULS experiment. The total experimental uncertainty of the thermal neutron cross section for the ^{241}Am(n,f) reaction

TABLE III

Comparison of Mean Values of the ^{241}Am Fission Cross Section from the Current Work with Those from ENDF/B-VI, JENDL-3.2, and the Data by Dabbs, Johnson, and Bemis

Energy Range (eV)	Average Cross Sections (b)			
	ENDF/B-VI	JENDL-3.2	Dabbs, Johnson, and Bemis	Current
0.1 to 0.89	4.753+0[a]	4.724+0	5.133+0	4.897+0 ± 0.199
0.89 to 3.55	2.046+0	1.853+0	2.182+0	1.914+0 ± 0.0875
3.55 to 20.0	7.982−1	7.106−1	8.438−1	7.636−1 ± 0.0317
20.0 to 200	2.558−1	1.893−1	2.524−1	2.514−1 ± 0.0111
200 to 1000	9.701−2	9.708−2	10.224−2	10.965−2 ± 0.00628
1000 to 10000	3.031−2	3.009−2	3.110−2	3.570−2 ± 0.00308

[a]Read as $4.753 \times 10^{+0}$.

was derived to be ~3.1% as the root of the sum of the squares of the aforementioned uncertainties.

The measured result is given in Table IV and is compared with earlier evaluated and experimental data. The evaluated value in ENDF/B-VI is in good agreement with the current result, and the JEF-2.2 and the Mughabghab data are also close to the measurement. The data in JENDL-3.2 and that measured by Dabbs, Johnson, and Bemis are lower by 4.2 and 2.9%, respectively. Although the average value of the other six earlier experimental data is in agreement with the current measurement within the uncertainty, the value of Gavrilov et al. seems to be lower by 11% than the current data.

Because we carefully prepared the ^{241}Am sample and used a pure sample, the measured cross section should be free from reactions because of impurities. This is confirmed by the fact that the current measurement of the thermal neutron cross section for the ^{241}Am(n,f) reaction is in good agreement with most of the recent evaluated values at 0.0253 eV, as mentioned earlier. The current result may also be taken to provide confirmation that the KULS data with the ^{241}Am sample are not affected by impurities in the sample.

The result of the ^{241}Am fission cross section was reported at Gatlinburg as being higher by a factor of ~3 than the evaluations and Dabbs, Johnson, and Bemis measurement.[25] This has now been found to be mainly because of plutonium impurities in the sample, which was obtained on the market.[26] The current results replace the earlier published measurements, which were affected by plutonium impurities.

TABLE IV

Thermal Neutron Cross Sections (2200 m/s Value) for the ^{241}Am(n,f) Reaction

Cross Section (b)	Reference
3.15 ± 0.097	Current
3.153	ENDF/B-VI (1991) (Ref. 13)
3.019	JENDL-3.2 (1995) (Ref. 14)
3.177	JEF-2.2 (1994) (Ref. 15)
3.20 ± 0.09	Mughabghab (1989) (Ref. 16)
3.06 ± 0.19	Dabbs, Johnson, and Bemis (1983) (Ref. 6)
3.0	Hanna et al. (1951) (Ref. 17)
3.0 ± 0.2	Cunningham and Ghiorso (1951) (Ref. 18)
3.13 ± 0.15	Hulet et al. (1957) (Ref. 19)
3.15 ± 0.10	Bak et al. (1967) (Ref. 20)
2.8 ± 0.25	Gavrilov et al. (1975) (Ref. 21)
3.2 ± 0.15	Zhuravlev et al. (1975) (Ref. 22)

VI. CONCLUSION

The cross section for the ^{241}Am(n,f) reaction has been measured from 0.1 eV to 10 keV relative to that for the ^{235}U(n,f) reaction, making use of the BTB-type double fission chambers and a lead slowing-down spectrometer coupled to the KURRI electron linac. The ENDF/B-VI data and the data measured by Dabbs, Johnson, and Bemis (uncertainties more than 6%) are in good agreement with the current measurement within the uncertainties (4 to 9%). The JENDL-3.2 data are also in general agreement with the measurement, although the evaluated values are underestimated by a factor ranging from 1.2 to 2.3 between 22 and 140 eV. Above 1 keV, the current result is higher by 16.5 ± 1.5% than the evaluations and the Dabbs, Johnson, and Bemis data. In the comparison, these evaluated and measured data were broadened by the energy resolution function of the spectrometer, KULS. Some of the previous experimental data that were measured partially in the relevant energy region are not always in agreement with the current measurement.

The thermal neutron cross section for the ^{241}Am(n,f) reaction at 0.0253 eV was measured to be 3.15 ± 0.097 b. This was obtained with a pure Maxwellian distribution field using the BTB chambers. Good agreement can be seen between the current measurement and the values evaluated in ENDF/B-VI, JEF-2.2, and by Mughabghab. The JENDL-3.2 and the Dabbs, Johnson, and Bemis data are lower by 4.2 and 2.9%, respectively, than the current value. Most of the experimental data, which were measured from the 1950s to the 1970s, are close to that of the current result, although the measurement by Gavrilov et al. (uncertainty ±9%) is lower by ~11%.

ACKNOWLEDGMENTS

The authors would like to express their sincere thanks to M. Nakazawa of The University of Tokyo for the reconstruction of the lead slowing-down spectrometer for this work. They are grateful to T. Tsuruta of the Atomic Energy Research Institute, Kinki University, for his kind guidance on how to make uniformity measurements of the electrodeposited layers using solid-state track detectors. They are also indebted to T. Nakagawa of the Nuclear Data Center, JAERI, for supplying nuclear data. Technical assistance by H. Yamamoto and A. Kohashi of Kyoto University is appreciated.

This study was supported by a Grant-in-Aid of Scientific Research from the Ministry of Education, Science, and Culture (06452430 and 06302081) and by the Cooperative Use Program of KURRI.

REFERENCES

1. D. LANCASTER, "Actinide Burning in a Standard Pressurized Water Reactor," *Proc. Int. Conf. and Technology Exposition Future Nuclear Systems: Global '93*, Seattle,

Washington, September 12–17, 1993, p. 609, American Nuclear Society (1993).

2. J. TOMMASI, M. DELPECH, J. P. GROUILLER, and A. ZAETTA, "Long-Lived Waste Transmutation in Reactors," *Proc. Int. Conf. and Technology Exposition Future Nuclear Systems: Global '93*, Seattle, Washington, September 12–17, 1993, p. 1252, American Nuclear Society (1993).

3. T. WAKABAYASHI et al., "Feasibility Studies of an Optimized Fast Reactor Core for MA and FP Transmutation," *Proc. Int. Conf. Evaluation of Emerging Nuclear Fuel Cycle Systems: Global '95*, Versailles, France, September 11–14, 1995, p. 800, Commissariat à l'Energie Atomique (1995).

4. J. L. KLOOSTERMAN and J. M. LI, "Transmutation of Americium in Fission Reactors," *Proc. Int. Conf. Evaluation of Emerging Nuclear Fuel Cycle Systems: Global '95*, Versailles, France, September 11–14, 1995, p. 1106, Commissariat à l'Energie Atomique (1995).

5. T. MUKAIYAMA et al., "Research and Development of Transmutation of High Level Radioactive Waste," *J. At. Energy Soc. Japan*, **37**, *3*, 159 (1995).

6. J. W. T. DABBS, C. H. JOHNSON, and C. E. BEMIS, Jr., "Measurement of the ^{241}Am Neutron Fission Cross Section," *Nucl. Sci. Eng.*, **83**, 22 (1983).

7. B. R. LEONARD, Jr., et al., *Bull. Am. Phys. Soc.*, **4**, 31 (1959).

8. C. D. BOWMAN et al., *Phys. Rev.*, **137**, B326 (1965).

9. V. F. GERASIMOV, *Yaderno-Fizicheskie Issledovaniya*, **2**, 16 (1966).

10. P. A. SEEGER et al., *Nucl. Phys.*, **A96**, 605 (1967).

11. H. DERRIEN and B. LUCAS, *Proc. Int. Conf. Nuclear Cross Sections and Technology*, Washington, D.C., March 3–7, 1975, Vol. 2, p. 637, U.S. Government Printing Office (1975).

12. D. B. GAYTHER and B. W. THOMAS, "Measurement of the Neutron Capture and Fission Cross-Sections of ^{241}Am," *Proc. 4th All-Union Conf. Neutron Physics*, Kiev, Union of Soviet Socialist Republics, Part 3, p. 3 (1977).

13. "ENDF-201, ENDF/B-VI Summary Documentation," BNL-NCS-17541, 4th ed. (ENDF/B-VI), R. F. ROSE, Ed., Brookhaven National Laboratory (1991).

14. T. NAKAGAWA et al., *J. Nucl. Sci. Technol.*, **32**, *12*, 1259 (1995); see also "Evaluation of Nuclear Data for Americium Isotopes," JAERI-M, 89-008, Japan Atomic Energy Research Institute (1989).

15. C. NORDBORG and M. SALVATORES, "Status of the JEF Evaluated Data Library," *Proc. Int. Conf. Nucl. Data Science and Technology*, Gatlinburg, Tennessee, May 9–13, 1994, Vol. 2, p. 680, American Nuclear Society (1994).

16. S. F. MUGHABGHAB, "Neutron Cross Sections," *Neutron Resonance Parameters and Thermal Cross Sections*, Vol. 1, Part B, Academic Press, New York (1984).

17. G. C. HANNA et al., *Phys. Rev.*, **81**, 893 (1951).

18. B. B. CUNNINGHAM and A. GHIORSO, *Phys. Rev.*, **82**, 558 (1951).

19. E. K. HULET et al., *Phys. Rev.*, **107**, 1294 (1957).

20. M. A. BAK et al., *Atomnaya Energiya*, **23**, 316 (1967).

21. V. D. GAVRILOV et al., *Atomnaya Energiya*, **41**, 85 (1975).

22. K. D. ZHURAVLEV et al., *Atomnaya Energiya*, **39**, *4*, 285 (1975).

23. R. E. SLOVACEK, D. S. CRAMER, E. B. BEAN, J. R. VALENTINE, R. W. HOCKENBURY, and R. C. BLOCK, "^{238}U(n,f) Measurements Below 100 keV," *Nucl. Sci. Eng.*, **62**, 455 (1977).

24. C. WAGEMANS, *Nucl. Instrum. Methods Phys. Res.*, **A236**, 429 (1985).

25. K. KOBAYASHI et al., "Fission Cross Section Measurement of Am-241 Between 0.1 eV and 10 keV with Lead Slowing-Down Spectrometer," *Proc. Int. Conf. Nucl. Data Science and Technology*, Gatlinburg, Tennessee, Vol. 1, p. 242 (1994).

26. M. MIYOSHI, "Measurement of Neutron Energy Dependent Fission Cross Section of ^{241}Am," MS Thesis, Kyoto University, Department of Nuclear Engineering (1995) (in Japanese).

27. M. OBU, "Preparation and Characteristics of Fission Chambers with Actinide Nuclides," JAERI-M 9757, Japan Atomic Energy Research Institute (1981).

28. K. KOBAYASHI, S. YAMAMOTO, A. YAMANAKA et al., "Characteristics of the Kyoto University Lead Slowing-Down Spectrometer Coupled to an Electron Linac," *Nucl. Instrum. Methods Phys. Res. A*, **385**, 145 (1997).

29. A. YAMANAKA et al., *J. Nucl. Sci. Technol.*, **30**, *9*, 863 (1993).

30. K. KOBAYASHI et al., *J. Nucl. Sci. Technol.*, **31**, *12*, 1239 (1994).

31. "MCNP—A General Monte Carlo Code for Neutron and Photon Transport, Version 3A," LA-7396-M, Rev. 2, Los Alamos National Laboratory (1986).

32. A. BERGMAN et al., *Proc. Ist Int. Conf. Peaceful Use of Atomic Energy*, Vol. 4, p. 135, United Nations (1955).

33. K. H. BECKURTS and K. WIRTZ, *Neutron Physics*, p. 342, Springer-Verlag, New York (1964).

34. S. USUDA and N. KOHNO, *Separation Science Technol.*, **23**, 1119 (1988).

35. N. SHINOHARA and N. KOHNO, *Appl. Radiat. Isot.*, **40**, 41 (1989).

36. T. TSURUTA et al., *J. Nucl. Sci. Technol.*, **29**, *11*, 1108 (1992).

37. K. KANDA et al., *Nucl. Instrum. Methods*, **148**, 535 (1978).

38. E. M. GRYNTAKIS et al., *Radiochimica Acta*, **22**, 128 (1975).

39. "Nuclear Data Standards for Nuclear Measurements," Technical Reports Series, No. 227, International Atomic Energy Agency (1983).

付録C

Journal of NUCLEAR SCIENCE and TECHNOLOGY, Vol. 36, No. 1, p. 20–28 (January 1999)

Measurements of Neutron-induced Fission Cross Section of Americium-243 from Thermal Neutron Energy to 15 keV Using Lead Slowing-down Spectrometer and Thermal Neutron Facility

Katsuhei KOBAYASHI[*1,†1], Tetsuya KAI[*1,†2], Shuji YAMAMOTO[*1], Hyun-Je CHO[*1,†3], Yoshiaki FUJITA[*1], Itsuro KIMURA[*2] and Nobuo SHINOHARA[*3]

[*1] *Research Reactor Institute, Kyoto University*
[*2] *Department of Nuclear Engineering, Kyoto University*
[*3] *Department of Materials Science and Engineering, Japan Atomic Energy Research Institute*

(Received May 21, 1998)

The neutron-induced fission cross section of ^{243}Am was measured relative to that of ^{235}U from thermal neutron energy to 15 keV making use of a double fission chamber with ^{243}Am and ^{235}U electrodeposited layers.

The data above 0.05 eV were measured using a lead slowing-down spectrometer coupled to an electron linear accelerator. A relative measurement to the ^{10}B(n, α) reaction was also made using a BF_3 counter at energies below 1 keV, and normalized to the absolute value obtained by using the cross section of the ^{235}U(n, f) reaction between 200 eV and 1 keV. The existing experimental data by Wisshak and Käppeler, and by Knitter and Budtz-Jørgensen are in general agreement with the current measurement in the relevant energy region. However, the data by Seeger are considerably higher. The evaluated nuclear data in JENDL-3.2, ENDF/B-VI and JEF-2.2, whose data were broadened by the energy resolution function of the spectrometer, have been compared with the measured result.

The fission cross section for thermal neutrons was measured in a neutron field with a pure Maxwellian spectrum. The derived result at 0.0253 eV is 81.3±2.5 mb. The data by Wagemans *et al.* and in ENDF/B-VI are close to the current measurement. However, the values by Asghar *et al.*, Gavrilov *et al.* and Mughabghab, and the evaluated data in JENDL-3.2 and JEF-2.2 are discrepant from the current result by a factor of 1.4 to 2.4.

KEYWORDS: neutron-induced fission cross sections, measurement, americium 243, resonance energy region, lead slowing-down spectrometer, back-to-back type double fission chamber, thermal neutron cross section, Maxwellian distribution, JENDL-3.2, ENDF/B-VI, JEF-2.2

I. Introduction

Americium-243 is a burdensome minor actinide which is abundantly produced next to the ^{237}Np and ^{241}Am nuclides in spent-fuels of light water reactors. Nuclear data of the minor actinides are of great importance for an understanding of the burn-up characteristic of MOX (Mixed Oxide) or Pu fuels and for the design of systems for spentfuel reprocessing or radioactive waste disposal. In recent years, a great interest has been taken in the nuclear transmutation of minor actinides using conventional or advanced reactors and accelerator-driven subcritical reactors[1]-[8]. The fission cross section is one of the fundamental data for the investigation of the transmutation. The neutron-induced fission cross section of ^{243}Am rises at ~0.3 MeV and reaches up to ~1.5 barns around ~MeV like a threshold reaction[9]. The cross section has appreciable values in the thermal, intermediate and resonance energy regions. Then, the fission cross section data are important not only for the systematic studies of fission mechanism but also for transmutation with light water reactors because the neutron fluxes are high in the lower energy region.

In recent years, considerable progress has been achieved in the fission cross section measurements for minor actinide isotopes[10]-[18]. Concerning the ^{243}Am nuclide, Wagemans *et al.* measured the thermal neutron fission cross section using a neutron guide at the Institut Laue-Langevin (ILL)[16]. The fission fragments were detected with a surface barrier detector. Knitter and Budtz-Jørgensen measured the ^{243}Am(n, f) cross sec-

[*1] *Kumatori-cho, Sennan-gun, Osaka-fu 590-0494.*
[*2] *Yoshida-honmachi, Sakyo-ku, Kyoto 606-8501.*
[*3] *Tokai-mura, Naka-gun, Ibaraki-ken 319-1195.*
[†1] Corresponding author, Tel. +81-724-51-2346, Fax. +81-724-51-2602, E-mail: koba@rri.kyoto-u.ac.jp
[†2] Present address: Japan Atomic Energy Research Institute, *Tokai-mura, Naka-gun, Ibaraki-ken 319-1195.*
[†3] Visiting Scientist from University of Ulsan, KOREA.

tions using a 7 MV Van de Graaff accelerator and an electron linear accelerator at Geel (GELINA) as pulsed neutron sources[17]. They measured the fission cross section with a back-to-back type double fission chamber relative to the standard fission cross section of ^{235}U. Wisshak and Käppeler also obtained the ^{243}Am(n, f) cross section with an NE-213 liquid scintillator using a 3 MV pulsed Van de Graaff accelerator[18]. Seeger measured the fission cross section by the neutron time-of-flight (TOF) method using a nuclear explosion[19]. However, the fission cross section data are not enough both in quality and quantity, especially in the thermal and resonance neutron energy regions[9][20]. According to the data base NESTOR-2[20] which was converted from EXFOR, the measured data are still scanty and no datum has been reported below 50 eV except for those at thermal neutron energy. Kikuchi[21] calculated the fission cross section based on the resonance parameters, which were determined in the total cross section measurements by Simpson *et al.*[22]. However, theoretical estimation is not always accurate enough for the minor actinide. For example, among the evaluated data files of ENDF/B-VI[23], JENDL-3.2[24] and JEF-2.2[25], there exist marked discrepancies at energies below a few hundreds of kilo-electron-volts. One of the reasons may be due to lack of the experimental data in the relevant energy region.

In the present study, we have prepared a high pure ^{243}Am sample by an anion-exchange method to remove the ^{239}Pu impurity produced through the α-decay of ^{243}Am. After the chemical purification, the cross section of the ^{243}Am(n, f) reaction has been measured in the range of 0.05 eV to 15 keV relative to that of the ^{235}U(n, f) reaction by making use of a back-to-back (BTB) type double fission chamber and a lead slowing-down spectrometer coupled to the 46 MeV electron linear accelerator (linac) of the Research Reactor Institute, Kyoto University (KURRI). Below 1 keV, in order to avoid the interference between the resonance peaks of ^{243}Am and ^{235}U, measurement has been done relative to the ^{10}B(n, α) reaction using a BF_3 counter. The result has been normalized to that measured relative to the ^{235}U(n, f) reaction with the BTB chamber at energies between 200 eV and 1 keV. The current measurement is compared with the existing experimental data[17]-[19] and with the evaluated data in ENDF/B-VI[23], JENDL-3.2[24] and JEF-2.2[25].

The thermal neutron cross section has also been measured with the aforementioned fission chamber in a standard neutron spectrum field having a pure Maxwellian distribution in the Kyoto University Reactor (KUR) at KURRI. The current result is compared with the previous experimental and the evaluated data[16][23]-[28].

II. Samples and Fission Chamber

1. Chemical Purification of Am-243

The americium sample, which had been prepared by using a mass separator, was purchased from Oak Ridge National Laboratory (ORNL). The isotopic purity of ^{243}Am is 99.96% and the major impurity is ^{241}Am of about 0.04%. By an anion-exchange method[29], the americium sample was purified from other actinides (U, Np, Pu and Cm) that disturb the cross section measurement for the ^{243}Am(n, f) reaction[30]. The sample was dissolved in a mixture of 0.1 ml concentrated nitric acid and 1 ml of ethyl alcohol. After the sample solution was charged into a column of 4 mm in diameter and 40 mm in height, which was packed with MCI GEL CA06Y anion-exchange resin, americium was isolated by eluting with a mixture of 0.5 M nitric acid and 80% of methyl alcohol at room temperature.

The ^{243}Am layer was prepared by an electrodeposition method: The solution of the americium sample purified by the anion-exchange method was evaporated until dryness, then dissolved in a mixture of 5 μl of 0.1 M nitric acid and 5 ml of isopropyl alcohol. The mixture solution was put into an electrodeposition cell and electrolyzed under the conditions of 200 V and 5 mA[31]. The ^{243}Am sample was electrodeposited on a stainless steel disk of 28 mm in diameter and 0.2 mm in thickness, and the active area was 20 mm in diameter. The ^{243}Am deposit was sintered with a gas burner to fix the americium layer on the disk by transforming the deposit into an americium oxide.

After the chemical purification and deposit preparation, the α-ray spectrum of the ^{243}Am deposit was measured with a silicon surface barrier detector. **Figure 1** shows the pulse height distribution of the ^{243}Am α-ray spectrum, where one can see small α-ray peaks due to residual impurities. Analyzing the α-ray spectrum, the activity ratios of ^{244}Cm/^{243}Am and ^{241}Am/^{243}Am in the sample deposit were determined to be 4×10^{-5} (atom ratio: 9.8×10^{-8}) and 7×10^{-3} (atom ratio: 4.1×10^{-4}), respectively. We found that no other actinides were detected in the sample deposit. It should be noted that even if a pure ^{243}Am sample has been obtained, the impurity of ^{239}Pu is gradually accumulated in the ^{243}Am

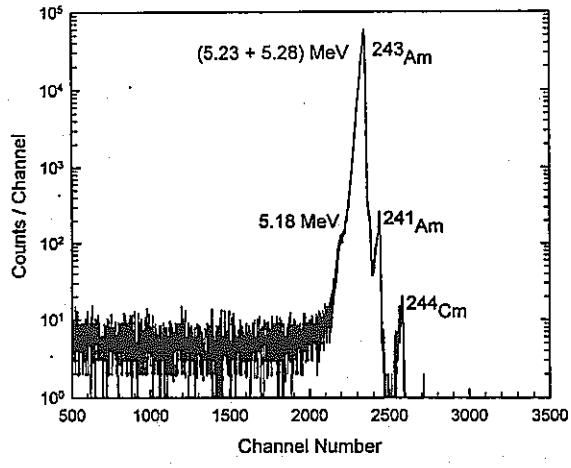

Fig. 1 Pulse height distribution of α-ray spectrum from the ^{243}Am sample

deposit through its α-decay. The impurity may influence the measurement of the ^{243}Am(n, f) cross section and make the apparent fission cross section larger, especially at the big resonance of 0.3 eV[32]. Therefore, we have to be careful with the growth of the ^{239}Pu as impurity in the ^{243}Am sample prepared in this study.

2. Number of Am-243 and U-235 Atoms

The amount of ^{243}Am deposited was determined by analyzing the α-ray spectrum having energies in the range of 5.18 to 5.28 MeV. Considering the detection efficiency, the α-ray intensities and the half-life, the number of the ^{243}Am atoms was found to be $(3.33\pm0.05)\times10^{17}$, as given in **Table 1**, where the errors were estimated by taking account of (a) counting statistics of the activity measurements, (b) uncertainties in geometrical detection efficiencies, and (c) uncertainties in the decay data used. The number of the atoms obtained by the α-ray measurement was confirmed by the measurement of the 74.7 keV γ-ray from ^{243}Am with a HPGe detector.

Highly enriched uranium oxide (^{235}U: 99.91%) purchased from ORNL was electrodeposited on a stainless steel disk by using the same technique as for the americium sample. Alpha-ray measurement was carried out, and the number of the ^{235}U atoms was determined as shown in Table 1, by analyzing the α-ray spectrum at energies of 4.152 to 4.597 MeV. The 185.7 keV γ-ray of ^{235}U was also measured.

3. Double Fission Chamber

An ionization chamber with two parallel plate electrodes has been employed for the current measurement. The chamber is made of aluminum and is 40 mm in diameter and 39 mm in length, and the wall thickness of the chamber is ~2 mm, as seen in **Fig. 2**. Since the back sides of the ^{243}Am and the ^{235}U deposits face each other, it is called a back-to-back (BTB) type double fission chamber. The distance between the electrode and the deposited layer is 8 mm. The electrodes act as anodes at +400 V, from which the fission fragment pulses are taken. The fission chamber is filled with a mixed gas of 97% Ar and 3% N_2 at a pressure of 1 atm. At this gas pressure, the mean range of α-rays reaches ~36 mm, while that of fission fragments is ~20 mm. Therefore, in this design, the fission chamber collects most of the energy of the fission fragments but not that of the α-rays, which results in getting good discrimination between pulses of α-ray and fission fragment. **Figure 3** shows a typical pulse height distribution of fission fragments from the ^{243}Am layer in a measurement for 4 h. The ^{235}U deposit of ~3.5 μg/cm^2 and the ^{243}Am deposit of ~43 μg/cm^2 were set at the center of the BTB chamber. Since the ^{243}Am and the ^{235}U deposits were thin, fission pulses could clearly be discriminated from background ones caused by the α-rays.

Table 1 Numbers of atoms for the ^{243}Am and the ^{235}U deposits obtained by α- and γ-ray measurements

Method	^{243}Am deposit	^{235}U deposit
α spectroscopy	$(3.33\pm0.05)\times10^{17}$	$(2.81\pm0.03)\times10^{16}$
γ spectroscopy	$(3.27\pm0.16)\times10^{17}$	$(2.86\pm0.04)\times10^{16}$

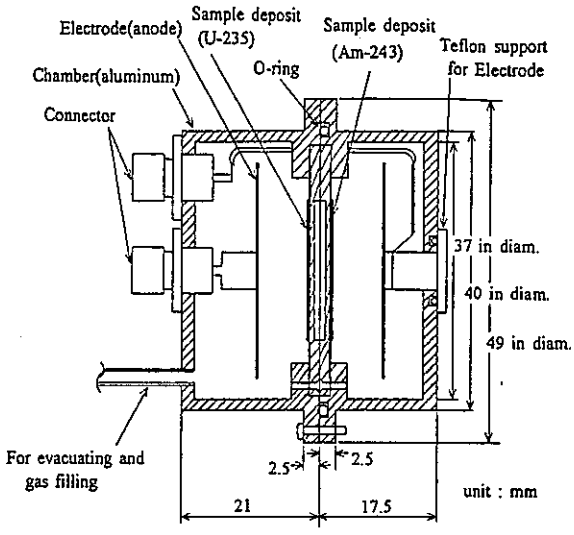

Fig. 2 Cross sectional view of the BTB chamber

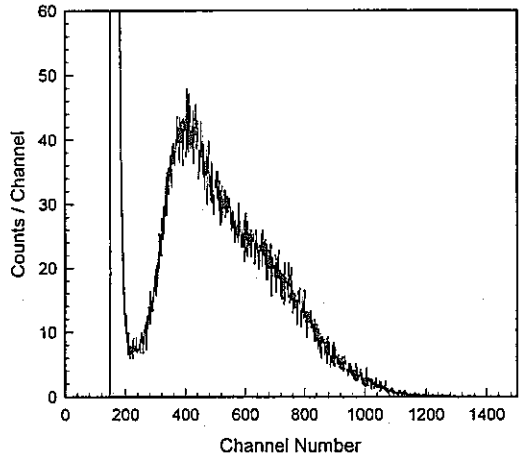

Fig. 3 Pulse height distribution of fission fragments for ^{243}Am measured with the BTB chamber

III. Lead Slowing-down Spectrometer

Lead is one of the heavy mass elements and most of its neutron total cross section is the elastic scattering cross section. When pulsed fast neutrons are put into the central region of a large lead assembly, the neutrons present convergence behavior and keep an asymptotic form at each energy corresponding to the slowing-down time. There exists a relation $E=K/t^2$ between the mean energy E in keV of the slowing-down neutrons and the slowing-down time t in μs[33][34], where K is

the slowing-down constant. The energy resolution of the slowing-down spectrometer is theoretically given as the full-width-at-half-maximum (FWHM) by[33][34]

$$(\Delta E/E)_{\mathrm{FWHM}} = 2.35 \times (\Delta\sigma/\sigma)_{\mathrm{Gaussian}} = 2.35 \times \{8/(3A)\}^{1/2} = 26.7\%, \quad (1)$$

where $(\Delta\sigma/\sigma)_{\mathrm{Gaussian}}$ is the standard deviation in a Gaussian function and A is the atomic mass (207.2) of lead.

A lead slowing-down spectrometer has been installed in coupling to the 46 MeV linac at KURRI. This Kyoto University Lead Slowing-down Spectrometer (KULS)[35] is composed of 1,600 lead blocks (each size: $10\times10\times20\,\mathrm{cm}^3$, purity: 99.9%) and the blocks are piled up to make a cube of $1.5\times1.5\times1.5\,\mathrm{m}^3$ (about 40 t in weight) without any structural materials, as shown in Fig. 4. The KULS is covered with Cd sheets of 0.5 mm in thickness to shield it against low energy neutrons scattered from the surroundings. At the center of the KULS, an air-cooled photoneutron target of tantalum is set to generate pulsed fast neutrons. One of the experimental holes in the KULS is covered by bismuth layers of 10 to 15 cm in thickness to shield a detector from high energy capture γ-rays (6 to 7 MeV) produced by the Pb(n, γ) reaction in the spectrometer. The bismuth layers are useful to reduce background counts due to photofissions in fission samples[36].

Characteristics of behavior of neutrons in the KULS have been studied by experiments using the resonance filter method[35]. The neutron slowing-down time and the energy resolution of the KULS were measured with a BF_3 counter and an Ar gas counter. The dips or the bumps that are observed in the slowing-down time spectrum correspond to the resonance energies of the filter material. The slowing-down constant K in the relation of $E=K/t^2$ was obtained by the least squares method using the measured relation between the neutron slowing-down time t in μs and the average neutron energy E in keV. The constant K was determined to be 190±2 and 156±2 (keV·μs^2) for the bismuth and the lead experimental holes, respectively[35]. The energy resolution for the experimental holes was also deduced from the measured data to be about 40% at energies between a few electron-volts and about 500 eV and was worse than that below a few electron-volts and above about 500 eV[35]. The relation between the neutron slowing-down time and the energy, and the energy resolution were also obtained by calculations using the Monte Carlo code MCNP[37]. The results were in good agreement with the experimental ones[35].

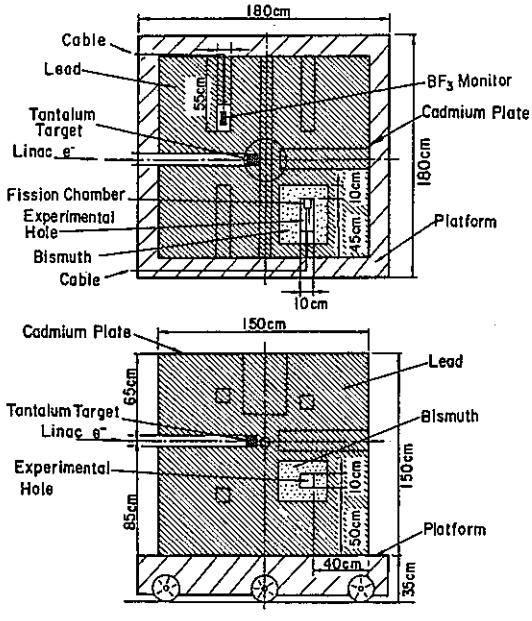

Fig. 4 Cross sectional view of Kyoto University Lead Slowing-down Spectrometer, KULS (Upper: Top view, Lower: Side view)

IV. Measurement and Analysis

1. Fission Ratio Measurement

The fission counts at the slowing-down time t (in μs) can be converted to those at energy E (in keV) by using the relation of $E=K/(t+t_0)^2$, where t_0 is for the zero time correction[35]. The energy-dependant cross section of the ^{243}Am(n, f) reaction is given by the following relation:

$$\sigma_{\mathrm{Am}}(E) = \frac{C_{\mathrm{Am}}(E)}{C_{\mathrm{U}}(E)} \cdot \frac{N_{\mathrm{U}}}{N_{\mathrm{Am}}} \sigma_{\mathrm{U}}(E), \quad (2)$$

where $C_{\mathrm{Am}}(E)$: Fission counts of ^{243}Am at energy E
$C_{\mathrm{U}}(E)$: Fission counts of ^{235}U at energy E
N_{U}: Number of ^{235}U atoms in the ^{235}U deposit
N_{Am}: Number of ^{243}Am atoms in the ^{243}Am deposit
$\sigma_{\mathrm{U}}(E)$: Energy-dependent reference cross section of the ^{235}U(n, f) reaction.

The fission cross section of ^{235}U is a well-known reference cross section and has been used to determine the neutron flux in the current measurement. The cross section values of $\sigma_{\mathrm{U}}(E)$ have been taken from ENDF/B-VI[23].

The lead slowing-down spectrometer KULS was driven by the 46 MeV electron linac at KURRI. The typical operating conditions of the linac during the experiments were as follows: The pulse repetition rate was 150 Hz, the pulse width 22 ns, the electron peak current ~0.8 A, and the electron energy ~31 MeV. After the measurement has been performed for more than ~120 h in the bismuth hole, the deposited layers of ^{243}Am and ^{235}U in the BTB chamber were interchanged, and another measurement in the hole was made for ~130 h to obtain the data with less systematic uncertainty.

A background run was carried out using the BTB chamber without the sample deposits. Few fission counts were observed in the slowing-down time spectrum for a run longer than 30 h. It was found that the effect of

the background counts to the $^{243}Am(n, f)$ cross section was ~0.2% at most in the minimum cross section region, whereas the background counts for the ^{235}U chamber could be ignored comparing to the foreground ones.

Neutrons may be scattered by the structural materials of the BTB chamber before arriving at the deposit layers. The inscattered neutrons, which are not directly observable, may be another source of disturbance or background for the current measurement. The effect of the inscattered neutrons was estimated by calculations using the MCNP code and slightly corrected for as done before[15].

2. BF_3 Counter

Below 200 eV, there exist strong neutron resonance peaks in the fission cross sections of ^{243}Am and ^{235}U. Therefore, we have employed the $^{10}B(n, \alpha)$ cross section that shows a smooth and a good $1/v$ energy dependence in the relevant energy region. The $^{10}B(n, \alpha)$ reaction is a well-known standard cross section and is often applied to cross section measurements as a reference. In order to measure the energy-dependent neutron flux in the resonance energy region, a BF_3 counter was placed in the bismuth hole of the KULS instead of the BTB chamber[15]. The BF_3 counter was of a cylindrical type, 50 mm in effective length, 12 mm in diameter with a gas pressure of 1 atm and high-voltage bias of 1,100 V. In the relative cross section measurement with the BF_3 counter, $C_U(E)$ and $\sigma_U(E)$ in Eq. (2) are replaced with those for the $^{10}B(n, \alpha)$ reaction, respectively. The ratio of N_U/N_{Am} is left same as before, because the measurement with the counter is a relative one.

3. Electronics and Data Taking

Two identical electronic circuits were employed for the fission count measurements by the ^{243}Am and the ^{235}U layers in the BTB chamber, as we did before[13][15]. Through the amplifiers and the discriminators, signals from the chamber were fed into a time digitizer, which was initiated by the linac electron burst. The slowing-down time data of the fission events were stored in a data acquisition system for each measurement of 4 to 5 h duration. Two sets of 4096 channels were allotted to the slowing-down time measurements for the BTB chamber with a channel width of 62.5 ns to 0.5 μs. Pulse height distributions of fission events from the ^{243}Am and the ^{235}U deposits were also measured with each 4096-channel pulse height analyzer together with the slowing-down time measurements.

For the relative measurement to the $^{10}B(n, \alpha)$ cross section, output signals from the BF_3 counter were also fed to the time digitizer through the amplifiers and the discriminators, and were stored in almost the same way as for the measurement with the BTB chamber.

V. Measurement of the Thermal Neutron Cross Section

1. Thermal Neutron Facility

The KUR at KURRI has a thermal neutron facility with a 1.4 m thick heavy water tank. The irradiation room is 2.4×2.4×2.4 m^3 and is surrounded by 90 cm-thick heavy concrete shields[38]. The leakage neutrons from the heavy water tank can be used as a thermal neutron source of a plane-type in a large space. Kanda *et al.* measured the neutron spectrum from the heavy water tank by the TOF technique using a fast chopper[39]. The measured spectrum showed good agreement with a Maxwellian distribution having a neutron temperature of 60°C. The cadmium ratio measured by gold foils with and without a cadmium cover of 0.7 mm in thickness was larger than 5,000, and so the contribution of epithermal neutrons to the thermal neutron cross section measurement can be neglected.

2. Experimental Method

The thermal neutron cross section for the $^{243}Am(n, f)$ reaction was measured employing the heavy water thermal neutron facility of the KUR, making use of the BTB chamber with the ^{243}Am and the ^{235}U layers. The chamber was set in the irradiation room and exposed to thermal neutrons for about 10 h during the nominal power operation of 5 MW of the KUR. The irradiation was repeated by exchanging the ^{243}Am layer with the ^{235}U in the BTB chamber. Fission pulses from each layer were led to each 2048-channel pulse height analyzer through the amplifiers and the discriminators. Each of the fission counts was obtained by integrating the pulse height distribution above the discrimination level.

3. Measurement and Analysis of the Cross Section

The thermal neutron cross section $\langle\sigma_{th}\rangle$ averaged over the Maxwellian distribution is given as

$$\langle\sigma_{th}\rangle = \frac{\sigma_{th}(v_o)}{1.128}\, g(T_n)\, \frac{\sqrt{T_o}}{\sqrt{T_n}}, \tag{3}$$

where v_o is 2,200 m/s, T_o is 293.6 K, T_n is the neutron temperature, and $g(T_n)$ is the Westcott's g factor[40]. Then the thermal neutron cross section σ_{Am} of the $^{243}Am(n, f)$ reaction at a neutron energy of 0.0253 eV is obtained as follows by rewriting Eq. (2) for the KULS measurement,

$$\sigma_{Am} = \frac{C_{Am}}{C_U} \cdot \frac{N_U}{N_{Am}} \cdot \frac{g_U(T_n)}{g_{Am}(T_n)}\, \sigma_U, \tag{4}$$

where C_{Am}: Fission counts of ^{243}Am
C_U: Fission counts of ^{235}U
$g_U(T_n)$: g factor of ^{235}U
$g_{Am}(T_n)$: g factor of ^{243}Am
σ_U: Cross section at 0.0253 eV of the $^{235}U(n, f)$ reaction.

The fission cross section of ^{235}U was taken from the evaluated data in ENDF/B-VI and the g factors of 1.017 for ^{243}Am and 0.9703 for ^{235}U were calculated by the method in Ref. (41) using the ENDF/B-VI data. We deduced the result by taking the average value of two C_{Am}/C_U data, which were obtained by exchanging the positions of the ^{243}Am and the ^{235}U layers in the BTB chamber. The fission counts were determined by linearly extrapolating the curve of the pulse height distribution near the discrimination level.

VI. Results and Discussion

Making use of the BTB chamber and the KULS, the cross section of the ^{243}Am(n, f) reaction was measured relative to that of the ^{235}U(n, f) reaction at energies from 0.05 eV to 15 keV. In the resonance energy region below 1 keV, the fission cross section was also measured relative to the ^{10}B(n, α) cross section to avoid the resonance interference between ^{243}Am and ^{235}U, and the result was normalized to the absolute value of the ^{243}Am fission cross section determined relative to the ^{235}U(n, f) cross section between 200 eV and 1 keV. The cross section data were obtained by summing up the slowing-down time data in intervals of ~0.12 lethargy width.

The dead time correction for the ^{235}U fission chamber was <0.03%, and that for the ^{243}Am was negligibly small. Concerning the effects of (a) absorption of the fission fragments in the ^{243}Am and the ^{235}U deposits, (b) anisotropic angular distribution of the fission fragments, and (c) photofission in the deposits on the resultant fission cross section of ^{243}Am, we have assumed that they are negligible as described in the earlier paper[13]. Since the ^{243}Am sample was chemically purified and almost free from impurities, no correction was made for the impurity effect, except for the ^{239}Pu growth which accumulated through the α-decay of ^{243}Am as noted below.

Figure 5 shows the apparent cross sections measured at 4 weeks, 5 months and 13 months after the chemical purification. One can see that the cross sections near 0.3 eV are getting larger with the time due to the accumulation of ^{239}Pu impurity by the α-decay of ^{243}Am. By repeating the experiments as seen in Fig. 5, we could experimentally investigate the time dependent influence of the ^{239}Pu impurity. **Figure 6** is the calculated results simulating the impurity growth of ^{239}Pu after the chemical purification. The calculated time-dependence of the ^{239}Pu impurity agreed well with the measurements shown in Fig. 5. Correcting for the time-dependent ^{239}Pu contribution, we could deduce the fission cross section of ^{243}Am measured at the time when the chemical process was done. The current result from 0.05 eV to 15 keV is shown in **Fig. 7** and compared with the existing experimental data. One can see in the figure that there are only very few experimental data below 10 keV. No datum has been measured before at energies below 50 eV except at thermal neutron energy[20]. The data by Knitter and Budtz-Jøgensen[17], and by Wisshak and Käppeler[18] are close to the current measurement in the

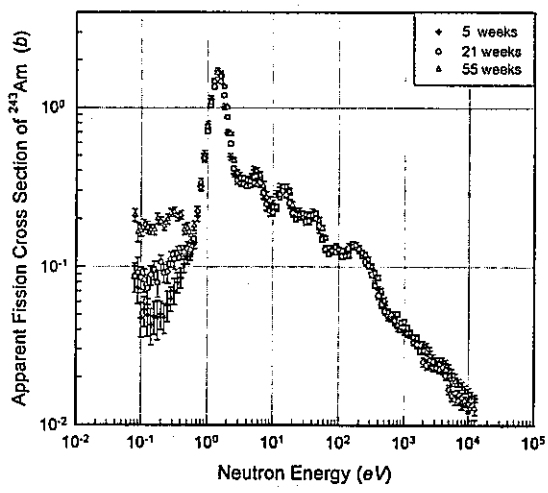

Fig. 5 Comparison of the measured data *vs.* the time after the chemical purification

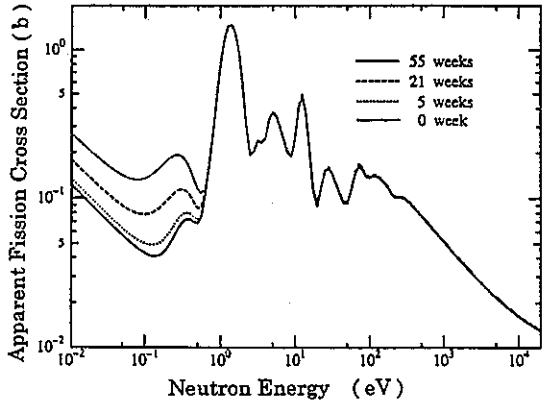

Fig. 6 Time-dependent contribution of ^{239}Pu impurity to the measurement of ^{243}Am fission cross section

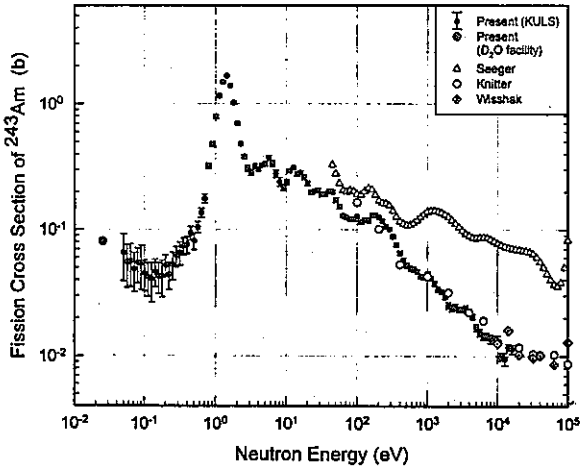

Fig. 7 Comparison of the existing experimental data of ^{243}Am with the current measurement

The data by Seeger are broadened by the energy resolution of the KULS.

relevant energy region. However, a bombshot experiment by Seeger[19] gives considerably higher values than the current measurement. In the figure, the data measured by Seeger have been broadened with the energy resolution function of the KULS.

The experimental uncertainties for the current measurement are summarized in **Table 2**. The discrimination level was set in the minimum count region between the fission and the noise counts in the pulse height distribution. Consequently, uncertainty to determine the fission counts was estimated to be 2.0% for ^{243}Am and 0.65% for ^{235}U, respectively. Considering the gain shift in the detection system, the discrimination level was checked and determined every 10 to 20 h during the experiment. The number of atoms in each ^{243}Am and ^{235}U deposit was determined by the α-ray measurements and confirmed by the γ-rays, as seen in Table 1. The uncertainties of the reference cross sections of the ^{235}U(n, f) and ^{10}B(n, α) reactions were estimated to be 2 to 4% and 2% (deviation from the $1/v$ form) in the relevant energy range[42][43]. The uncertainty related to the accumulated ^{239}Pu impurity is about 4% at most near 0.3 eV and is almost negligible above around 0.7 eV. The total uncertainty in the measured value of the ^{243}Am fission cross section is estimated to be more than 4%, and 40% at worst in the lower energy region.

The evaluated data in ENDF/B-VI, JENDL-3.2 and JEF-2.2 are compared with the current measurement in **Fig. 8**, where the evaluated data have been broadened with the energy resolution function of the KULS. Three evaluated data are discrepant each other. The ENDF/B-VI data are in general agreement with the measurement except for the energy region from 15 to 60 eV. At energies above 300 eV, the evaluated data are higher than the measurement. As seen in **Table 3**, the ENDF/B-VI data is lower by about 40% between 15 and 60 eV than the current data, although the discrepancies from the measurement are within 20% in other regions. The JENDL-3.2 data above 100 eV are lower by more than 20% than the current result, but higher below 0.2 eV on the contrary. The data in JEF-2.2 are markedly lower than the other evaluations and the measurement, although they are in good agreement at the resonance energy of 1.2 eV. Near the narrow dip of around 2.7 eV and the sharp bump at

Table 2 Experimental uncertainties for the current measurements

Uncertainties due to	Error (%)	
	KULS experiment	Thermal neutron cross section measurement
Statistical error for ^{243}Am	0.09 to 40.2	0.4
Statistical error for ^{235}U	0.08 to 1.5	0.04
Assignment of fission counts for ^{243}Am	<2.0	1.5
Assignment of fission counts for ^{235}U	<0.65	1.1
Number of atoms of ^{243}Am	1.5	1.5
Number of atoms of ^{235}U	1.2	1.2
g-factor of ^{243}Am	—	~1.0
g-factor of ^{235}U	—	0.12
Cross section of the ^{235}U(n, f) reaction	2 to 4	<1
Cross section of the ^{10}B(n, α) reaction	2	—
Setting ^{243}Am and ^{235}U deposits in the BTB chamber	<0.3	0.25
Correction for inscattered neutrons by the BTB chamber	<0.2	~0
Correction for the influence of the accumulated ^{239}Pu impurity	~0 to 4	0.2
Background subtraction	<0.2 to 0.5	~0

	Energy range (eV)	Error in average (%)
Total uncertainties	0.0253	3.1
	0.045–0.1	35.4
	0.1–0.7	19.8
	0.7–2.0	4.5
	2.0–15	6.1
	15–60	5.6
	60–200	5.2
	200–1,000	5.7
	1,000–10,000	7.0

Table 3 Comparison of mean values of the ^{243}Am fission cross section from current work with those from ENDF/B-VI, JENDL-3.2, and JEF-2.2

Energy range (eV)	Average cross section (b)			
	ENDF/B-VI	JENDL-3.2	JEF-2.2	Current
0.1–0.7	0.0579	0.0638	0.0290	0.0712±0.0122
0.7–2.0	0.8482	0.9498	0.7431	0.9200±0.0249
2.0–15	0.3066	0.2958	0.1191	0.3338±0.0144
15–60	0.1271	0.2344	0.0421	0.2089±0.0085
60–200	0.1361	0.1056	0.0235	0.1241±0.0043
200–1,000	0.0805	0.0501	0.0125	0.0710±0.0028
1,000–10,000	0.0298	0.0177	0.0062	0.0241±0.0013

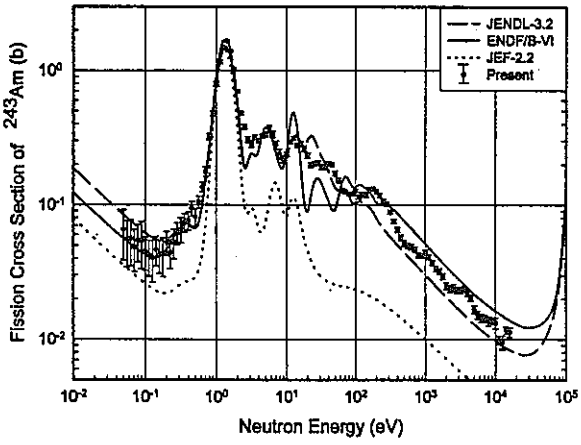

Fig. 8 Comparison of the evaluated fission cross section of ^{243}Am with the current measurement
The evaluated data are broadened by the energy resolution of the KULS.

12 eV, one can see discrepancies between the evaluated and the measured data. The reason would be due to the insufficient resolution function of the lead slowing-down spectrometer. It is obvious that the JEF-2.2 data are lower than the other evaluations and the current measurement except for the big resonance region at 1.2 eV.

The thermal neutron cross section of the ^{243}Am(n, f) reaction was obtained relative to the reference value of 586.2 b for the ^{235}U(n, f) reaction in ENDF/B-VI, after correction for the influence of the ^{239}Pu impurity which accumulated for 3 months after the chemical purification. The current result at 0.0253 eV is 81.3±2.5 mb and is compared with the existing experimental and evaluated data in Table 4. The current value is in good agreement with that extrapolated from the KULS data, as shown in Fig. 7. The main sources of uncertainties in the current measurement are also summarized in Table 2. Other uncertainties and corrections are considered to be small and can be neglected as in the KULS experiment. The total experimental uncertainty was estimated to be 3.1% as the root of quadratic sum of the aforementioned uncertainties.

Table 4 Thermal neutron cross section (2,200 m/s value) for the ^{243}Am(n, f) reaction

Cross section (mb)	Reference
81.3±2.5	Present work
74.0±4.0	Wagemans *et al.* (1989) (Ref. (16))
198.3±4.2	Asghar *et al.* (1979) (Ref. (27))
200±110	Gavrilov *et al.* (1976) (Ref. (28))
116.1	JENDL-3.2 (1998) (Ref. (24))
49.56	JEF-2.2 (1994) (Ref. (25))
74	ENDF/B-VI (1991) (Ref. (23))
198.3±4.3	Mughabghab (1984) (Ref. (26))

The data by Wagemans *et al.*[16] and in ENDF/B-VI[23] agree with the current measurement within the range of the experimental uncertainties. However, the data by Asghar *et al.*[27], Gavrilov *et al.*[28], Mughabghab[26] and in JENDL-3.2[24] are larger by a factor of 1.4 to 2.4 than the current result. The JEF-2.2 data[25] is lower by about 40%.

VII. Conclusion

The cross section of the ^{243}Am(n, f) reaction has been measured from 0.05 eV to 15 keV relative to that of the ^{235}U(n, f) reaction, making use of the BTB-type double fission chamber and the lead slowing-down spectrometer KULS at KURRI. The experimental data by Knitter and Budtz-Jørgensen, and by Wisshak and Käppeler are close to the current measurement in the overlapping energy region. However, the data measured by Seeger are considerably higher. The ENDF/B-VI data are in general agreement with the current measurement except for the energy regions from 15 to 60 eV and above 300 eV. The evaluated values in JENDL-3.2 are lower than the measurement above 100 eV and higher below 0.2 eV. The JEF-2.2 data are obviously low except for the resonance peak at 1.2 eV.

The cross section of the ^{243}Am(n, f) reaction at 0.0253 eV was obtained to be 81.3±2.5 mb using a pure Maxwellian distribution field and the BTB chamber. The current measurement is in good agreement with the value extrapolated from the KULS data. Although the

data by Wagemans *et al.* and in ENDF/B-VI are close to the current result, the JENDL-3.2 and other measured data are higher by a factor of 1.4 to 2.4 than the current measurement, while the JEF-2.2 data is lower by ~40%.

We could measure the cross section of the ^{243}Am(n, f) reaction in the lower/resonance energy region, where the experimental data have scarcely been obtained before.

ACKNOWLEDGMENTS

The authors would like to express their thanks to the linac staff of the Research Reactor Institute, Kyoto University (KURRI) for making it possible to operate the accelerator steadily. They are also indebted to the Nuclear Data Center, the Japan Atomic Energy Research Institute (JAERI), for supplying the evaluated nuclear data. Technical assistance by Hideki Yamamoto of Kyoto University is appreciated. One of the authors (H.C.) is grateful to Profs. Sang Kyun Nha and Seung Kook Ko of Department of Physics, University of Ulsan, Korea for their valuable discussions and encouragement to carry out the study.

This study was supported by a Grant-in-Aid of Scientific Research from the Ministry of Education, Science, Sports and Culture (06452430). A part of this work was also performed by the financial support from Power Reactor and Nuclear Fuel Development Corp. and under the Project Research of Cooperative Use Program at KURRI.

—REFERENCES—

(1) Lancaster, D.: *Proc. of Int. Conf. and Technol. Exposition on Future Nucl. Systems: Global '93*, Seattle, Washington, Sept. 12–17, 1993, ANS, La Grange Park, Illinois, p. 609 (1993).
(2) Tommasi, J., *et al.*: *ibid.*, ANS, La Grange Park, Illinois, p. 1252 (1993).
(3) Wakabayashi, T., *et al.*: *Proc. of Int. Conf. Evaluation of Emerging Nucl. Fuel Cycle Systems: Global '95*, Versailles, France, Sept. 11–14, 1995, Commissariat a l'Energie Atomique, p. 800 (1995).
(4) Kloosterman, J. L., Li, J. M.: *ibid.*, Commissariat a l'Energie Atomique, p. 1106 (1995).
(5) Mukaiyama, T., *et al.*: *Nihon-Genshiryoku-Gakkai Shi* (*J. At. Energy Soc. Jpn.*), **37**[3], 159 (1995), [in Japanese].
(6) Tommasi, J., *et al.*: *Proc. of Int. Conf. on Future Nuclear Systems: Global '97*, Yokohama, Japan, Oct. 5–10, 1997, Vol. 1, p. 224 (1997).
(7) Yokoyama, K., *et al.*: *ibid.*, Vol. 1, p. 230 (1997).
(8) Kloosterman, J. L., *et al.*: *ibid.*, Vol. 1, p. 338 (1997).
(9) McLane, V., *et al.*: "*Neutron Cross Sections*", Vol. 2, Neutron Cross Section Curves, Academic Press, (1988).
(10) Maguire, H. T., *et al.*: *Nucl. Sci. Eng.*, **89**, 293 (1985).
(11) Alam, B., *et al.*: *Nucl. Sci. Eng.*, **99**, 267 (1988).
(12) Danon, Y., *et al.*: *Nucl. Sci. Eng.*, **109**, 341 (1991).
(13) Yamanaka, A., *et al.*: *J. Nucl. Sci. Technol.*, **30**, 863 (1993).
(14) Carlson, A. D., *et al.*: *Proc. Int. Conf. Nucl. Data Science and Technology*, Gatlinberg, Tennessee, May 9–13, 1994, ANS, Vol. 1, p. 40, (1994).
(15) Yamamoto, S., *et al.*: *Nucl. Sci. Eng.*, **126**, 201 (1997).
(16) Wagemans, C., *et al.*: *Nucl. Sci. Eng.*, **101**, 293 (1989).
(17) Knitter, H.-H., Budtz-Jørgensen, C.: *Nucl. Sci. Eng.*, **99**, 1 (1988).
(18) Wisshak, K., Käppeler, F.: *Nucl. Sci. Eng.*, **85**, 251 (1983).
(19) Seeger, P. A.: *LA*-4420, (1970).
(20) Nakagawa, T.: "*Neutron Data Storage and Retrieval System*", JAERI Nuclear Data Center, (1995).
(21) Kikuchi, Y.: *JAERI-M*-82-096, (1982).
(22) Simpson, O. D., *et al.*: *Nucl. Sci. Eng.*, **55**, 273 (1974).
(23) Rose, R. F. (Ed.): ENDF-201, ENDF/B-VI Summary Documentation, *BNL-NCS*-17541, 4th Ed. (ENDF/B-VI), (1991), and ENDF/B-VI MOD 2 Evaluation, by P. G. Young, (1996).
(24) Shibata, K., Narita, T. (Eds.): *JAERI-Data/Code* 98-006 (part II), (1998).
(25) Nordborg, C., Salvatores, M.: *Proc. Int. Conf. Nucl. Data Science and Technology*, Gatlinberg, Tennessee, May 9–13, 1994, ANS, Vol. 2, p. 680 (1994).
(26) Mughabghab: "*Neutron Cross Sections*", Vol. 1, Neutron Resonance Parameters and Thermal Cross Sections, Part B, Academic Press, (1984).
(27) Asghar, M., *et al.*: *Ann. Nucl. Energy*, **6**, 561 (1979).
(28) Gavrilov, V., *et al.*: *Sov. At. Energy*, **41**, 808 (1976).
(29) Usuda, S., Kohno, N.: *Sep. Sci. Technol.*, **23**, 1119 (1988).
(30) Shinohara, N., Kohno, N.: *J. Nucl. Sci. Technol.*, **34**, 398 (1997).
(31) Shinohara, N., Kohno, N.: *Appl. Radiat. Isot.*, **40**, 41 (1989).
(32) Kai, T., *et al.*: *JAERI-Conf* 97-005, p. 280 (1997).
(33) Beckurts, K. H., Wirtz, K.: "*Neutron Physics*", Springer-Verlag, p. 357 (1964).
(34) Bergman, A. A., *et al.*: *Proc. 1st Int. Conf. on Peaceful Uses for Atomic Energy*, United Nations, P/642, Vol. 4, p. 135 (1955).
(35) Kobayashi, K., *et al.*: *Nucl. Instrum. Methods Phys. Res. A*, **385**, 145 (1997).
(36) Nakagome, Y., *et al.*: *Phys. Rev. C*, **43**, 1824 (1991).
(37) MCNP-A General Monte Carlo Code for Neutron and Photon Transport, Version 3A, *LA*-7396-*M*, Rev. 2, (1986).
(38) Kobayashi, K., *et al.*: *J. Nucl. Sci. Technol.*, **31**, 1239 (1994).
(39) Kanda, K., *et al.*: *Nucl. Instrum. Methods*, **148**, 535 (1978).
(40) Westcott, C. H., *et al.*: *Proc. 2nd Int. Conf. on Peaceful Use of Atomic Energy*, Geneva, United Nations, New York, Vol. 16, 70 (1958).
(41) Gryntakis, E. M., *et al.*: *Radiochim. Acta*, **22**, 128 (1975).
(42) "*Nuclear Data Standards for Nuclear Measurements*", Technical Rep. Series, No. 227, IAEA (1983).
(43) Nakazawa, M., *et al.*: *JAERI* 1325, (1992).

付録D

Journal of NUCLEAR SCIENCE and TECHNOLOGY, 31[12], pp. 1239～1247 (December 1994).

Measurements of Thermal Neutron Cross Section and Resonance Integral for $^{237}Np(n,\gamma)^{238}Np$ Reaction

Katsuhei KOBAYASHI,

*Research Reactor Institute, Kyoto University**

Akihiro YAMANAKA† and Itsuro KIMURA

*Department of Nuclear Engineering, Kyoto University***

(Received January 12, 1994)

Making use of a standard neutron spectrum field with a pure Maxwellian distribution, the thermal neutron cross section for the $^{237}Np(n,\gamma)^{238}Np$ reaction was measured at a neutron energy of 0.0253 eV by the activation method. The result is 158±3 b, which is obtained relative to the reference value of 98.65±0.09 b for the $^{197}Au(n,\gamma)^{198}Au$ reaction. Although the data in JENDL-3 is larger by about 15% than the present value, the recently revised data in JENDL-3.2 is close to the present. The ENDF/B-V, ENDF/B-VI, JEF-2 and Mughabghab's data are also larger by 7～15%. Old measurements are larger by 7～18% than the present data.

The resonance integral for the $^{237}Np(n,\gamma)^{238}Np$ reaction was also measured relative to the reference value of 1,550±28 b for the $^{197}Au(n,\gamma)^{198}Au$ reaction with a $1/E$ standard neutron spectrum field. By defining the Cd cut-off energy as 0.5 eV for the $^{237}Np(n,\gamma)^{238}Np$ reaction, the present resonance integral is 652±24 b, which is in good agreement with the JENDL-3, -3.2, ENDF/B-V, -VI, JEF-2 and Mughabghab's data. However, most of the old experimental data are, in general, larger by 24～38% than the present measurement.

***KEYWORDS:* neptunium 237 target, neutron beams, gamma radiation, neptunium 238, nuclear reactions, gold 197 target, gold 198, thermal neutrons, cross sections, Maxwellian distribution field, resonance integrals, 1/E neutron spectrum field, activation method**

I. INTRODUCTION

Neptunium-237 is one of the minor actinides with a long half-life, which is abundantly produced in light water reactors. In order to make nuclear power more acceptable and practical, much interest has been paid to the disposal of radioactive waste matter these days[1]～[7]. One of the waste disposal methods for ^{237}Np is to adopt the nuclear transmutation using reactor neutrons[8]. Quite a number of experimental data for the $^{237}Np(n,f)$ cross section have been obtained in the MeV energy region and these data are rather well evaluated. The fission cross sections are about 10～500 mb at energies below about 500 keV. In this lower energy region, large discrepancies are seen among the existing experimental data[9]. Very recently, the present authors have measured the $^{237}Np(n,f)$ cross section by using a lead slowing-down spectrometer coupled to an electron linear accelerator[10]. The $^{237}Np(n,\gamma)^{238}Np$ reaction cross section, which is a combination of $1/v$ and resonance cross sections in the low energy region, is much higher than the fission cross section, and hence this reaction would be more effective for the nuclear transmutation of ^{237}Np than the $^{237}Np(n,f)$ reaction in the lower energy region, considering the reaction

* *Kumatori-cho, Sennan-gun, Osaka 590-04.*
** *Yoshida honmachi, Sakyo-ku, Kyoto 606-01.*
† Present address: Hitachi Works, Hitachi, Ltd., *Saiwai-cho, Hitachi-shi 317.*

rates averaged over the energy spectrum of neutrons for light water reactors.

Calculations for fuel burn-up and for the reactor design aiming at the transmutation of high level radioactive materials have been carried out[1)~6)8)]. In these cases, well-evaluated nuclear data are indispensable[11)]. It is said that the evaluated nuclear data, which would be often based on the experimental results, are not always enough for the estimation of nuclear transmutation, especially for the $^{237}Np(n,\gamma)^{238}Np$ reaction. The number of energy dependent cross sections for this reaction is limited. In addition, most of the thermal neutron cross sections and the resonance integrals are rather old[12)~17)]. In the previous measurements, information on the neutron spectrum field used was not always enough as a standard.

In the present study, the thermal neutron cross section and the resonance integral for the $^{237}Np(n,\gamma)^{238}Np$ reaction have been measured by the activation method, making use of standard neutron fields with a pure Maxwellian distribution and a $1/E$ neutron spectrum, respectively.

II. Neutron Spectrum Fields

1. Thermal Neutron Spectrum Field

The Kyoto University Reactor (KUR) of the Research Reactor Institute, Kyoto University (KURRI) is a highly enriched uranium-fueled light water-moderated research reactor, whose nominal power is 5 MW. Beside the core, there is a heavy water thermal neutron facility with a heavy water tank of 1.4 m in length. Outside the heavy water tank, there are a void region of 48 cm in thickness, 40×40 cm square and a removable bismuth layer of 60 cm in diameter and 15 cm in thickness, as illustrated in **Fig. 1**. The irradiation room is about 2.4×2.4×2.4 m³ and surrounded by 90 cm thick heavy concrete shields. The leakage neutrons from the heavy water tank can be used as a thermal neutron source of plane-type in a large space.

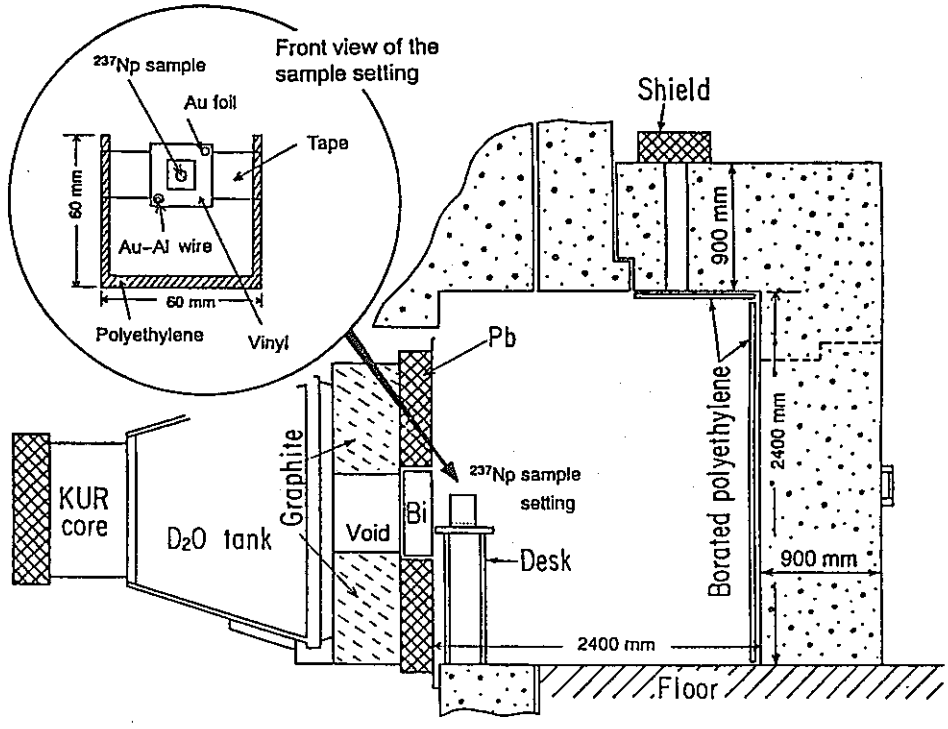

Fig. 1 Experimental arrangement for thermal neutron cross section measurement at heavy water thermal neutron facility of KUR. The extended figure shows the setting arrangement of the ^{237}Np and the Au samples.

Kanda *et al.* measured the neutron spectrum from the heavy water tank by the time-of-flight technique using a fast chopper [18]. The obtained spectrum showed good agreement with a Maxwellian distribution having neutron temperature of 60°C. The Cd-ratio measured by Au foils with and without Cd-cover of 0.7 mm in thickness was more than 5,000 at the bismuth layer, and epi-thermal neutrons could be almost negligible[18][19].

2. $1/E$ Neutron Spectrum Field

The Kinki University Reactor (UTR-KINKI) is a highly enriched uranium-fueled light water-moderated and graphite-reflected research reactor[20], which has the separate cores at an interval of 46 cm. The nominal output power is 1 W. At the center of the internal graphite reflector between the two divided cores as shown in **Fig. 2**, a graphite stringer of 9.6×9.6 cm square and 66 cm long can be withdrawn to make a void region or a central cavity for sample irradiation. The neutron energy spectrum at the central graphite cavity has been calculated[21] using the SRAC code system[22]. In this calculation, geometrical conditions for the separate cores were assumed to be a cylindrical ring. The two-dimensional transport S_N code TWOTRAN[23] was employed to calculate the neutron spectrum in the central void region. The 122 group constants were produced from ENDF/B-IV data. The results of the neutron spectra are shown in **Fig. 3**(a), (b). The calculated spectrum satisfactorily agrees with a standard $1/E$ neutron spectrum from about 1 eV to a few 100 keV.

By adjusting the above calculated spectrum with multi-foil activation data for 5 kinds of (n, γ) reactions and 4 kinds of threshold reactions[20], the neutron spectrum at the central graphite cavity of the UTR-KINKI was also obtained using the NEUPAC code[24]. This code contains energy dependent group cross section libraries for important neutron dosimetry reactions in ENDF/B-V. We adopted 144 energy groups from 0.01 eV to 16.4 MeV. The results of the adjusted spectrum are shown in Fig. 3, and compared with the above transport calculations. It has been found that the neutron spectrum at the core center gives a good $1/E$ shape in the relevant energy range. Moreover, the neutron flux distribution is almost flat in the central cavity of the UTR-KINKI[20].

The sandwiched foil method has been also employed to measure epi-thermal neutrons at the main resonances for 4 kinds of (n, γ)

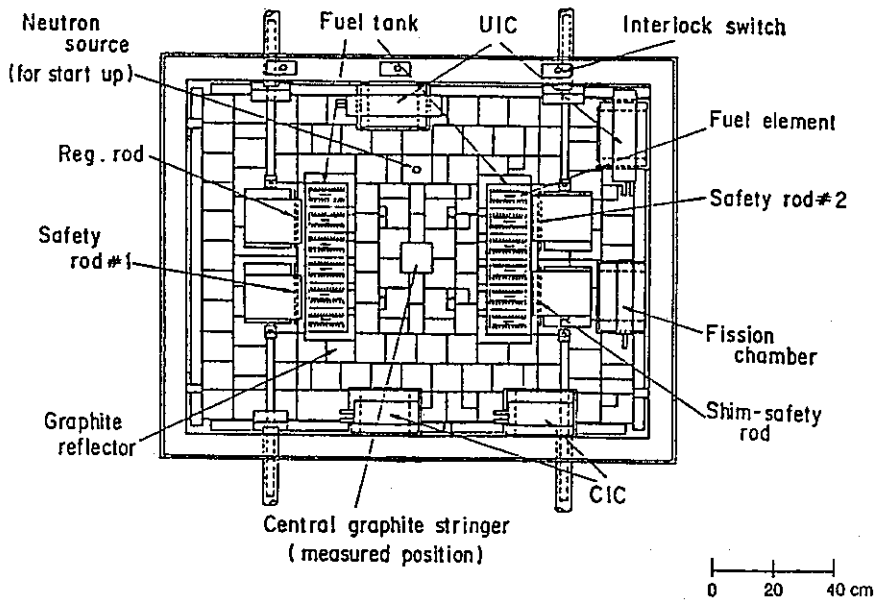

Fig. 2 Top view of UTR-KINKI core for present experiment. A graphite stringer at the central region can be withdrawn to make a cavity for the sample irradiation.

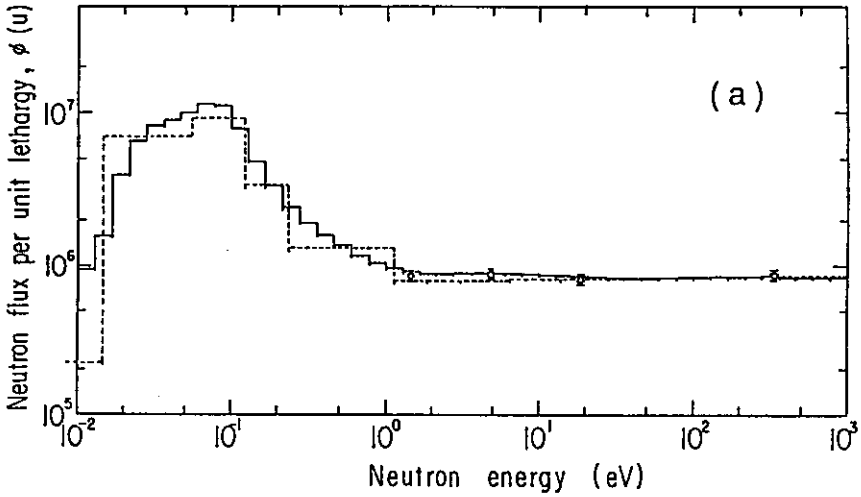

○□△▽: Measurement by resonance sandwich foils
- - - - - - -: Calculation, ———: Adjusted spectrum

(a) Lower energy region

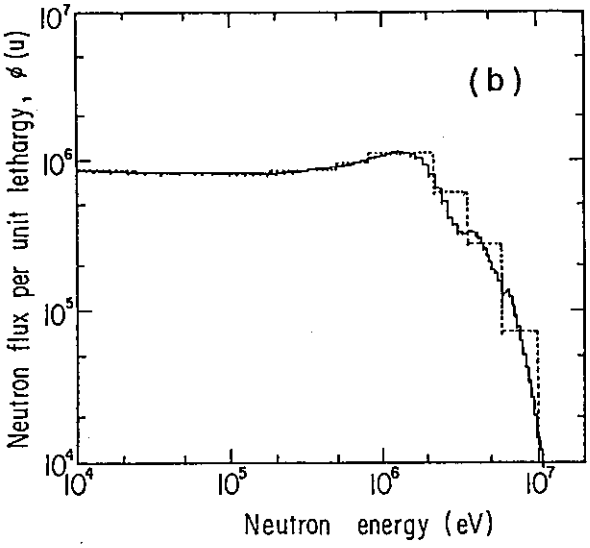

(b) Higher energy region

Fig. 3(a),(b) Neutron energy spectra obtained at central graphite cavity of UTR-KINKI[20]

reactions[20]. Neutron fluxes at 1.46, 4.94, 18.8 and 337 eV resonances for ^{115}In, ^{197}Au, ^{186}W and ^{55}Mn are shown in Fig. 3(a), respectively. These results are in good agreement with the calculated and the adjusted spectra in the $1/E$ spectrum region.

III. Measurement of Thermal Neutron Cross Section

1. Experimental Methods

The heavy water thermal neutron facility of the KUR has been used for the measurement of the thermal neutron cross section for the ^{237}Np$(n,\gamma)^{238}$Np reaction. The ^{237}Np samples, which were chemically purified as aqueous solution[10], were prepared in the form of dried filter-paper 1.5×1.5 cm square with drops of the solution. The sample was sealed with vinyl sheet of 0.05 mm in thickness, 2.5×2.5 cm square, and was attached to a 3 mm thick polyethylene holder with adhesive tape, as seen in Fig. 1.

Thermal neutron flux was monitored with an Au foil of 3 mm in diameter and 50 μm thick or with a piece of Au-Al alloy wire, 0.5 mm in diameter and 0.0314% in weight of Au. The monitor sample was put on the corner of the vinyl sheet for the ^{237}Np sample and these samples were set at about 10 cm from the Bi surface, as shown in Fig. 1. Irradiation time was about 10 hours during the 5 MW operation of the KUR. Nine irradiations were made, and neutron fluxes for six of them were obtained with the Au-Al alloy wire monitor and the remainings were measured by the Au foil. The thermal neutron flux at the irradiation position in front of the Bi layer reached about 1.5×10^9 $n/cm^2\cdot s$ at the nominal KUR power level of 5 MW.

The total amount of the ^{237}Np atoms was experimentally determined by the γ-ray measurement of 312 keV from ^{233}Pa, which was in radioactive equilibrium to ^{237}Np, and was found

to be $10^{16}\sim10^{17}$ for each sample. Induced activities of ^{238}Np from the irradiated ^{237}Np sample and the ^{233}Pa were simultaneously measured with a high purity Ge (HPGe) detector. These γ-ray photo-peaks were clearly observed in the pulse height spectrum. Gold samples were also measured with the same Ge detector. These samples were set at a distance of about 5 cm from the detector. Gamma-ray energies and intensities used for the present data processing are shown in **Table 1**, in which the data used for the determination of number of ^{237}Np atoms are included[25]. The g-factors[26] for both of ^{237}Np and ^{197}Au are also given in the table. The detection efficiency of the Ge detector used was experimentally calibrated by the mixed γ-ray standard sources purchased from Amersham.

Table 1 Nuclear data of ^{237}Np, ^{233}Pa, ^{238}Np, ^{197}Au and ^{198}Au used for present measurements

Isotope	Half-life	γ-ray energy (MeV)	γ-ray intensity (%)	g-factor
^{237}Np	2.14×10^{6} yr			0.982
^{233}Pa	27.0 d	0.312	37.0	
^{238}Np	2.12 d	0.984	27.8	
^{197}Au				1.0051
^{198}Au	2.694 d	0.412	95.5	

2. Measurement of Cross Section

The thermal neutron cross section σ_x averaged over the Maxwellian distribution spectrum is defined as

$$\sigma_x=\frac{\sigma_x(v_0)}{1.128}S_x g_x(T_n)\sqrt{\frac{T_0}{T_n}},$$

and the measured reaction rate is given in the following relation:

$$R_x=\varepsilon_x N_x \sigma_x \phi,$$

where v_0=2,200 m/s, T_0=293.6 K, T_n is the neutron temperature, S_x the self-shielding coefficient, $g_x(T_n)$ the g-factor, ε_x the detection efficiency, N_x the number of atoms for the relevant reaction and ϕ the neutron flux.

In the present measurement, the thermal neutron cross section for the ^{237}Np$(n,\gamma)^{238}$Np reaction at a neutron energy of 0.0253 eV (corresponding to a velocity of 2,200 m/s) has been measured relative to that for the ^{197}Au$(n,\gamma)^{198}$Au reaction as a standard, by rewriting the above relations as follows:

$$\sigma_x(v_0)=\frac{\varepsilon_{Au}}{\varepsilon_x}\cdot\frac{R_x}{R_{Au}}\cdot\frac{N_{Au}}{N_x}\cdot\frac{S_{Au}}{S_x}\cdot\frac{g_{Au}(T_n)}{g_x(T_n)}\sigma_{Au}(v_0),$$

where x and Au denote the parameters for ^{237}Np and ^{197}Au, respectively.

The self-shielding coefficient[27] for the Au foil was about 0.9 in our measurement. The coefficients for the Au-Al alloy wire and the ^{237}Np sample were neglected and the corrections were not made for these samples.

IV. Measurement of Resonance Integral

1. Experimental Methods

A standard $1/E$ neutron spectrum field at the UTR-KINKI has been used for the measurement of the resonance integral for the ^{237}Np$(n,\gamma)^{238}$Np reaction. The ^{237}Np samples were also made in the form of dried filter-paper, which was the same as those used for the thermal neutron cross section measurement. For the neutron flux monitor with Au sample, a metallic foil of 12.7 mm in diameter and 50 μm in thickness was used. Each of the ^{237}Np sample and the Au foil was put in a Cd-cover of 0.5 mm in thickness and stuck on an Al holder, which was set at the central graphite cavity of the UTR-KINKI, as illustrated in **Fig. 4**. The ^{237}Np sample was set between the Au foils, which were used for the neutron flux monitor. Nine irradiations for the ^{237}Np sample were made for 5 h each together with the Au monitor foils during the 1 W operation of the reactor. Induced activities from the ^{237}Np and the Au foils were measured with a HPGe detector, whose detection efficiency was calibrated with standard γ-ray sources.

The nuclear data used for the present activation measurements were also taken from Table 1. The experimental methods are similar to those for the thermal neutron cross section measurement.

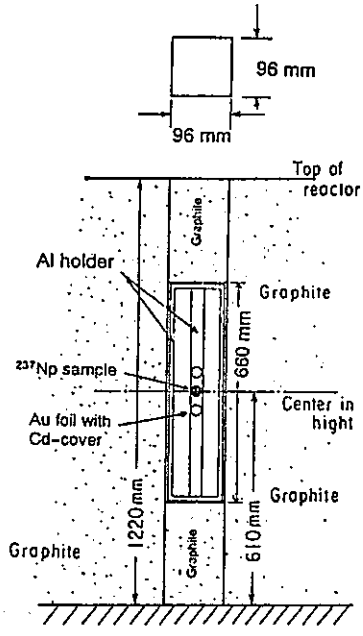

Fig. 4 Experimental arrangement for ^{237}Np and Au samples at central graphite cavity of UTR-KINKI

2. Measurement of Resonance Integral

The resonance integral is defined by the relation;

$$I_x=\int_{E_{Cd}}^{\infty}\sigma_x(E)dE/E,$$

where $\sigma_x(E)$ is the cross section as a function of energy E, and E_{Cd} is a Cd cut-off energy, which is usually defined as 0.5 eV[28][29]. The resonance integral for the ^{237}Np$(n,\gamma)^{238}$Np reaction has been measured relative to that for the ^{197}Au$(n,\gamma)^{198}$Au reaction, as seen in the following relation:

$$I_x=\frac{\varepsilon_{Au}}{\varepsilon_x}\cdot\frac{R_x}{R_{Au}}\cdot\frac{N_{Au}}{N_x}\cdot\frac{S_{Au}}{S_x}I_{Au},$$

where I_{Au} is the standard value of the Au resonance integral, ε the detection efficiency, R the reaction rate, N the number of atoms and S the self-shielding coefficient, and the subscripts Au and x mean the data for ^{197}Au and ^{237}Np, respectively. The neutron self-shielding coefficient for the Au foil was obtained by the calculations using the continuous energy Monte Carlo code VIM[30]. For the ^{237}Np sample, the self-shielding correction was neglected because the sample was diluted in the form of dried filter-paper with the drops of the ^{237}Np solution.

As seen in Fig. 3, the neutron spectrum at the central graphite cavity of the UTR-KINKI deviates from the $1/E$ standard spectrum below about 1 eV. Moreover, it is noticed that ^{237}Np has a big resonance at 0.49 eV. Making use of the neutron spectrum at the UTR-KINKI, energy dependent reaction rate curve for the ^{237}Np$(n,\gamma)^{238}$Np reaction was calculated with the VIM code[30]. **Figure 5** shows the calculated reaction rate which is observed in the energy region above 0.2 eV. In order to derive the resonance integral, which is defined as an integral of the reaction rate for relevant cross section above E_{Cd}=0.5 eV, we have made a correction of the measured reaction rate by taking the ratio of the calculated reaction rate integral above 0.5 eV to that above 0.2 eV.

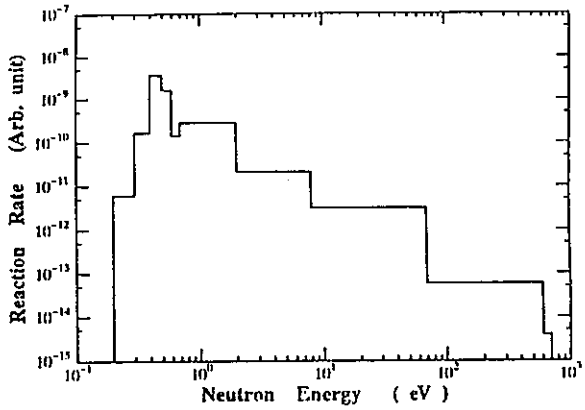

Fig. 5 Calculated reaction rate for ^{237}Np$(n,\gamma)^{238}$Np reaction using neutron spectrum obtained at UTR-KINKI

V. Results and Discussion

1. Thermal Neutron Cross Section

The thermal neutron cross section of ^{237}Np$(n,\gamma)^{238}$Np reaction for 2,200 m/s neutrons was obtained, relative to the well known reference cross section value of 98.65±0.09 b for the ^{197}Au$(n,\gamma)^{198}$Au reaction. Three of the 9 measured data were obtained with the Au foil monitors and the results were 156.4, 156.5 and 161.3 b, respectively. Other 6 data, which were measured with the Au-Al alloy wire monitors, were in the values from 155.9 to 160.1 b. These 9 data are in good agreement with each other within about 3.4%,

and it is found that there exists consistency between the data measured by the Au foil and the Au-Al alloy wire. Main sources of the uncertainties are due to the statistical errors (1.0~2.0%), the detection efficiencies (1.5~2.2%), number of atoms, especially for ^{237}Np (about 1.8%), geometrical factor for irradiation of the samples (about 0.5%), and errors (0.8~1.2%) including some other corrections. The experimental uncertainties were carefully analyzed and the covariance matrix for the ^{237}Np$(n,\gamma)^{238}$Np and the ^{197}Au$(n,\gamma)^{198}$Au reactions was derived by considering the correlations between the measured data as done before[35]. The resultant variance and covariance data gave the standard deviation of about 2% for the ^{237}Np$(n,\gamma)^{238}$Np cross section measurement and the off-diagonal element of 0.05, respectively. The present value obtained is shown in **Table 2**, and compared with the existing experimental and the evaluated data[9][12]~[16][29][31]~[34].

Table 2 Thermal neutron cross section (2,200 m/s value) for ^{237}Np$(n,\gamma)^{238}$Np reaction

Present	158±3 b	
JENDL-3.2 ('93)	164.6	Ref. (33)
JENDL-3 ('90)	181.0	Ref. (29)
ENDF/B-VI ('91)	181.0	Ref. (32)
ENDF/B-V ('79)	169.1	Ref. (31)
JEF-2 ('93)	181.0	Ref. (34)
Mughabghab ('84)	175.9±2.9	Ref. (9)
Gryntakis ('87)	169±3	Ref. (16)
Weston ('81)	180±6	Ref. (15)
Eberle ('71)	187±6	Ref. (14)
Hellstrand ('70)	172±3	Ref. (13)
Schuman ('69)	185±12	Ref. (12)

In order to check the effect on the undesirable ^{237}Np$(n,\gamma)^{238}$Np reaction by epi-thermal neutrons, we have also made a neutron irradiation of the ^{237}Np sample with a Cd-cover of 0.5 mm in thickness at the heavy water thermal neutron facility of the KUR. We have found no induced activities of ^{238}Np in the ^{237}Np sample.

As seen in Table 2, previous measurements of the thermal neutron cross section are between 169 and 187 b and are larger by 7~18% than the present value. The Mughabghab's datum is larger by 11%. The evaluated data in JENDL-3, ENDF/B-V, -VI and JEF-2 whose libraries are based on experimental data, are also larger by about 7~15% than the present measurement. These discrepancies may be due to the fact that the previous measurements are not always good enough from the points of the experimental technique, purity of the sample prepared and the neutron spectrum field used as a standard. Very recently, the evaluated cross sections of ^{237}Np in JENDL-3 have been revised as JENDL-3.2[33] by taking account of recent data. The thermal neutron cross section in JENDL-3.2 is closer to our present data.

2. Resonance Integral

The resonance integral for the ^{237}Np$(n,\gamma)^{238}$Np reaction was obtained by normalizing the measured data to the reference value of 1,550±28 b for the ^{197}Au$(n,\gamma)^{198}$Au reaction. All of the 9 experimental data were between 644 and 671 b and showed good agreement with each other. The experimental uncertainties are due to the statistical counts (5~10% for ^{237}Np and 0.5~1% for ^{197}Au), the reference value for the ^{197}Au$(n,\gamma)^{198}$Au reaction, the Cd cut-off correction in the ^{237}Np reaction (about 1%) and the self-shielding effect for the Au foil (1.2%). Some of other uncertainties due to the detection efficiencies, number of atoms, geometrical factor and other corrections are almost similar to those in the thermal neutron cross section measurement. Considering the correlations between the measured data as described above, the experimental uncertainties were analyzed[35] to obtain the variance and covariance matrix for the ^{237}Np$(n,\gamma)^{238}$Np and the ^{197}Au$(n,\gamma)^{198}$Au reactions. The experimental uncertainty derived from the variance data is 3.7% for the ^{237}Np$(n,\gamma)^{238}$Np reaction, and the off-diagonal element in the covariance matrix is 0.48. The present result is given in **Table 3** and compared with the previous data[9][12][13][16][17][29][31]~[34].

Since ^{237}Np has a big resonance at 0.49 eV, the effective Cd cut-off energy is much lower than 0.5 eV whose value is used for the definition of the resonance integral. In the

Table 3 Resonance integral for $^{237}Np(n,\gamma)^{238}Np$ reaction

Present	652±24 b	
JENDL-3.2 ('93)	662.0	Ref. (32)
JENDL-3 ('90)	663.0	Ref. (28)
ENDF/B-VI ('91)	655.0	Ref. (31)
ENDF/B-V ('79)	662.6	Ref. (30)
JEF-2 ('93)	655.0	Ref. (33)
Mughabghab ('84)	640±50	Ref. (9)
Gryntakis ('87)	821.5±58.0	Ref. (16)
Hellstrand ('70)	640±50	Ref. (13)
Schuman ('69)	807±40	Ref. (12)
Scoville ('68)	900±300	Ref. (17)

experimental determination of the resonance integral for the $^{237}Np(n,\gamma)^{238}Np$ reaction, therefore, the measured data were corrected. In the present measurement, the correction factor for the reaction rate due to the difference from the Cd cut-off energy of 0.5 eV was estimated to be 0.7 by the Monte Carlo calculations using the VIM code. Without this correction, the resonance integral is 931±35 b.

We have investigated the effect which is observed in the resonance integral by changing the Cd cut-off energy, and found that a 10% change with energy results in only a 0.2% shift in the integral data, if the cross section is assumed to be $1/v$ shape. Moreover, we have made corrections for the fact that the neutron energy spectrum in the UTR-KINKI deviates from the ideal $1/E$ spectrum, especially at energies below 1 eV.

Recent evaluations of JENDL-3, -3.2, ENDF/B-V, -VI, JEF-2 and by Mughabghab are in good agreement with the present measurement, as shown in Table 3. However, most of the experimental values which are rather old are larger by 24~38% than the present value, except for that by Hellstand. The reason why the old experimental data are much larger than the present value may be due to the fact that the Cd cut-off energy correction was not made properly. Moreover, another problem may be due to the use of the irradiation field deviating from a $1/E$ neutron spectrum as a standard.

VI. Conclusion

The thermal neutron cross section for the $^{237}Np(n,\gamma)^{238}Np$ reaction at 0.0253 eV was measured with the pure Maxwellian distribution field at the heavy water thermal neutron facility of the KUR, and the resonance integral for the same reaction was measured with the $1/E$ neutron spectrum field at the central graphite cavity of the UTR-KINKI, relative to the $^{197}Au(n,\gamma)^{198}Au$ reaction cross section for both ^{237}Np cross section measurements. For the thermal neutron cross section measurement, most of the previous experimental data are larger by 7~18% than the present data (158±3 b), and the evaluated values in JENDL-3, ENDF/B-V, -VI and JEF-2 are also larger by 7~15% than the present result. The Mughabghab's evaluation is also larger by 11%. The value in JENDL-3.2 (164.6 b) is close to the present measurement. On the other hand, the evaluated resonance integrals in JENDL-3, -3.2, ENDF/B-V, -VI, JEF-2 and by Mughabghab are in good agreement with the present result (652±24 b). However, some of the old measurements are larger by 24~38% than the present value.

Acknowledgment

The authors would like to express their sincere thanks to Prof. R. Miki of Kinki University for his useful discussions and great encouragement to carry out this work.

This study was supported by the Grant-in-Aid of Science Research from the Ministry of Education, Science and Culture (No. 03452302). A part of this work was also performed by the Visiting Research Program of the Kinki University Atomic Energy Research Institute under the support and cooperation by the Section of Kinki University Cooperation Research Use, Faculty of Engineering, Osaka University.

The authors are much indebted to the Nuclear Data Center of Japan Atomic Energy Research Institute for supplying the nuclear data of ^{237}Np. The Monte Carlo calculations were carried out with the FACOM M-Series Computers at the Data Processing Center of Kyoto University.

References

(1) Mukaiyama, T., *et al.*: Conceptual study of actinide burner reactors, *Proc. of 1988 Int.*

Reactor Phys. Conf., Jackson Hale, Vol. IV, 369.
(2) BERWALD, D.H., DUDERSTADT, J.J.: *Nucl. Technol.*, 42, 34 (1979).
(3) TAKANO, H., *et al.*: Concept of actinide transmutation with intense proton accelerator, *Proc. of 6th Int. Conf. on Emerging Nuclear Energy Systems, Monterey, USA*, (1991).
(4) JOURNET, J., *et al.*: Minor actinides transmutation in oxide fueled fast reactors, *Proc. of Int. Conf. and Technol. Exposition on Future Nuclear System; Emerging Fuel Cycles and Waste Disposal Options*, p. 99 (1993), ANS.
(5) DOBBIN, K.D., *et al.*: Evaluating the efficacy of a minor actinide burner, *ibid.*, p. 131.
(6) BULTMAN, J.H.: Actinide breeding and burning in metallic and oxide fueled ALMR cores, *ibid.*, p. 170.
(7) KONING, A.J., *et al.*: Nuclear data evaluation for accelerator-based transmutation of radioactive waste, *ibid.*, p. 437.
(8) PRUNIER, C., *et al.*: Some specific aspects of homogeneous Am and Np based fuels transmutation through the outcomes of the superfact experiment in PHENIX fast reactor, *ibid.*, p. 158.
(9) MCLANE, V., *et al.*: *"Neutron Cross Sections"*, Vol. 2, Neutron Cross Section Curves, (1988), Academic Press.
(10) YAMANAKA, A., *et al.*: *J. Nucl. Sci. Technol.*, 30[9], 863 (1993).
(11) HAAS, M.N.: Nuclear fuel cycle data needs, Ref. (4), p. 435.
(12) SCHUMAN, R.P., BERREGH, J.R.: Resonance integral measurements, *IN*-1296, (1968).
(13) HELLSTRAND, E., *et al.*: Studies of the capture cross section of ^{237}Np and ^{241}Am in different reactor spectra, *BNL* 50242, (1970).
(14) EBERLE, S.H., *et al.*: Project actiniden, *KFK*-1456, (1971).
(15) WESTON, L.W., TODD, J.H.: *Nucl. Sci. Eng.*, 79, 184 (1981).
(16) GRYNTAKIS, E., *et al.*: *"Handbook on Nuclear Activation Data"*, Technical Rep. Ser. No. 273, p. 199 (1987), IAEA.
(17) SCOVILLE, J.J., ROGERS, J.W.: Resonance integrals measured in the advanced reactivity measurement facilities, *IN*-1195, (1968).
(18) KANDA, K., *et al.*: *Nucl. Instrum. Methods*, 148, 535 (1978).
(19) KOBAYASHI, T.: Private communication, (1983).
(20) KOBAYASHI, K., *et al.*: *Annu. Rep. Kinki Univ., At. Energy Res. Inst.*, 25, 21 (1988).
(21) MIKI, R., ITOH, T., TOTAKA, M.: *ibid.*, 23, 33 (1986).
(22) TSUCHIHASHI, K., *et al.*: *JAERI* 1285, (1983).
(23) LATHROP, K.D., BRINKLEY, F.W.: *LA*-4848-*MS*, (1973).
(24) NAKAZAWA, M., SEKIGUCHI, A.: *Proc. of 2nd ASTM-Euratom Symp. on Reactor Dosimetry, NUREG/CP*-0004, Vol. 3, 1423 (1977).
(25) BROWNE, E., FIRESTONE, R.: *"Table of Radioactive Isotopes"*, (1986), John Wiley & Sons, New York.
(26) MUGHABGHAB, S.F.: *"Neutron Cross Sections"*, Vol. 1, Neutron Resonance Parameters and Thermal Cross Sections, Part B, (1984), Academic Press.
(27) HELM, F.H.: *Nucl. Sci. Eng.*, 16, 235 (1963).
(28) MUGHABGHAB, S.F., *et al.*: *"Neutron Cross Section"*, Part A, (1981), Academic Press.
(29) SHIBATA, K., *et al.*: Japanese Evaluated Nuclear Data Library, Version-3, JENDL-3, *JAERI* 1319, (1990).
(30) BLOMQUIST, R.N., *et al.*: *ORNL/RSIC*-44, p. 31 (1980).
(31) KINSEY, R. (Ed.): ENDF/B Summary Documentation, *BNL-NCS*-17541, (3rd Ed.) (ENDF/B-V), (1979).
(32) ROSE, R.F. (Ed.): *ibid.*, (4th Ed.) (ENDF/B-VI), (1991).
(33) JAERI Nuclear Data Center: JENDL-3.2, Rev. 2 of JENDL-3, Private communication, (1993).
(34) OECD/NEA Data Bank, (1993).
(35) KOBAYASHI, K., KIMURA, I., MANNHART, W.: *J. Nucl. Sci. Technol.*, 19[5], 341 (1982).

Nuclear Instruments and Methods in Physics Research A 385 (1997) 145–156

ELSEVIER

NUCLEAR INSTRUMENTS & METHODS IN PHYSICS RESEARCH Section A

付録E

Characteristics of the Kyoto University Lead Slowing-down Spectrometer (KULS) coupled to an electron linac

Katsuhei Kobayashi[a,*], Shuji Yamamoto[a], Akihiro Yamanaka[b,1], Yoshihiro Nakagome[a], Yoshiaki Fujita[a], Satoshi Kanazawa[b], Itsuro Kimura[b]

[a] *Research Reactor Institute, Kyoto University, Kumatori-cho, Sennan-gun, Osaka 590-04, Japan*
[b] *Department of Nuclear Engineering, Kyoto University, Yoshidahonmachi, Sakyo-ku, Kyoto 606-01, Japan*

Received 20 September 1995; revised form received 17 September 1996

Abstract

A lead slowing-down spectrometer coupled to a 46 MeV electron linear accelerator (linac) was installed at Research Reactor Institute, Kyoto University (KURRI). The size of this Kyoto University Lead Slowing-down Spectrometer (KULS) is $1.5 \times 1.5 \times 1.5$ m^3, and it is covered with Cd sheets 0.5 mm thick. One of the eleven experimental holes in the KULS is covered with 10 to 15 cm thick bismuth layers to suppress high energy capture gamma-rays from lead.

The characteristics of this KULS have been experimentally obtained and the results are compared with the predicted values by Monte Carlo calculations using the MCNP code. 1) The slowing-down constant K in the relation $E = K/t^2$ between the neutron slowing-down time t and energy E is 190±2 (keV μs^2) for the bismuth hole and 156±2 (keV μs^2) for an ordinary lead hole, respectively. The K values agree with the calculated ones. 2) The measured energy resolution $\Delta E/E$ at full-width-at-half-maximum (FWHM) was about 40% for both holes, while the calculated values were lower by about 10% than the measured ones in the relevant energy region. 3) The neutron energy spectrum from 0.01 eV to 20 MeV and the spatial distribution of neutrons in the KULS were measured by the foil activation method. The angular neutron spectrum perpendicular to the linac electron beam was also obtained experimentally in the energy range from a few eV to about 10 MeV by the neutron time-of-flight (TOF) method. The measured results are compared with the calculated ones in which we have used the three evaluated nuclear data JENDL-3, ENDL-85 and ENDF/B-IV for lead. Through the comparison a check on the nuclear data has been performed.

1. Introduction

Lead is one of the heavy mass elements and it has no inelastic scattering cross section below about 600 keV, where the neutron total cross section mainly consists of elastic scattering cross section, since the absorption cross section is very small. Therefore, when pulsed fast neutrons are put into the central region of a large lead assembly, the neutrons are slowed down by repeating many elastic scattering processes, because of little leakage of neutrons. The slowing-down neutrons present focusing behaviour and keep an asymptotic form at each energy corresponding to the slowing-down time [1]. There exists a relation $E = K/t^2$ between the mean energy E in keV of the slowing-down neutrons and the mean slowing-down time t in μs [1], where K is the slowing-down constant. The energy resolution of the slowing-down neutrons is theoretically given at full-width-at-half-maximum (FWHM) by [1]

$$(\Delta E/E)_{\mathrm{FWHM}} = 2.35 \times (\Delta\sigma/\sigma)_{\mathrm{Gaussian}} = 2.35 \times (8/3A)^{1/2} = 27\%,$$

where, $(\Delta\sigma/\sigma)_{\mathrm{Gaussian}}$ is the standard deviation in a Gaussian function and A is the atomic mass (207.2) of lead.

Hence a large lead assembly was proposed to be applicable as a neutron spectrometer and practically used by Bergman et al. [2] for the first time. Since that, in some laboratories or universities, lead slowing-down spectrometers coupled to a D–T pulsed neutron source by a Cockcroft–Walton accelerator have been installed and widely applied to measurements of neutron capture and fission cross sections in the intermediate and/or resonance neutron energy region [1–7].

* Corresponding author.
[1] Present address: Hitachi Works, Hitachi Ltd., Saiwai-cho, Hitachi-shi, Ibaraki 317, Japan.

PII S0168-9002(96)00900-X

Most of electron linear accelerators have been developed in 1960s as an intense neutron source and neutron time-of-flight (TOF) method has often been used for neutron cross section measurements [8]. The usage of a lead slowing-down spectrometer coupled to an electron linear accelerator (linac) was proposed for the measurement of small amount of samples with low cross sections and for the cross section measurement of radioactive materials to give high background level. The first spectrometer was installed at the Rensselaer Polytechnic Institute (RPI) as an intense neutron spectrometer [9]. Since neutrons can be detected at the distance of tens of centimeters from the pulsed neutron source in the lead slowing-down spectrometer, higher neutron intensities by more than thousands times than those at the measuring station of 5 m flight path for the conventional neutron TOF method can be obtained [9]. Making use of the spectrometer, the RPI groups have made measurements of sub-threshold fission cross sections [9,10] of ^{238}U and ^{232}Th and measured fission cross sections of trans-uranium nuclides [11–13] in the energy range from about 1 eV to several tens of keV. Recently, the spectrometer was also applied to the nondestructive assay of spent fuels [14,15].

In the present work, we have experimentally investigated characteristic behaviour of neutrons in the lead slowing-down spectrometer coupled to a 46 MeV electron linear accelerator (linac) at the Research Reactor Institute, Kyoto University (KURRI). The spectrometer was originally installed at University of Tokyo [5] and transferred to KURRI in 1991. With this Kyoto University Lead Slowing-down Spectrometer (KULS), we first obtained the relation between neutron slowing-down time and energy and the neutron energy resolution by the experiments with resonance filters and by the calculations using the continuous energy Monte Carlo code MCNP [16]. Secondly, making use of the NEUPAC and the SAND-II codes [17,18], the neutron flux spectrum in the KULS has been analyzed by the adjustment method with activation foil data. Radial flux distributions of neutrons have also been measured by Au foils and Ni wires. In addition, neutron TOF method has been employed to measure the angular neutron flux spectrum in the KULS, as we have done before [19,20]. These experimental results have been compared with calculations performed by the MCNP code using the evaluated nuclear data files of ENDF/B-IV [21], ENDL-85 [22] and JENDL-3 [23]. The nuclear data for lead is useful to understand the characteristics of a lead slowing-down spectrometer.

2. Lead slowing-down spectrometer

The lead slowing-down spectrometer was recently installed by coupling to the 46 MeV linac at KURRI. Specific features of the Kyoto University Lead Slowing-down Spectrometer (KULS) are as follows.

1) The KULS is a cube of $1.5\times1.5\times1.5$ m^3 and about 40 tons in weight, and is set on a platform car in the linac target room so that it can be removed when the conventional neutron TOF measurement is made, as shown in Fig. 1.

2) The number of the lead blocks used was about 1600 (each size: $10\times10\times20$ cm^3, and purity: 99.9%). Each block was carefully cleaned with alcohol or acetone and piled up to make the cube without any structural steel. All sides of the KULS were covered with cadmium sheet of 0.5 mm in thickness to shield low energy neutrons scattered from the surroundings.

3) Two types of photoneutron targets were employed: one was a cylindrical lead block (8 cm in diameter and 5 cm thick) casted with an aluminum pipe for air cooling, and the other was a tantalum target assembly (8 cm in diameter and 6 cm in effective thickness), which was made to set 12 sheets of tantalum plates in all (1 to 5 mm in each thickness) in a cylindrical titanium case. The tantalum target assembly was also cooled by compressed air flow. The photoneutron target is separated from the linac vacuum system to prevent troubles by which the linac machine is disturbed. The temperature on the target case was monitored with thermocouples and the linac operating conditions were controlled so that the temperature was kept less than 300°C. During the KULS experiments, the linac beam power on the target was about 200 to 500 W.

4) For the multi-purpose and/or parallel measurements, as seen in Fig. 1, we added eight experimental/irradiation

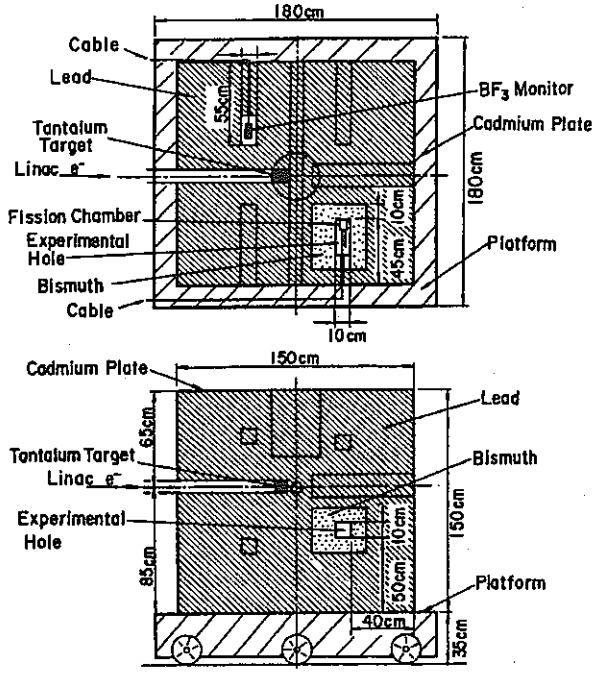

Fig. 1. Cross sectional view of Kyoto University Lead Slowing-down Spectrometer, KULS.

holes (10×10 cm^2, 55 or 45 cm in depth) to the spectrometer which were originally designed at University of Tokyo [5]. One of the good points of the KULS is that one of the lead holes was covered by a bismuth layer of 10 to 15 cm (neutron source side of the hole) in thickness to shield high energy gamma-rays (6 to 7 MeV) by the Pb(n,γ) reaction in the spectrometer. The bismuth layers are useful to reduce background counts due to photofissions in the fission event measurement [10].

5) An advantageous point of the KULS is the design to be able to measure the neutron energy spectrum in the KULS by the conventional TOF method. At a distance of 12.5 cm behind the photoneutron target, a through hole of 8 cm in diameter is provided at a right angle to the incident electron beam, as shown in Fig. 1. Moreover, in the forward and the upper directions there are large experimental plugs of lead, each of which has an axial irradiation hole of 3 mm in diameter along the central axis. Activation foils or wires can be set to measure the flux distribution of neutrons.

3. Experimental method and measurement

3.1. Slowing-down time and energy

The relation between neutron slowing-down time and energy in the KULS has been measured in the bismuth hole and the lead hole at the opposite upper position to the bismuth hole, as shown in Fig. 1. For the investigation of the experimental reliability, two types of detectors were employed: one was a BF_3 counter (12 mm in diameter, 50 mm in length, 1 atm. pressure) for the neutron transmission measurement through a resonance filter which gave the dip structure in the slowing-down time spectrum, and the other was an Ar gas counter (12.7 mm in diameter, 63.5 mm in length, 1 atm. pressure) for the capture γ-ray measurement with a resonance filter which showed the bump structure in the slowing-down time spectrum. The detector was placed at the bottom of the bismuth or the lead hole covered with and without the resonance filter and the setting position was about 40 cm distant from the photoneutron target in the KULS. Table 1 shows the resonance filters and their main resonance energies used in the present measurement. Since the resonance energies for these filters are well known [24], we can calibrate the relation between slowing-down time t at the center of the dip spectrum by the BF_3 counter or of the bump spectrum by the Ar gas counter and its energy E, as a function of $E = K/(t + t_0)^2$, where K is slowing-down constant and t_0 is constant for the zero time correction.

Output pulses from the BF_3 or the Ar gas counter were transmitted through the pre-amplifier, the main amplifier and the discriminator and were stored in a multi-channel analyzer of 4096 channels as a function of the neutron slowing-down time. The channel width of 62.5 to 500 ns was selected. Another BF_3 counter was set in a lead hole as seen in Fig. 1, to monitor the neutron source intensity during the experiment.

Table 1
Resonance filters and their main resonance energies used in the present measurement

Material	Energy [eV]	Thickness [mm]	Form
In	1.46	0.2	foil
Te	2.33	7.0	powder
Ta	4.28	0.2	foil
Ta	10.4		
Au	4.91	0.05	cylinder
Ag	5.19	0.5	cylinder
Ag	16.3		
Cd	27.5	0.3	cylinder
Mo	44.9	7.0	powder
Co	132	0.3	cylinder
Cu	230	1.0	cylinder
Cu	579		
Mn	336	7.0	powder

3.2. Energy resolution

The energy resolution of neutrons in the KULS has been experimentally obtained from the dip or the bump spectrum, as performed in the above measurements, making use of the BF_3 and the Ar gas counters. The dip or the bump spectrum was fitted with a Gaussian function to give the energy resolution at full width at half maximum $(\Delta E/E)_{FWHM} = 2.35(\Delta\sigma/\sigma)_{Gaussian}$ using the standard deviation. In the transmission measurement with a resonance filter, corrections are required for the dip spectrum broadened by certain width of the resonance cross section and by the certain thickness of the resonance filter. Then, the capture γ-ray measurement using a sharp resonance peak like a delta function would be better to determine the energy resolution, because one can derive the energy resolution without any corrections in the measured data. Table 1 lists not only the big resonance filters but also the Cu and Cd filters with sharp resonances at 230, 579 and 27.5 eV, respectively.

3.3. Neutron spectrum and flux distribution measured by activation method

With the photoneutron target of lead placed near the center of the KULS, we have irradiated eleven kinds of activation foils at the distance of 12.5 cm behind the target, as seen in Fig. 1. During the irradiations, lead plugs were put into the through hole. Table 2 shows the activation foils and the fourteen nuclear reactions used in the present measurement. Gamma-rays from these induced activities were measured with a HPGe detector, whose detection efficiency was calibrated using a mixed radioactive standard source. The linac operations were performed with a

Table 2
Nuclear reaction, half life, gamma-ray energy and its intensity used for the present data processing

No.	Reaction	Half life[a]	Gamma-ray[a] energy [MeV]	Gamma-ray[a] intensity [%]
1	$^{197}Au(n,\gamma)^{198}Au$	2.694 d	0.412	95.5
2	$^{55}Mn(n,\gamma)^{56}Mn$	2.579 h	0.847	98.93
3	$^{59}Co(n,\gamma)^{60}Co$	5.271 y	1.173	99.90
4	$^{186}W(n,\gamma)^{187}W$	23.85 h	0.686	29.3
5	$^{24}Mg(n,p)^{24}Na$	14.66 h	1.369	100.0
6	$^{27}Al(n,p)^{27}Mg$	9.462 m	0.844	73.0
7	$^{27}Al(n,\alpha)^{24}Na$	14.66 h	1.369	100.0
8	$^{46}Ti(n,p)^{46}Sc$	83.83 d	0.889	99.98
9	$^{47}Ti(n,p)^{47}Sc$	3.341 d	0.159	68.2
10	$^{48}Ti(n,p)^{48}Sc$	1.821 d	0.984	100.0
11	$^{58}Ni(n,p)^{58}Co$	70.92 d	0.811	99.53
12	$^{54}Fe(n,p)^{54}Mn$	312.2 d	0.835	99.98
13	$^{64}Zn(n,p)^{64}Cu$	12.70 h	0.511	35.8
14	$^{115}In(n,n')^{115m}In$	4.486 h	0.336	45.8

[a]The nuclear data were taken from Ref. [25].

pulse width of 33 ns, a repetition rate of 30 Hz, an electron peak current of about 2 A and an electron energy of 32 MeV, respectively.

The activation data were analyzed by spectrum adjustment method employing the NEUPAC and the SAND-II codes [17,18]. The NEUPAC code contains energy dependent group cross sections of 135 groups from 0.01 eV to 16.4 MeV, including the error matrices [26] for neutron dosimetry reactions in ENDF/B-V. For the SAND-II code, the original code was revised to produce the analytical uncertainties using the Monte Carlo method [27,28]. Moreover, a subroutine program was added for the self-shielding correction in the foil. The group cross sections of 642 energy bins were used and taken from the JENDL Dosimetry File [29]. As an initial spectrum for the adjustment with the NEUPAC and the SAND-II codes, the spectral result calculated with the MCNP code was used, as described later.

Neutron flux distribution in the KULS was measured in the radial irradiation holes and the through hole. Nickel wires of 1 mm in diameter were radially set in the experimental holes to measure fast neutron fluxes by the $^{58}Ni(n,p)^{58}Co$ reaction. Gold foils, each of 5 mm × 10 mm and 50 μm thick, were put on the nickel wire in every 10 cm distance for the measurement of slow neutrons by the $^{197}Au(n,\gamma)^{198}Au$ reaction. At the position of 12.5 cm behind the neutron source and the bottom of the bismuth and the lead holes, neutron fluxes were also measured with Ni foils (12.7 mm in diameter and 0.5 mm thick) and Au foils (12.7 mm in diameter and 50 μm thick). With the Au foils and Mn–Cu foils (Mn:Cu = 88:12, 12.7 mm in diameter, 0.2 mm thick), cadmium ratio measurement (Cd-cover: 0.5 mm thick) was made in the bismuth and the lead holes by their (n,γ) reactions. These induced activities were measured with the above HPGe detector.

3.4. Neutron spectrum measured by TOF method

Making use of the Ta photoneutron target, angular neutron flux spectrum of $\mu = 0$ ($\theta = 90°$) to the incident electron beam was measured from a few eV to 10 MeV by the neutron TOF method. The experimental arrangement is shown in Fig. 2. A horizontal through hole of 8 cm in diameter was stuffed with a lead plug in the backward region to make a re-entrant hole and to extract neutrons at the position of $r = 12.5$ cm from the photoneutron target.

In order to experimentally investigate the reproducibility of the neutron spectrum measurement, different types of two neutron detectors were employed: one was composed of a bank of three ^{6}Li glass (12.7 cm in diameter and 1.27 cm thick) scintillation detectors at the 22 m station and the other was ^{10}B-vaseline-plug NaI(Tl) (12.7 cm in diameter and 5.08 cm thick) scintillation detectors at the 24 m station. When the ^{10}B-vaseline-plug NaI(Tl) detectors were used for the spectrum measurement, the ^{6}Li glass detectors were removed from the TOF neutron beam. Relative detection efficiencies for these neutron detectors were experimentally calibrated by making use of a borated graphite standard pile [30]. The background measurement was performed by removing the backward lead plug to make a through hole. Through the amplifiers and the discriminator, output signals from the detectors were fed into a time digitizer, which was initiated by the linac electron burst, and the TOF data were stored in a data acquisition system. The channel width was 20 ns to 0.25 μs and the number of channel was 4096.

The linac was operated with the pulse width of 10 ns, the repetition rate of 180 Hz, the electron peak current of about 1 A and the electron energy of about 32 MeV, respectively. A BF_3 counter was set in an experimental hole of the KULS to monitor the neutron intensity between

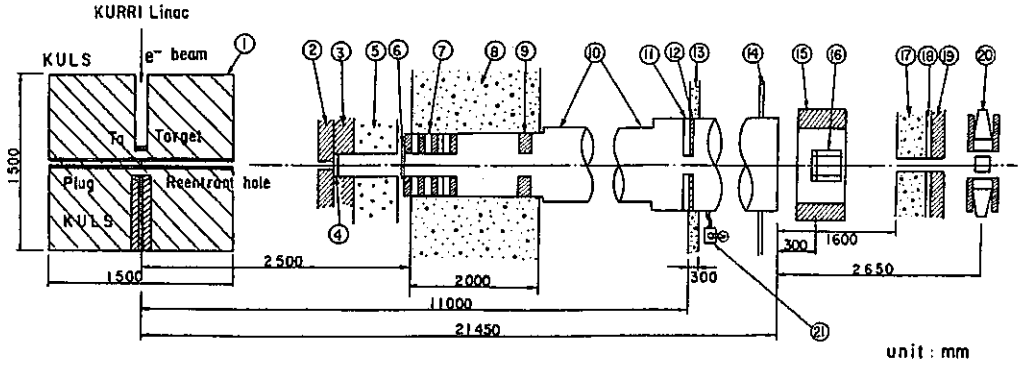

Fig. 2. Experimental arangement for the linac TOF method. (1) KULS, (2) Pb collimator, (3) Pb shield, (4) U-filter, (5) Heavy concrete (6) Cd-filter, (7) Pb+B_4C collimator, (8) Concrete wall, (9) Pb collimator, (10) Flight tube, (11) B_4C collimator, (12) Pb collimator, (13) Concrete wall, (14) Wall of measuring house, (15) Detector shield of Pb, (16) ^{6}Li glass detectors, (17) Concrete shield, (18) Cd shield, (19) Pb shield, (20) ^{10}B-vaseline-plug NaI(Tl) detectors, (21) Rotary pump.

the experimental runs. An uranium filter of 2 cm in thickness was placed in the TOF beam to shield the neutron detectors against the intense γ-ray flash from the linac burst. Moreover, a Cd-filter of 0.5 mm in thickness was placed in the TOF beam to suppress overlap of thermal neutrons from the previous pulses. The relation between neutron TOF and its energy was calibrated with resonance energies of 132 eV for Co, of 336 eV and 2.37 keV for Mn and of 27.7 keV for Fe filters. Good linearity was found between the neutron TOF and the channel number.

4. Calculations

The continuous energy Monte Carlo code MCNP [16] has been employed to analyze the time-dependent spectrum of slowing-down neutrons in the KULS. This code can track the time behavior of neutrons every 10^{-8} s. The calculations were performed with three dimensional Cartesian coordinate, and the geometrical parameters and/or size of the KULS were referred as the spectrometer was. For the calculations, the photoneutron source spectrum was taken from the experimental data, which were previously measured by the neutron TOF method [20]. Tally boxes of $10\times10\times10$ cm^3 for the MCNP calculations were put at the positions of the bismuth and the lead holes. Fig. 3 shows the calculated time-dependent neutron spectra for average energies from 70 keV to 3.6 eV at the bismuth hole about 40 cm distant from the Ta photoneutron source. In the figure, the mean time in μs after the pulsed neutron burst is shown for the each corresponding spectrum. The time behavioral spectra seem to be asymptotic form at energies below a few keV and after that, the spectrum form is kept in the slowing-down process, although small dips are observed at 0.8, 2.31 and 12.09 keV due to the sharp resonances of bismuth. From the calculated time-dependent spectra, we can obtain the relation between neutron slowing-down time and its average energy and also the energy resolution at FWHM.

The time-dependent spectra were integrated over a few tens of milliseconds to get the steady state neutron spectrum from about 0.1 eV to 10 MeV. For these calculations, one million random histories were performed. The statistical errors were poor in the lower energy region and 20 to 30% at neutron energies of a few eV, although the error was about 1% at hundreds of keV. There was scarcely difference in shape between the scalar neutron flux and the angular neutron flux in the lead hole. Activation data support the fact that the angular flux distribution of neutrons is almost symmetric around the neutron source in the KULS, as described later.

The MCNP code has its own nuclear data libraries, which were generated from the evaluated nuclear data files of ENDF/B-IV [21] and ENDL-85 [22]. New data library [31] generated from JENDL-3 [23] was also available for the MCNP calculations. Comparison of the calculated neutron spectrum and the measured one would be useful for the integral investigation of the nuclear data for lead, to understand the characteristics of the lead slowing-down spectrometer.

5. Results

5.1. Slowing-down time and energy

The measured relation between the neutron slowing-down time t in μs and the average neutron energy E in keV is summarized in Fig. 4. By the least squares fitting with these measured data, the slowing-down constant K appeared in the relation of $E = K/(t_0 + t)^2$ was obtained to be

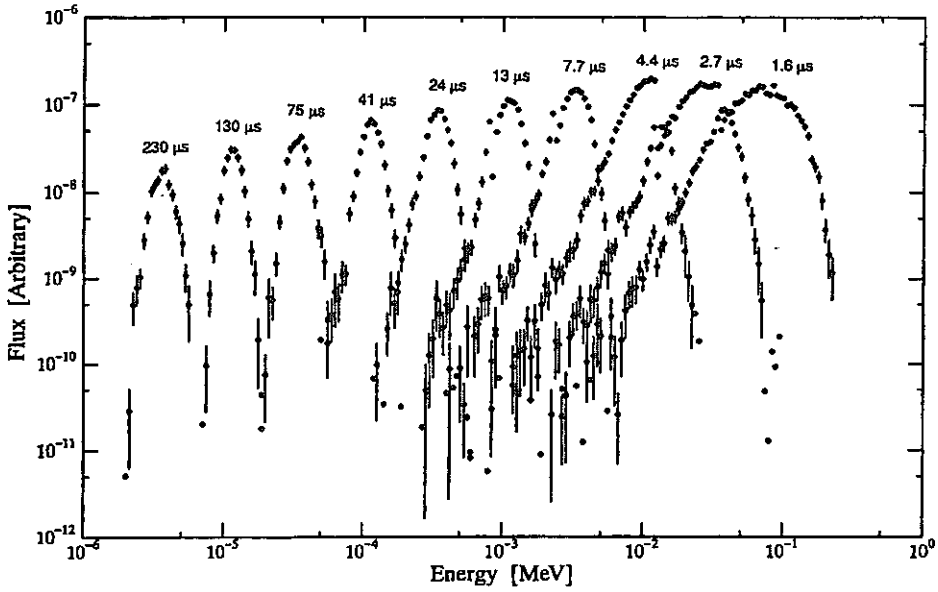

Fig. 3. Calculation of time dependent neutron spectra in the Bi hole after the pulsed neutrons were driven into the Ta target.

190±2 (keV μs^2) for the bismuth experimental hole and 156±2 (keV μs^2) for the lead one in the KULS, respectively. For both experimental holes, the constant t_0 was derived to be 0.2 to 0.3 μs. The present value of the constant K for the lead hole is in good agreement with 155 (keV μs^2), which was obtained by Wakabayashi et al. [5] before it was transferred from the University of Tokyo to KURRI. The bismuth hole was originally provided at KURRI.

As seen in Fig. 3, the time-dependent spectra from a few eV to hundreds keV calculated with a certain time bin were fitted with a Gaussian function, especially near the peak region. Making use of the slowing-down time corresponding to the Gaussian peak, the constant K for the bismuth hole was derived as 191±3 (keV μs^2), which was in excellent agreement with the experimental results mentioned above. In the same manner, the constant K for the lead hole was obtained with the calculations. The resultant value for the lead hole is 157±4 (keV μs^2), which is in good agreement with the present experimental value and that measured by Wakabayashi et al.

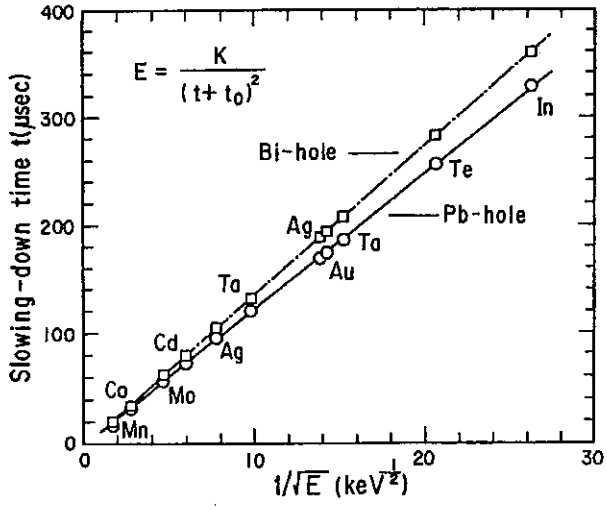

Fig. 4. Relation between neutron slowing-down time and mean energy in Bi and Pb holes of the KULS.

5.2. Energy resolution

After the neutron transmission data measured by the BF_3 counter were corrected for the resonance width and the sample filter thickness, neutron energy resolution of the KULS was obtained by fitting the resonance dip data in the slowing-down time spectrum, and derived from the FWHM in the Gaussian distribution. Resonance capture measurements using the Ar gas counter could give the appropriate energy resolution at sharp and narrow resonances of 230 and 579 eV for copper and 27.5 eV for cadmium without any corrections for the resonance peak width. Fig. 5 illustrates the present results measured in the bismuth hole. It is seen that the measured energy resolution is about 40% at energies from a few eV to about 500 eV and that the resolution is going to be larger in the lower and the higher energy regions. The results for the lead hole were in good agreement with those for the bismuth hole measured by the BF_3 and the Ar gas counters, as shown in Table 3.

The time-dependent spectra calculated with the MCNP code were also fitted with a Gaussian function. The resultant energy resolutions at FWHM are summarized in

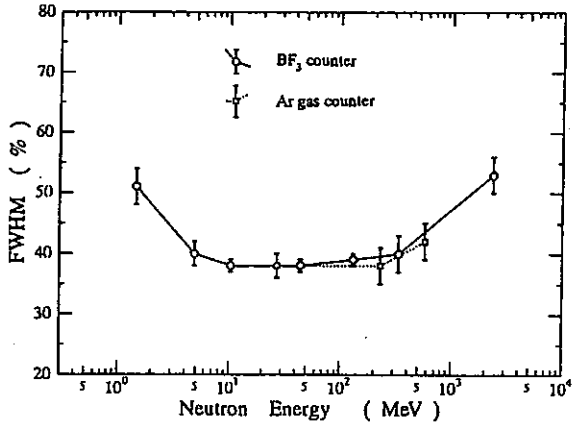

Fig. 5. Energy resolution measured by resonance filters in Bi hole of the KULS. (———○———) neutron transmission method using the BF_3 counter. (- - -□- - -) capture gamma-ray measurement using the Ar gas counter (Error lines are indicated).

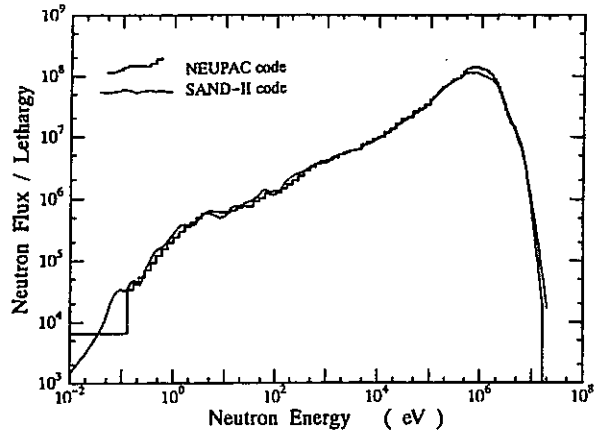

Fig. 6. Neutron spectra obtained by the activation data analysis for the lead photoneutron source.

Table 3 and are compared with the measured data using the BF_3 and the Ar gas counters in the bismuth and the lead holes, respectively. Although good agreement can be seen between the measured energy resolutions in both holes, the calculated values are generally lower by about 10% than the measured ones. It may be said that the difference is due to some other effects, such as impurity in the KULS.

5.3. Neutron spectrum and flux distribution measured by activation method

Making use of fourteen kinds of activation data, neutron spectrum from the lead target has been obtained in the energy region from 0.01 eV up to 20 MeV by the SAND-II code and up to 16.4 MeV by the NEUPAC code. The initial spectrum for both analysis codes has been taken from the MCNP calculation, and the adjusted results are shown in Fig. 6. In the figure, neutron fluxes are given by the absolute values from the activation reaction rates. The spectral uncertainties in these results are 2 to 3% at least and 7 to 8% above 10 MeV and below a few hundreds keV where the activation responses are poor. Both spectra, adjusted with different type of analysis codes, are in general agreement with each other except for energies around 1 MeV, although small deviations are observed in the resonance neutron energy region within the order of analysis error. The discrepancy around 1 MeV would be due to the difference between the dosimetry cross section libraries for some threshold reactions. In the MeV energy region, the spectral shape is close to that of lead photoneutron source and harder than that of $1/E$ spectrum in the slowing-down neutron energy region. From the Cd-ratio

Table 3
Energy resolution [%] in Bi and Pb holes of the KULS

Measurements				Calculations		
Energy	BF_3 counter	Ar gas counter		Energy	MCNP code	
[eV]	Bi hole	Bi hole	Pb hole	[eV]	Bi hole	Pb hole
1.46	51±3			3.02		35.7
4.9	40±2			3.56	37.4	
10.4	38±1			10.0		28.5
27.5		38±2	37±2	11.6	31.6	
44.9	38±1			29.8		28.2
132	39±2			33.8	35.7	
230		38±3	40±3	99.1		29.8
336	40±3			113	34.5	
579		42±3	42±4	298		33.7
2370	53±3			339	38.3	
				990		38.1
				1091	43.2	
				2988		50.3
				3208	51.8	

measurements using Au and Mn–Cu foils, it was found that there existed scarcely thermal neutrons in the KULS as displayed in Fig. 6, since the Cd-ratio was almost unity.

By the $^{58}Ni(n,p)^{58}Co$ reaction used in the above activation measurement, fast neutron flux was obtained at $r =$ 12.5 cm behind the neutron source (at the center of the horizontal through hole). Making use of the spectrum-averaged cross section for the KULS, the resultant fast neutron flux was 2.9×10^{8} n/cm^2/s, which was the result normalized to 100 W operation of the linac, although the linac power was about 63 W during the irradiation. This neutron flux is in good agreement with the normalized integral value between 1 keV and 20 MeV, appeared in Fig. 6. Fast neutron fluxes at the bottom of the bismuth and the lead holes ($r = 35$ to 50 cm from the source) were also measured with nickel foils. The results were 1.8×10^{7} to 7.1×10^{6} n/cm^2/s/100 W depending upon the distance from the source, respectively. Experimental uncertainties for these neutron fluxes were 5 to 7%.

The spatial distribution of neutrons in the KULS was experimentally determined by the activation method. The results are given in Fig. 7 for the epi-thermal neutron flux distribution by the $^{197}Au(n,\gamma)^{198}Au$ reaction and in Fig. 8 for the fast neutron flux distribution by the $^{58}Ni(n,p)^{58}Co$ reaction. Although the epi-thermal neutron flux may be higher by 5 to 10% in the forward direction, it is seen that not only flux distribution of epithermal neutrons but also that of fast neutrons are approximately symmetric in the KULS. From Figs. 7 and 8, in addition, it may be realized that the neutron flux distribution in the KULS is not affected by the room-returned neutrons, at least, at the position to set the detector in the experimental hole.

5.4. Neutron spectrum measured by TOF method

The angular neutron flux spectrum of $\mu = 0$ was measured at the position of $r = 12.5$ cm behind the Ta photoneutron target in the KULS, making use of the ^{6}Li glass detectors from a few eV up to 4.5 MeV and of the ^{10}B-vaseline-plug NaI(Tl) detectors from a few eV up to 10 MeV. The results are shown in Figs. 9 and 10 and are compared with the time-integrated spectra calculated by the MCNP code. By the MCNP calculations, we have also found that the angular neutron fluxes and scalar neutron fluxes are in general agreement in spectral shape.

The measured data were summed with energy interval of $\Delta u = 0.1$ in lethargy unit to give better statistics. The statistical errors were 2 to 10%, in general, and about 50% at worst at lower energies as seen in the figures. The neutron source normalization was made for the calculated spectra, and the measured spectrum was normalized to the calculated ones by the spectrum integration above 100 keV in Figs. 9 and 10, respectively. Fluctuations in the calculated spectra are caused by poor statistics in the Monte

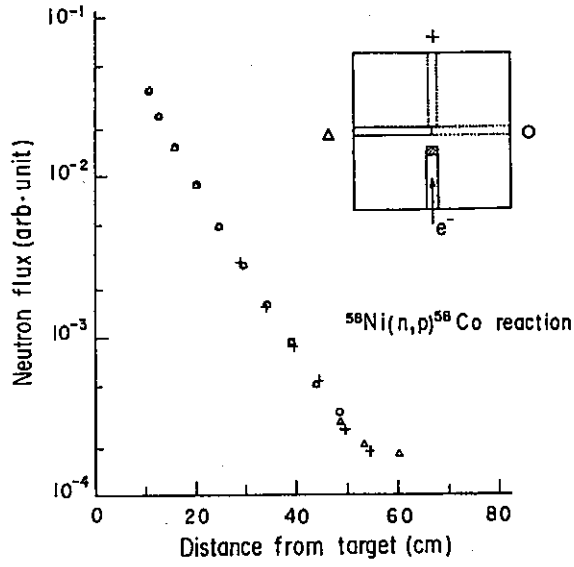

Fig. 8. Spatial distribution of fast neutrons measured by the $^{58}Ni(n,p)^{58}Co$ reaction in the KULS.

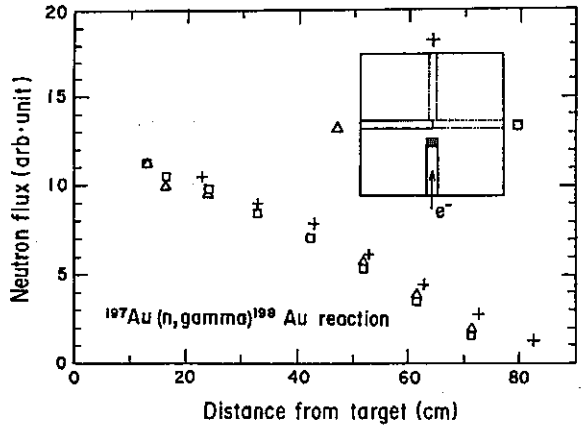

Fig. 7. Spatial distribution of epi-thermal neutrons measured by the $^{197}Au(n,\gamma)^{198}Au$ reaction in the KULS.

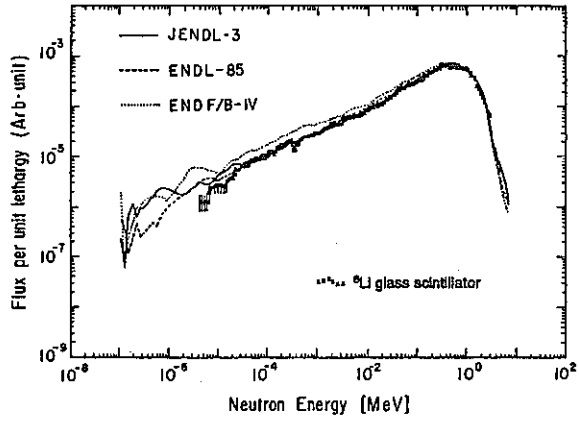

Fig. 9. Neutron spectra measured with ^{6}Li glass scintillators and calculated with the MCNP code for the Ta photoneutron source.

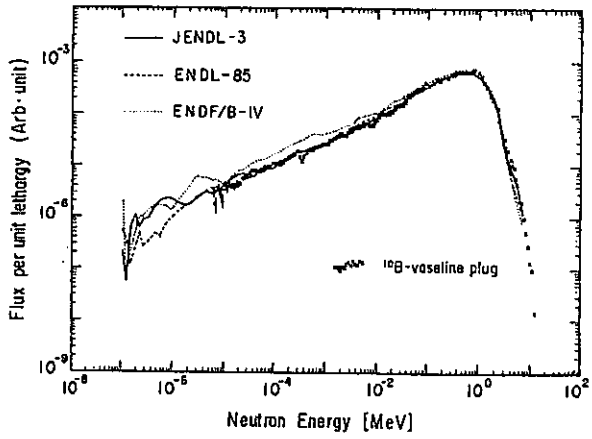

Fig. 10. Neutron spectra measured with ^{10}B-vaseline-plug NaI(Tl) detectors and calculated with the MCNP code for the Ta photoneutron source.

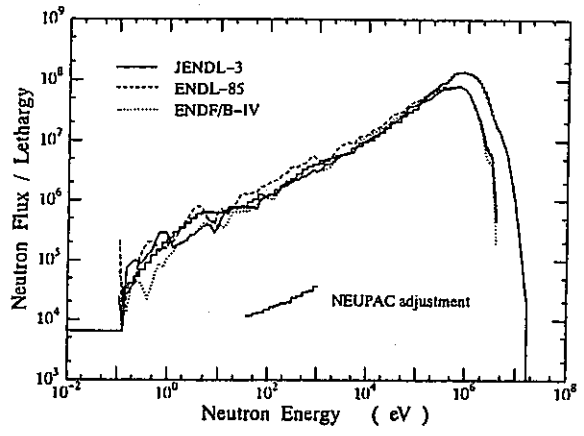

Fig. 11. Comparison of neutron flux spectra analyzed by the NEUPAC code and calculated by the MCNP code.

Carlo calculations, especially below 10 eV the uncertainties are about 300%. As seen in Figs. 9 and 10, good agreement is obtained in general between the measured spectrum and those calculated with the evaluated nuclear data libraries of JENDL-3 and ENDL-85, while the ENDF/B-IV spectrum is higher below 100 keV than the measured and the other calculated spectra. The difference is about 25% around 10 keV and 50% around 100 eV, respectively, for both ^{6}Li glass and ^{10}B-vaseline-plug NaI(Tl) detectors' measurements. It has also been found that the agreement is good between the experimental results by the detectors. This fact implies that the systematic uncertainty in the measured spectrum may be small.

Around 336 eV in the measured spectra in Figs. 9 and 10 one can see a dip structure due to the big resonance of manganese, which is included as an impurity in the steel case of lead plug. In the MCNP calculations, the manganese impurity has not been considered. If the antimony impurity exists in lead of the KULS, this may absorb lower energy neutrons and make the fluxes lower in the lower energy region. Moreover, the measured TOF data had poor counting rate and the background counting rate was almost half of the foreground one. Lower neutron fluxes near 10 eV may be due to the neutron absorption by Sb, poor counting rate or inappropriate background subtraction for the TOF measurement.

In Fig. 11, the neutron spectra by the NEUPAC and the MCNP codes are compared. In the slowing-down energy region below 100 keV, these spectra are in general agreement with each other, although the lead target produces higher energy neutrons than the Ta target above several hundreds of keV [20]. The ENDF/B-IV spectrum below about 100 keV is also higher than that analyzed by the activation data, as seen in Figs. 9 and 10, although large deviations are observed among the spectra. From the comparison of the results in Figs. 6, 9–11, good agreement can be seen between the TOF spectra and the MCNP calculations by the JENDL-3 and the ENDL-85 data, so that it may be said that the NEUPAC and the SAND-II spectra by the activation data are in good agreement with the TOF spectra in the slowing-down energy region.

6. Discussion

In the present study on the characteristics of the KULS, good agreement can be seen in general between the experiments and the calculations related to the neutron slowing-down time and its energy and to the energy resolution. It has been also found that the energy resolution of the KULS is larger than 27% for the theoretically predicted value at FWHM [1,2]. Making use of the MCNP code, we have more investigated the KULS characteristics from the points of 1) the spectrometer size, 2) the impurities in lead blocks, and 3) the spectral shape of the neutron sources.

At first, we have tried to make one dimensional calculations for the neutron fluxes and energy spectra not only in the KULS of $1.5\times1.5\times1.5$ m^3 (effective radius = 93.1 cm) but also in lead slowing-down spectrometers of $1.2\times1.2\times1.2$ m^3 (effective radius = 74.4 cm), $1.8\times1.8\times1.8$ m^3 (effective radius = 112 cm) and $2.0\times2.0\times2.0$ m^3 (effective radius = 124 cm) as typical cases of the spectrometer size, respectively. At the radial positions of more than 10 cm from the photoneutron source, it is found that the relation of neutron slowing-down time and energy is almost independent of the size of the spectrometer and of the distance from the neutron source, except for the neutron intensity. Even in case that the neutron source position shifts 10 cm from the KULS center, the relation of slowing-down time and energy and the energy resolution are almost same as before at 10 cm from the source. Neutron leakage with the KULS is higher than those with the bigger spectrometers, and the neutron fluxes in the 30

to 40 cm region from the neutron source of the KULS are about 70% and 35% of those in the bigger spectrometer of radius = 112 cm at 10 keV and 10 eV, respectively. From the point of the spectrometer size, one can see that the energy resolution in the KULS (1.5 m cubic) is larger than those in other bigger spectrometers, especially in the higher energy region as appeared in Fig. 12.

If the KULS is made of bismuth material only, the slowing-down constant K becomes larger and can be calculated as 308 (keV μs^2). In the KULS, 10 to 15 cm thick layers of bismuth blocks are partially used and those blocks may make the slowing-down constant larger than that made by lead material only. One may be able to understand the reason why the slowing-down constant K in the bismuth hole is larger than that in the lead hole.

Concerning the impurities which may contribute to the energy resolution of the KULS, we have taken account of antimony (0.05% Sb in weight) added to the lead as hardener and of water (10 to 1000 ppm of H_2O in weight) adhered to the lead surface. From the calculated results, we found that the Sb impurity was effective in absorbing epi-thermal neutrons and made the neutron fluxes lower, although the impurity did not give a severe influence to the energy resolution. In Figs. 9 and 10, the reason why the experimental spectra deviate from the MCNP calculations below about 30 eV would be explained by the neutron absorption of Sb. Fig. 13 shows the FWHM data depending upon the Sb and water impurities in the KULS. From the results, it is said that the energy resolution is not affected much by the adhered water up to 100 ppm. Even if the lead blocks were oxidized or some water was adhered to the lead, more than 10 ppm water would not be considered because the blocks were carefully cleaned to pile up.

As far as the neutron energy spectrum in the KULS is concerned, good agreement can be seen between the calculations and the TOF measurements, although the impurities in the KULS are not considered. However, the

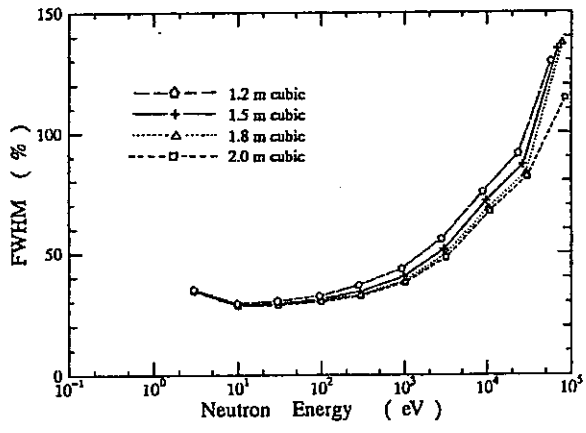

Fig. 12. Comparison of the calculated FWHM with different sizes of lead slowing-down spectrometers.

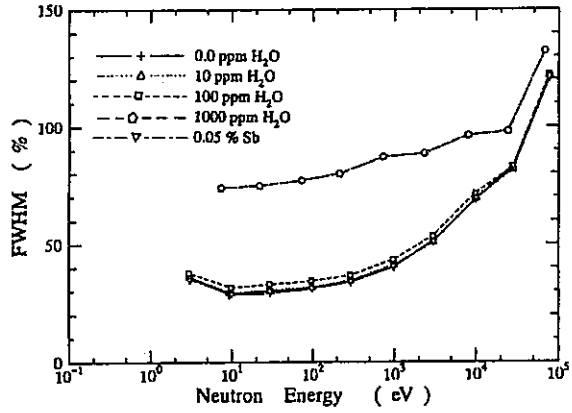

Fig. 13. Comparison of the calculated FWHM with Sb and H_2O impurities in the KULS.

calculated energy resolutions of the KULS are 5 to 10% lower than the measured ones, as given in Table 3. The difference may be due to some effects by such as small amount of impurities which are not considered in the present calculations.

With the different types of neutron source spectra, neutron behavior in the KULS has been investigated. We have selected the following spectra: 1) Ta photoneutron source, 2) 14 MeV neutrons, and 3) 500 keV neutrons whose energy is lower than the threshold level (0.57 MeV) for the inelastic scattering cross section of lead. The 14 MeV neutrons are widely spread after a few interactions with lead, and the slowing-down time spectrum may become similar to that from the Ta photoneutrons. The slowing-down time spectrum by the 500 keV neutrons already shows asymptotic form above 1 keV, as seen in Fig. 14, and the calculated energy resolution at 100 eV, for example, is about 28% at FWHM, while the energy resolution obtained with the Ta photoneutron source is about 30% in the lead hole. This fact implies that the energy resolution of the KULS is broadened by the inelastic scattering processes with lead. In the lower energy region, up-scattering neutrons may also broaden the energy resolution.

As we have investigated above, main factors to make the energy resolution broadened are thought to be the effects due to the size of the KULS, the inelastic scattering of fast neutrons and the impurities in the KULS. It may be said that the practical energy resolution of the KULS was broadened by the superposition of these effects.

As seen in Figs. 6, 9 and 10, it may be realized that there scarcely exist thermal neutrons in the KULS and that the neutron spectrum is close to that obtained in a large core of fast breeder reactors [32]. The neutron spectral shape in the KULS is simple and no structure can be observed. We have characterized the neutron spectrum in the KULS through the present experiments and the calculations. It can be expected to use the KULS in future not

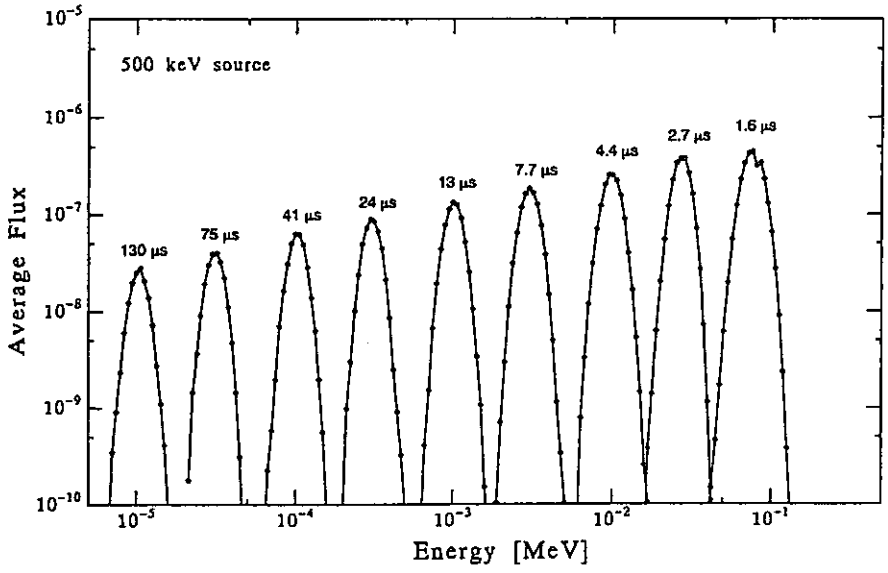

Fig. 14. Calculation of time dependent neutron spectra in the KULS driven by 500 keV neutrons.

only for measurements of energy dependent nuclear data but also for integral experiments as a reference neutron spectrum field.

7. Conclusion

The characteristic behavior of neutrons in the Kyoto University Lead Slowing-down Spectrometer, KULS of $1.5\times1.5\times1.5$ m^3, was obtained by the experiments using resonance neutron filters and by the calculations with the MCNP code. The slowing-down constant K in the relation of $E=K/t^2$ was experimentally determined to be 190 ± 2 (keV μs^2) for the bismuth hole and 156 ± 2 (keV μs^2) for the lead hole, respectively. The energy resolution of the KULS was obtained to be around 40% in the relevant energy region for the bismuth and the lead holes, making use of the Ar gas counter for the sharp resonances at 230 and 579 eV of Cu and at 27.5 eV of Cd, and of the BF_3 counter for the neutron transmission measurement using resonance filters.

Monte Carlo calculations using the MCNP code were also performed to determine the relation between the neutron slowing-down time and its average energy and to obtain the energy resolution and the neutron spectrum in the KULS. The calculated results agreed in general with these measurements, and the calculated energy resolutions were lower by about 10% than the measured ones.

Spatial distribution of neutrons in the KULS was measured by the activation method and the results showed almost symmetric around the photoneutron source. The neutron flux spectrum in the KULS was obtained by the spectrum adjustment method with activation data in the energy range from 0.01 eV to 20 MeV. The angular neutron spectrum was also measured by the TOF method from 4 eV to 10 MeV, and the TOF measurement was compared with the spectra calculated with the JENDL-3, the ENDL-85 and the ENDF/B-IV cross section data. The calculated spectra are in general agreement with the measured one except for that the ENDF/B-IV spectrum seems to be 25 to 50% higher than the TOF measurement below about 100 keV. The present result would be useful for the integral investigation of lead cross section which is related to the neutron transport in the lead slowing-down spectrometer. The neutron flux spectrum per unit lethargy in the KULS is proportional to the square root of energy in the slowing-down neutron energy region and show similar spectral tendency to the TOF measurement and the activation analysis. Since there exist scarcely thermal neutrons in the KULS, the neutron field there would be expected to be a quasi-standard field for integral measurements in the epithermal/resonance neutron energy region.

Acknowledgments

The authors would like to express their sincere thanks to Prof. M. Nakazawa of University of Tokyo for the reconstruction of the lead slowing-down spectrometer. They are also indebted to Mr. K. Nishio of Kyoto University for his kind assistance in the Monte Carlo calculations.

This study was supported by the Grant-in-Aid of Scientific Research from the Ministry of Education, Science and Culture (No. 03452302 and No. 63460234) and by the Cooperative Use Program of KURRI. The calculations were carried out with the FACOM M-Series Computers at the Data Processing Center of Kyoto University.

References

[1] K.H. Beckurts and K. Wirtz, Neutron Physics (Springer, New York, 1964) p. 342.

[2] A.A. Bergman, A.I. Isacoff, I.D. Murin, F.L. Shapiro, I.V. Shtranikh and M.V. Cazarnovsky, Proc. 1st Int. Conf. on Peaceful Uses for Atomic Energy, United Nations, P/642, Vol. 4 (1955) p. 135.

[3] Y.P. Popov, Proc. Lebedev Phys. Inst., Academy of Sci., USSR, Vol. 24 (1964) p. 111.

[4] F. Mitzel and H.S. Plendl, Nukleonik 6 (1964) 371.

[5] H. Wakabayashi, A. Sekiguchi, M. Nakazawa and O. Nishino, J. Nucl. Sci. Technol. 7 (1970) 487.

[6] A.A. Bergman, A.E. Samsonov, Yu. Ya. Stavisskii, V.A. Tolstikov and V.B. Chelnokov, Proc. Nuclear Constants, Obninsk Reports, Vol. 7 (1971) p. 37.

[7] M. Fujino, F. Takahashi and H. Yamamoto, J. Nucl. Sci. Technol. 13 (1976) 566.

[8] J.A. Harvey (ed.), Experimental Neutron Resonance Spectroscopy (Academic Press, New York and London, 1970).

[9] R.E. Slovacek, D.S. Cramer, E.B. Bean, J.R. Valentine, R.W. Hockenbury and R.C. Block, Nucl. Sci. Eng. 62 (1977) 455.

[10] Y. Nakagome, R.C. Block, R.E. Slovacek and E.B. Bean, Phys. Rev. C 43 (1991) 1824.

[11] H.T. Maguire, Jr., C.R.S. Stopa, R.C. Block, D.R. Harris, R.E. Slovacek, J.W.T. Dabbs, R.J. Dougan, R.W. Hoff and R.W. Lougheed, Nucl. Sci. Eng. 89 (1985) 293.

[12] B. Alam, R.C. Block, R.E. Slovacek and R.W. Hoff, Nucl. Sci. Eng. 99 (1988) 267.

[13] Y. Danon, R.E. Slovacek, R.C. Block, R.W. Lougheed, R.W. Hoff and M.S. Moore, Nucl. Sci. Eng. 109 (1991) 341.

[14] E.C. Vanterpool, R.E. Slovacek, D.R. Harris and R.C. Block, Nucl. Sci. Eng. 110 (1992) 186.

[15] N.M. Abdurrahman, R.C. Block, D.R. Harris, R.E. Slovacek, Y. Lee and F. Rodriguez-Vera, Nucl. Sci. Eng. 115 (1993) 279.

[16] MCNP – A General Monte Carlo Code for Neutron and Photon Transport, Version-3A, LA-7396-M, Rev.2, Los Alamos National Laboratory (1986).

[17] M. Nakazawa and A. Sekiguchi, Proc. 2nd ASTM-Euratom Symp. on Reactor Dosimetry, NEUREG/CP-0004, Vol. 3 (1977) p. 1423.

[18] W.N. McElroy, S. Berg and G. Gigas, Nucl. Sci. Eng. 27 (1967) 533.

[19] S.A. Hayashi, I. Kimura, K. Kobayashi, S. Yamamoto, H. Nishihara, T. Mori and S. Kanazawa, J. Nucl. Sci. Technol. 24 (1987) 702.

[20] K. Kobayashi, I. Kimura and T. Mori, Nucl. Sci. Eng. 99 (1988) 157.

[21] D. Garber (ed.), BNL-17541 (ENDF-201) (1975).

[22] R.J. Howerton, D.E. Cullen, R.C. Haight, M.H. MacGregor, S.T. Perkins and E.F. Plechaty, UCRL-50400, Vol. 15 (1975).

[23] K. Shibata, T. Nakagawa, T. Asami, T. Fukahori, T. Narita, S. Chiba, M. Mizumoto, A. Hasegawa, Y. Kikuchi, Y. Nakajima and S. Igarasi, JAERI 1319 (1990).

[24] S.F. Mughabghab, M. Divadeenam and N.E. Holden, Neutron Cross Sections, Vol. 1, Neutron Resonance Parameters and Thermal Cross Sections, Part A (Academic Press, Inc., New York, 1981); and S.F. Mughabghab, Neutron Cross Sections, Vol. 1, Neutron Resonance Parameters and Thermal Cross Sections, Part B (Academic Press, Inc., New York, 1984).

[25] E. Browne and R.B. Firestone, Table of Radioactive Isotopes (Wiley-Interscience, New York, 1986).

[26] T. Iguchi, Private communication (1985).

[27] Z. Li, Y. Wang and J. Gao, Measurements of Neutron Flux Spectra in SPR, Japan-China Symp. on Research and Test Reactor, UT-1, JAERI (1988).

[28] K. Kobayashi, I. Kimura, Z. Li and Y. Wang, Proc. 7th ASTM-Euratom Symp. on Reactor Dosimetry, eds. G. Tsotridis et al. (Kluwer, London, 1992) p. 263.

[29] M. Nakazawa, K. Kobayashi, S. Iwasaki, T. Iguchi, K. Sakurai, Y. Ikeda and T. Nakagawa, JEARI 1325 (1992).

[30] I. Kimura, K. Kobayashi, S.A. Hayashi, S. Yamamoto, M. Ando, S. Kanazawa, H. Nishihara and Y. Higashihara, Nucl. Instr. and Meth. 137 (1976) 85.

[31] K. Kosako, Y. Oyama and H. Maekawa, JAERI-M 91-187 (1991).

[32] A.E. Waltar and A.B. Reynolds, Fast Breeder Reactors (Pergamon, New York, 1981).